ALMA MATER STUDIORUM - UNIVERSITÀ DI BOLOGNA
CAMPUS DI CESENA
SCUOLA DI INGEGNERIA E ARCHITETTURA

CORSO DI LAUREA MAGISTRALE IN INGEGNERIA BIOMEDICA

DEVELOPMENT AND MECHANICAL CHARACTERIZATION OF A BIOSTABLE NYLON 6.6 ELECTROSPUN NANOFIBROUS MULTISCALE DEVICE FOR TENDON AND LIGAMENT REPLACEMENT AND SIMULATION

(Sviluppo e caratterizzazione meccanica di un dispositivo elettrofilato multiscala biostabile nanofibroso in nylon 6.6 per la sostituzione e la simulazione di tendini e legamenti)

Tesi in
MECCANICA DEI TESSUTI BIOLOGICI

Relatore

Prof. Ing. Luca Cristofolini

Presentata da

Carlo Gotti

Co-Relatore

Ing. Alberto Sensini

Sessione III
Anno accademico 2016-2017

Contents

Contents 1

ABSTRACT 5

ABSTRACT (Italian version) 7

1: **INTRODUCTION** 9

1.1: Structural connective tissues: tendons and ligaments 9

1.1.1: Hierarchical structure of tendons and ligaments *10*

1.1.2: Mechanical properties *13*

1.2: Tendons and ligaments mechanisms of injury and common cases 20

1.3: State of the art of tendons and ligaments replacement 22

1.3.1: Synthetic biostable materials and devices for tendon and ligament replacement *23*

1.3.2: Tissue engineering with 3D scaffolds *28*

1.4: The Electrospinning technique 29

1.4.1 The Operating principles *29*

1.4.2 Working parameters *31*

1.4.3 Electrospinning in tendon and ligament tissue replacement *34*

1.5: Developments and applications: soft-robotics – an overview 35

1.5.1 Soft Robots: actuation modes and prototypes *35*

1.5.2 Soft exoskeletons and prosthesis *39*

1.6: *In vitro* tendon and ligament simulators 48

2: **AIMS** 51

3: **MATERIALS AND METHODS** 53

3.1: Materials 53

3.2: Production of electrospun nylon 6.6 bundles and ring bundles 54

3.3: Production of the multiscale nylon 6.6 device and sheath 57

3.4: Design of grips and modification of electrospinning machine 61

3.5: Morphological characterization: optical microscopy and scanning electron microscopy 66

3.6: Mechanical characterization of bundles, ring bundles and multiscale nylon 6.6 device 67

3.6.1 Mechanical characterization of single bundles *67*

3.6.2 Mechanical characterization of ring bundles *69*

3.6.3 Mechanical characterization of multiscale nylon 6.6 device *69*

3.6.4 Data analysis *70*

4: **RESULTS** 73

4.1: Morphological properties 73

4.1.1 Morphology of nanofibers and bundles *73*

4.1.2 Morphology of multiscale nylon 6.6 device *75*

4.2: Mechanical properties 77

4.2.1 Mechanical properties of single bundles *77*

4.2.2 Mechanical properties of ring bundles *78*

4.2.2 Mechanical properties of multiscale nylon 6.6 device *79*

5: **DISCUSSION** 83

5.1: Morphological properties 83

5.2: Mechanical properties 87

5.3: Future directions 91

6: **CONCLUSIONS** 95

7: **REFERENCES** 97

ABSTRACT

Ligaments and tendons injuries are a widespread clinical problem worldwide, that compromises joint stability and patients' daily movements and quality of life. Furthermore, their treatments have a high cost on the public healthcare system. Besides many procedures investigated in the past decades, involving allograft, autograft and synthetic devices, these presented many unsolved drawbacks. In fact there are no implantable devices, both for tissue regeneration and replacement, able to accurately reproduce, from the morphological and the mechanical point of view, their complex hierarchical structure and biomechanical properties. Moreover, there are no devices nowadays that are able to simulate tendons and ligaments *in vitro*, neither for biomechanical tests of new devices or surgical techniques, and for the training of surgeons.

For these reasons, in this work, thanks to the electrospinning technique, an innovative biostable nanofibrous nylon 6.6 multiscale device was produced, investigated and tested, both from a morphological and mechanical point of view. Obtained nanofibers had a mean diameter of 257 ± 43 nm, the same order of magnitude of tendons and ligaments fibrils. From these nanofibers, ring-shaped continuous bundles were obtained, manually wrapping the nanofibrous mats. The mean diameter of these bundles was 0.48 ± 0.05 mm, in line with fascicles diameter of tendons and ligaments reported in literature. Ring bundles were then assembled in a multiscale device, by electrospinning a novel randomly oriented nylon 6.6 sheath along the group of bundles, thanks to a customized electrospinning device. This contributed to their packing and tightening, mimicking the role of the epitenon/epiligament sheath. The mechanical characterization was performed, using *ad hoc* custom-made grips, at a strain rate typical of tendon and ligament injuries. The ring bundles reported a mean ultimate stress of 63 ± 11 MPa, Young's modulus of 808 ± 89 MPa and ultimate strain of 10 ± 1.2 %. These values are in the same order of magnitude of tendon and ligament fascicles. The multiscale nylon 6.6 device reported a mean ultimate load of 333 ± 11 N, Young's modulus of 321 ± 81 MPa and ultimate strain of 9.0 ± 0.2 %. These values are in line with many biological structures, with comparable dimensions, like patellar tendon, anterior

longitudinal spine ligament, medial collateral ankle ligament and anterior/posterior cruciate ligaments. Considering the results obtained, the multiscale nylon 6.6 device is proposed as a possible novel implantable biostable device, a valid simulation tool, but also as a component for those soft robots, exoskeletons and orthoses, that need fibrous cable driven actuation, in order to simulate the physiological behaviour of human tendons and ligaments.

ABSTRACT (Italian Version)

Le lesioni a tendini e legamenti rappresentano una criticità clinica a livello mondiale in grado di compromettere la stabilità articolare e la qualità della vita dei pazienti. Inoltre, il trattamento medico di questi infortuni risulta molto oneroso per il sistema sanitario pubblico. Nonostante negli ultimi decenni più soluzioni siano state proposte, comprendenti allograft, autograft e dispositivi sintetici, questi presentano notevoli criticità irrisolte. Non vi sono infatti dispositivi impiantabili, sia per la rigenerazione che la sostituzione di questi tessuti, in grado di riprodurne accuratamente sia dal punto di vista morfologico che meccanico, la complessa struttura gerarchica e le proprietà biomeccaniche. Inoltre, non vi sono ad oggi dispositivi in grado di simulare *in vitro* tendini e legamenti, sia per quanto riguarda test biomeccanici di nuovi dispositivi o di tecniche chirurgiche, nonché per l'addestramento dei chirurghi stessi.

Per i suddetti motivi, in questo lavoro di tesi, grazie alla tecnica dell'elettrofilatura, è stato prodotto, analizzato e testato, sia dal punto di vista morfologico che meccanico, un nuovo dispositivo multiscala, biostabile, in nylon 6.6, composto da nanofibre. Le nanofibre ottenute hanno mostrato un diametro di 257 ± 43 nm, corrispondete allo stesso ordine di grandezza delle fibrille di tendini e legamenti. Da queste nanofibre sono poi stati ottenuti dei bundles continui a forma di anello, avvolgendo manualmente le membrane di nanofibre. Il diametro medio calcolato di questi bundles è risultato 0.48 ± 0.05 mm, valori in linea con il diametro medio dei fascicoli di tendini e legamenti riportati in letteratura. I bundles ad anello sono poi stati assemblati in un dispositivo multiscala, elettrofilandovi sopra una guaina di nanofibre di nylon 6.6 disposte in configurazione random. Per l'elettrofilatura della guaina è stato utilizzato un dispositivo modificato *ad hoc*. Questo procedimento ha contribuito all'impacchettamento e al restringimento del diametro del fascio di bundles, riproducendo il ruolo svolto in ambito biologico dalla guaina tendinea e legamentosa. È stata successivamente eseguita una caratterizzazione meccanica, utilizzando afferraggi *ad hoc* e una velocità di deformazione paragonabile a quella tipica degli infortuni di questi tessuti. I bundles ad anello hanno riportato una tensione a rottura di 63 ± 11 MPa, un modulo di Young di 808 ± 89 MPa e una

deformazione a rottura di 10 ± 1.2 %, valori che sono risultati nello stesso ordine di grandezza di quelli di fascicoli di tendini e legamenti. Il dispositivo multiscala in nylon 6.6 invece, ha riportato valori ti carico a rottura di 333 ± 11 N, un modulo di Young di 321 ± 81 MPa e una deformazione a rottura di 9.0 ± 0.2 %. Questi valori sono in linea con varie strutture biologiche di paragonabili dimensioni, quali il tendine patellare, il legamento spinale longitudinale anteriore, il legamento deltoideo e il legamento crociato, sia anteriore che posteriore. Alla luce dei risultati ottenuti, il dispositivo multiscala in nylon 6.6 viene proposto come un possibile dispositivo impiantabile biostabile, un valido strumento di simulazione, ma anche come componente per quei soft robot, esoscheletri e ortesi, che necessitano di una attuazione guidata da cavi fibrosi che simulino l'andamento fisiologico di tendini e legamenti umani.

1: INTRODUCTION

1.1: Structural Connective Tissues: Tendons and Ligaments

The connective tissue provides structural and metabolic support to animal tissue[1]. It originates from the mesenchymal cells which are pluripotential and capable of generating different kinds of connective cells: osteoblasts, chondroblasts, adipocytes, macrophages, lymphocytes, mastocytes and fibroblasts[2]. Besides the cellular part, the distinctive feature of connective tissue is its abundant extracellular matrix[3]. It is interposed between cells and can be divided by its ratio of ground substance to fibrous tissue[4]. In this classification, tendons and ligaments are composed of dense, regular connective tissue. It is mainly characterized by collagen fibers, usually oriented in the same direction of the load which they have to support, and a low count of cells, almost fibroblasts[5].

The principal function of tendons is to transfer the contraction force between a skeletal muscle and a bone. In this way, the muscle does not have to be directly connected to the bone, making joint movements and upright posture possible[6]. When the skeletal muscle is activated, it shortens itself. If it is connecting the two sides of a skeletal joints, this contraction will lead to the reduction of the joint angle, narrowing the two bones[7]. The tendon permits the detaching of the muscle from the bone, this frees up space at the joint insertion allowing the flexion of the forearm that otherwise would be impaired by the presence of the bigger muscle[7]. The tendon is connected to the muscle through the myotendinous junction and, when pulled by the muscle, it exhibits a high resistance with low strain, transferring the load to the bone via the osteotendinous junction[8]. Tendons do not only transfer forces in a linear way, their fibrous configuration makes them flexible and so capable of bending around the bones[5]. These contact zones act like pulleys and are also made of osteo-fibrous tissue[1]. For example, several tendons from the superficial flexor muscle of the fingers link the forearm to the fingers themselves passing through the carpal tunnel[9]. Healthy tendons exhibit a brilliant white colour due to the low presence of the cellular part and therefore of the vascularization[1,10]. Their length and width vary considerably with their function: the ones associated with big and

powerful muscles, are usually short and wide compared to the dedicated to precise movements ones. They also vary between individuals and even the same tendon varies significantly with age[11]. Their shape can range from wide and flat to cylindrical, fan-shaped and ribbon-shaped[1].

Ligaments, like tendons, are made of connective tissue. Their function is to connect bone to bone providing mechanical stability limiting unwanted joint motions.[6,8] Like tendons they are made of bundles of collagenous fibers. Ligaments can also prevent a joint from a forbidden movement[6].

1.1.1: Hierarchical structure of tendons and ligaments

Tendons and ligaments structure is determined by their extracellular matrix, which is composed predominantly by collagen, proteoglycans and elastin, with the first one dominating in terms of composition[1]. The lowest structural level unit of tendons and ligaments is the tropo-collagen molecule; contrarily, there is no general consensus about the upper structural levels nomenclature and subdivision[8 3] . This is probably due to the huge variability in this type of soft connective tissue and the limitations of the instruments used. In this work the hierarchical structure is referred primarily to the work of Kannus[1], Goh[8] and Kastelic[3], all of whom show a certain accordance, and the description will follow a bottom-up approach.

- **Tropo-collagen Molecules**: this is the lowest structural level identified. This is, in fact, the most stable disposition in which the collagen aggregates. It is composed by three aminoacidic chains twisted together to form a triple-helix with a repeating sequence of three amino acids in the form "glycine – proline – X" or "glycine – X – hydroxyproline" where the X stands for a random other amino acid. The most common structure identified is type I collagen. These particular structure, permits to the collagen to be insoluble in physiological environment[8].
- **Microfibrils:** A microfibril is a package of up to five tropo-collagen molecules intertwined with a right-handed twist. It has a diameter of about 3.5 nm and can be considered the basic structural unit of the collagen fibril.

- **Fibrils:** According to tomographic image investigations[12], the cross-section of a fibril is usually made up of four microfibrils surrounded by a ring of ten microfibrils. The diameter of these ranges from 20 to 150 nm as reported by researchers[1,8]. These fibrils increase their diameter until the animal has grown and vary in different tendons and ligaments[13].
- **Fibers**: Collagen fibers are usually assembled in bundles, in which the diameters of the fibers vary consistently in the same individual with anatomical site and in different species. Generally, can be identified in the order of magnitude of 100 μm[7]. The collagen concentration inside them is correlated with their diameter. Fibers are highly aligned inside bundles and their configuration is quite similar both in tendons and ligaments[6]. At this level the hierarchical structure is more evident but, despite this, the nomenclature is not unique. Accordingly to Kannus et al[1], a bunch of collagen fibers forms a primary fiber bundle, a group of primary fiber bundles forms a secondary fiber bundle. A group of the latter forms a tertiary fiber bundle. The primary one is also called sub-fascicle, the secondary fascicle. It was also observed that cells are cross connected between the fibers and microscopic crimps are present. This is attributed to the helical structure of tropo-collagen molecules that gives a wavy configuration to the whole fiber that can be observed even under the light microscope. [3] This configuration vanishes when the tissue is stretched (under load) and is recovered when it goes back to the resting state. It is thought that these crimps help to deconcentrate the forces facilitating a more uniform distribution[7]. Each of these structures (from primary to tertiary) is surrounded by a fine sheath of a reticular network of connective tissue called endotenon/endoligament. It binds individual fibers and larger structures together. It also presents a high amount of proteoglycan components between the endotenon and surface of fascicle in order to allow the fibers to glide on each other preserving also the integrity of blood vessels, nerves and lymphatics during the movement[7,14].
- **Tendon / Ligament:** The ultimate structure is the tendon or the ligament itself, usually made up of an aggregate of more tertiary bundle structures.

Speaking about a tendon, it is surrounded by the epitenon, another sheath of connective tissue relatively dense (8-10 nm in thickness). The fibers contained inside this membrane are longitudinal, oblique and even transverse unlike the ones in the fascicles. The outer face of the epitenon, is sometime contiguous with another sheath (paratenon) located in some tendons, the ones which do not have a synovial sheath, in order to reduce friction. Synovia sheaths are present in some contact points with bones and act like a lubricated tunnel in which the tendon can glide[1]. The tissue junctions are the part of the ligament or tendon in which it connects to the bone (and the muscle in the case of the tendon). The bone insertion is named enthesis, in this region the tendon or ligament presents highly mineralized collagen fibers[6]. Approaching the bone these fibers cover gradually larger areas. The composition of the tissue and its shape in these sites is due to the need to spread the load on a wider area in order to reduce the stress concentrations. The gradual mineralization is due to the concentration of forces that is otherwise observed in discontinuity points. In a similar manner, at the myotendinous junction, a series of terminal cytoplasmic extensions are observed at the end of the muscle cells[15,16]. These filaments extend in the extracellular matrix of the tendon leading to a higher surface area to volume ratio that can reduce the stress.

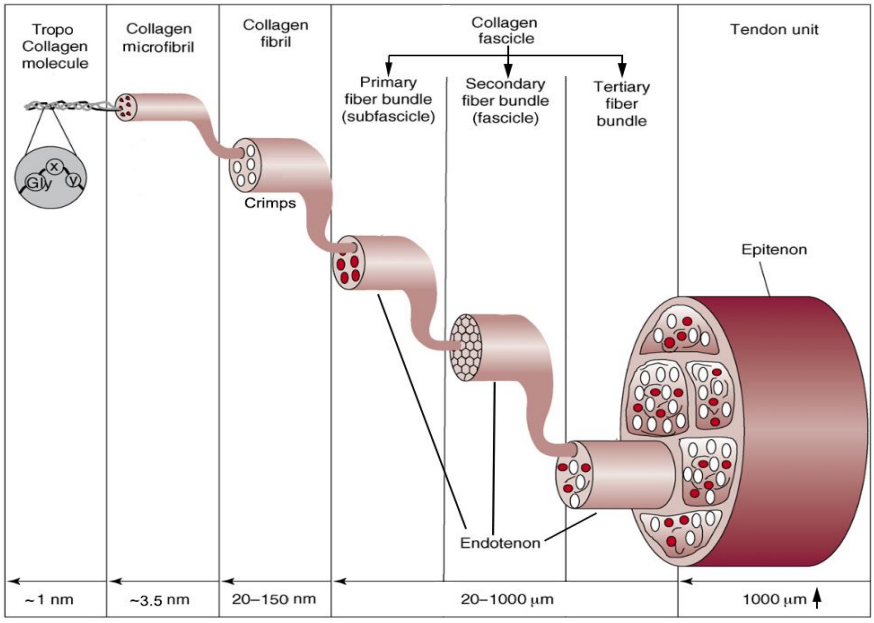

Figure 1.1.1: Tendon Structure. (Adapted from Liu et al.[17])

Apart from the collagen hierarchical structure, these connective tissues are composed also by a low percentage of elastin (1-2%), ground substances and a very low quantity of inorganic substances (less than 0.2% of the dry mass). Even if the role of elastic fibers in this kind of tissue in not completely known, it is supposed it can help to recovery the wavy configuration after a stretch[18]. These fibers are approximately 0.3-2 μm in diameter.[1] Ground substances consist mainly in proteoglycans, glycosaminoglycans (GAGs) and glycoproteins that surround the collagen structure. Proteoglycans have a protein core with one or more GAGs bounded; they are negatively charged and highly hydrophilic in a way that they can absorb up to 50 times their weight in water[19]. These macromolecules confer to the collagen structure a high resistance to shear and compressive and tensile stresses.

1.1.2: Mechanical Properties

As showed above, soft connective tissues, such as tendons and ligaments, have a hierarchical architecture. In this section the same point of view will be used to investigate the mechanical properties and characterization of the different levels of structures composing these tissues. Subsequently, a description of the whole tissue behaviour under stress will be shown, focusing on the tendon because it is almost always easier to mechanically test and to obtain geometrical measures like section (and thus stress) of a macroscopic structure. The time-dependent behaviour will also be discussed. These tests are done trying to imitate the way a natural tendon is stressed, this happens usually with a uniaxial tensile stress.

The first structural level identified was the **tropo-collagen molecules.** Applying a tensile stress to the whole tissue causes a stretching in each internal component, thus also the tropo-collagen as said before, these molecules are present in a triple helix chain structure and are connected by many types of covalent cross-links, Van der Waals and hydrogen bonds[8]. These connections allow the tropo-collagen molecules to distribute the stress between them and not to take up concentration peaks that, otherwise, would result in a rupture of the chains. These molecules are proteins that possesses domains which, under tensile stress, begin to

move and then to deform. Once the domains are unfolded, the secondary structures (chains) begin to be denatured leaving a straight molecule. The following diagram (Fig. 1.1.2) shows the force – displacement relationship of a tropo-collagen molecule under uniaxial extension. These data are achieved by stretching the molecule with an atomic force microscopy[20].

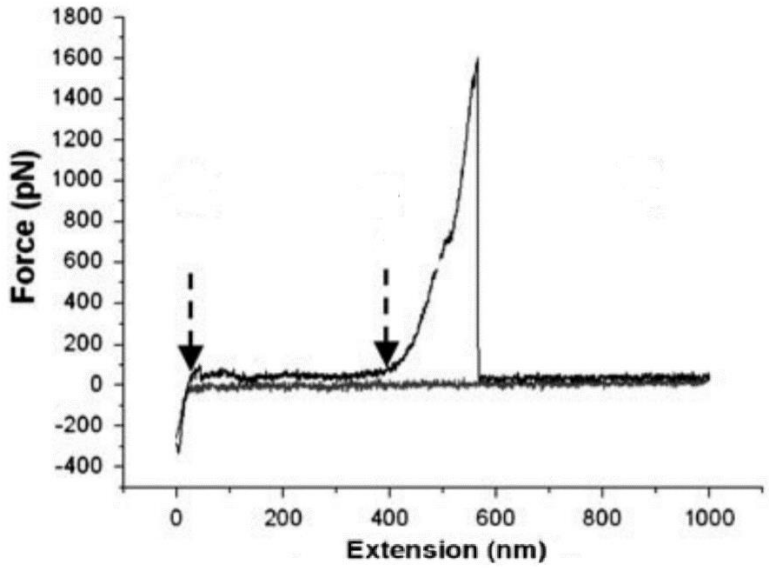

Figure 1.1.1: Force-displacement diagram of a single tropo-collagen monomer achieved by atomic force microscope. The firs arrow indicate when the tip of the microscope leave the surface, the second arrow when the force begin to rise.[20]

There is a first region of the curve in which there is an extension without a corresponding increase in force. This is due to the straightening of the slacks between tropo-collagen molecules and the alignment of the bonds that are not parallel to the axis of the molecule (and the direction of stress). Then, from the second arrow, the force begins to rise accordingly to the unwinding of the triple helix before and to the elastic deformation later, ending with the rupture[20].

The upper level structure identified was the **microfibril,** a kind of supertwist of a bunch of tropo-collagen molecules. Even at this level, the interdigitation between narrow microfibrils allow a better distribution of the axial forces between them. It was shown[21] that, when stretched, tropo-collagen molecules slide slower compared to microfibrils. This difference in time is probably a strategy to "dump"

the stress, permitting a gradual distribution from the microfibrils to the tropo-collagen molecules. As said before, the microfibril has a right-handed twist; this, in addition, can improve its stability in case of torsional forces, behaving as a sort of shield against the rupture of the helical structure. [8]

In (Fig. 1.1.3) the stress-strain relationship of a collagen **fibril** is shown. It was achieved stretching a fibril using a MEMS[22].

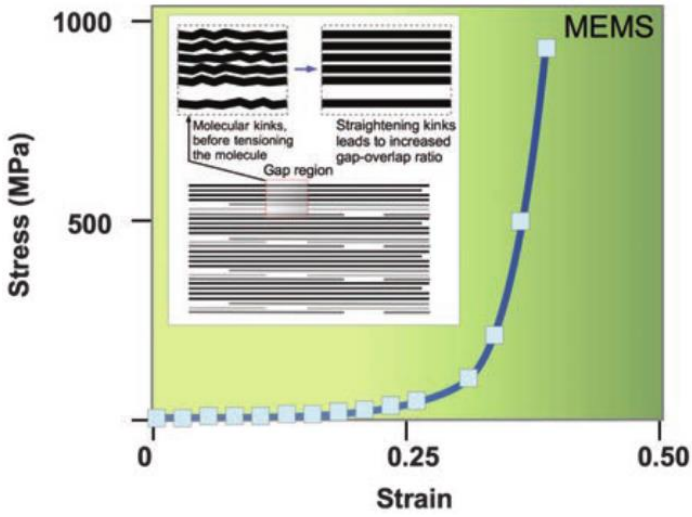

Figure 1.1.3: Stress - strain relationship of a collagen fibril.[8]

It shows the true stress (force over instantaneous sectional area that decreases with the shrinking of the fiber) versus the Eulerian strain. The curve shares the same macroscopic aspect from the one typical from tropo-collagen molecule. A first strain region without stress, increase due to the repositioning of the bonds along the axis followed by a toe-region that can be more or less visible. After that, there is a marked increase in the slope of the curve that starts the linear region in which the deformation is still recoverable if the load is removed. Here the fibril (and its components), is aligned on the same axis of the force. During the axial deformation, the interfibrillar matrix, rich in proteoglycans, deforms in shear[8]. The shear stress is generated on the fibril surface.[8] When the load exceeds this region, it can happen that the proteoglycan-rich interfibrillar matrix disrupts its bonds with the fibrillar matrix, and slides over its surface becoming plastic[23–25]. At this, point the deformation is not recoverable and removing the load will result in a permanent residual deformation.

The upper level of structure, the **fibers**, are harder to investigate because their characterization varies a lot because of different length, diameter, orientation or site[26,27] (insertions sites present different fiber composition)[6,15,16,28]. This means that during the test these fibers are not uniformly loaded. However, studies have reported that fiber strain is recoverable until about 5% deformation[29,30]. As said before, along fibers (packed as bundle or fascicle) microscopic crimps are observed. It was observed that these crimps disappear at about 3% of deformation acting like another shock absorber[31–33].

Fibers are aggregate in bundles, which can be primary (subfascicle), secondary (fascicle) or tertiary. In (Fig. 1.1.4) a stress-strain graph oh human Achilles tendon fascicle is shown.

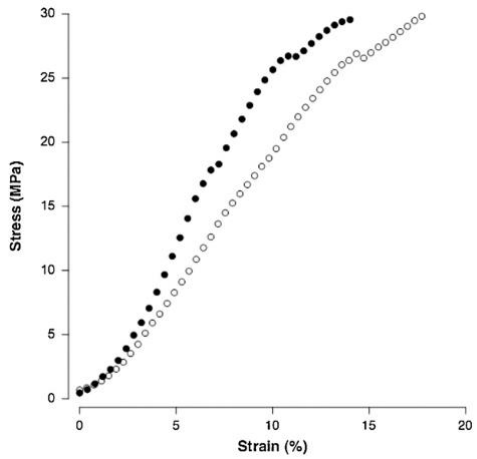

Figure 1.1.4: Stress - strain relationship for human Achilles tendon fascicle. Filled circles = Afro American. Open circles = Caucasian[34].

The upper level is represented by the whole tissue. In (Fig. 1.1.5) a typical stress-strain relationship of a tendon is shown. It shares again a similar shape compared to the characterization of its internal components.

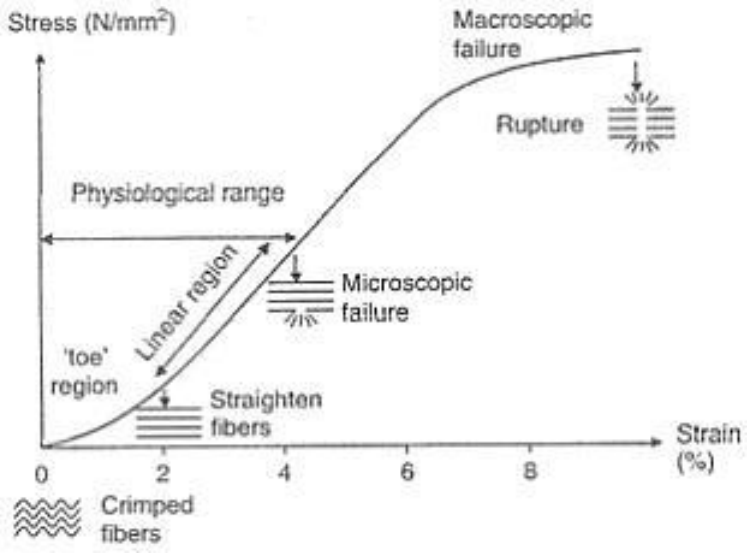

Figure 1.1.5: Typical stress-strain curve of a tendon. The curve is coupled with a simple representation of the corresponding behaviour of the collagen fibers.[35]

In (Fig. 1.1.6) the analogue relationship is drawn for a ligament.

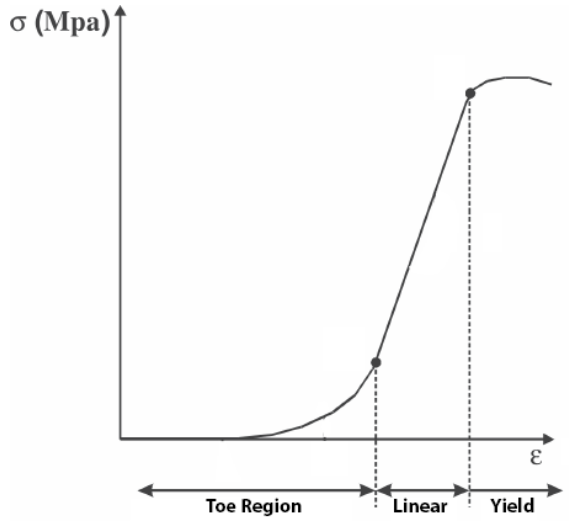

Figure 1.1.6: Stress - strain relationship of a human ligament (adapted from Campbell-kyureghyan et al)[36].

The first part is the toe-region, in which the increasing force reduces the laxity of the collagen fibers aligning them to the direction of the load. Here the structure is "reshaped" without a true deformation. Ligaments usually present a more evident toe region (Fig. 1.1.6). This is due to their function, they have to permit the joint

movement undergoing a certain amount of strain and then becoming suddenly stiffer to avoid non-physiological movements[37]. *In vivo*, this preload is automatically done by muscles that keep tendon deformation point at the start of the linear region[37]. From this point, further increasing the load, the curve enters a linear region in which the fibers are elastically deformed. Inside this region ends the physiological range of stimulation, proceeding further with the stress determines the disruption of some fibers that gradually decrease the slope of the curve (the stiffness). This is called the plastic region. The stress continues to rise until the number of broken fibers determines the failure of the structure: the curve can now show a plateau in which deformation increases without a rise of the stress, followed by the total disruption of the tendon[8]. This behaviour will not be the same if tested at different strain rate[38]. Arising the latter, the Young's modulus that is usually chose equal to the slope in the elastic region, will increase in the same way as the failure stress[38]. This is due to the different mechanisms that predominate at slower or higher strain rates, a behaviour known as viscoelasticity. In the next picture (Fig. 1.1.7) an example of stress-strain behaviour of a human anterior cruciate ligament at different strain rates is proposed.

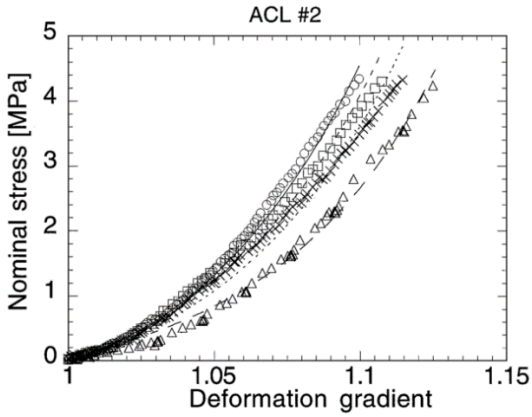

Figure 1.1.7: Stress-displacement curves at different strain rates for human ACL. The displacement rates varies from 12mm s^{-1} (o) to 0.3mm s^{-1} (Δ)[38]

Other studies[39,40] show how soft connective tissues exhibit a normal creep and stress relaxation behaviour. Furthermore, it was also shown how, during a cyclical test, the stress versus strain curves for individual loading cycles became less linear and

with a softer slope (decreases in stiffness) during the cycles[40]. The hysteresis that is also present increases its area from one cycle to another one.

Once discussed the mechanical characterization of the whole tendon and its internal structures, in the next picture (Fig 1.1.8) is depicted a comparison between the stress-strain curve of tropo-collagen molecule, collagen fibril and the whole tissue. These results can vary consistently but normally it can be said that the stiffness decreases going from the lower structural level to the highest one[41].

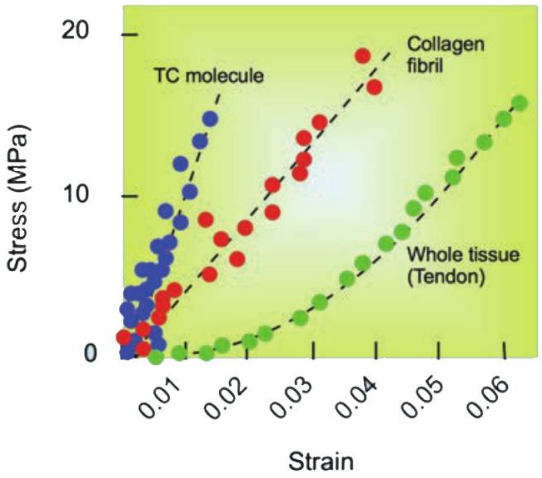

Figure 1.1.8: Stress - strain relationship for tropo-collagen, fibril and tendon.[8]

1.2: Tendon and ligament mechanisms of injury and common cases

Ligament and tendon injuries are widespread problems worldwide[42,43]. It has been reported that more than a half of about 30 million musculoskeletal injuries worldwide involves tendons and ligaments[43]. The cost sustained annually by US for tendon and ligament related problems is estimated at up to 30$ billion[42]. It has been reported that more than 150000 procedures of treatment of anterior cruciate ligament (ACL) ruptures are done annually only in the US[44]. The consequences of these injuries can compromise the joint stability and, accordingly, the daily movements of patients and quality of life[42,45].Tendon and ligament injuries can be both acute or chronic[46]. In the former scenario, the injury usually differs from tendons to ligaments for their different function. The role of tendons is to transfer the joint force of the muscle, so the most obvious danger is to suffer an acceleration or force that exceeds the tendon limit. For example, up to 90% of Achilles tendon injuries in sports are related to strong accelerations[47]. It was also reported that more than an half of sport-related injuries affect tendons[48]. These are called extrinsic factors which predominate in acute injuries[46]. Despite this, it was shown that in many sudden ruptures of the Achilles tendon a degenerative change that was present prior to the rupture was found[49,50]. Kannus and Jozsa showed how in 97% of 891 spontaneously ruptured tendons was already present a degenerative situation, compared to the 33% of 445 control tendons[49]. These changes is often caused by degenerative tendinopathy of which the etiology remains unclear.[46] Tendinopathy is a general term used to enclose several different tendon pathologies[43]. Intrinsic factors such as misalignment, biomechanical faults are also associated with a presence of tendinopathy[46]. As showed, tendons can bear an applied stress without damage only if the strain remains in the linear region. It must be also remembered that the stress-strain behaviour of these tissues is related to the strain rate. The physiological strain for a tendon is usually up about to 5%, beyond this point the fibers begin to disrupt[29]. With repetitive overloading the tendon responds with either inflammation of the sheath or degeneration of its body, or both.[46] Tendons have a repair mechanisms mediated by tenocytes but, they need enough time to heal

, caused by the low vascularization. Because of this, fatigue damages will result in a weaken and eventually in a broken tendon. Even at physiological stresses tendons suffer from microtraumas which need to be healed and may result in an injury if not enough time is given for this process, in a way similar to fatigue fractures of bones[51]. For example chronic problems caused by overuse of tendons are probably responsible for 30% of all running-related injuries[46,52]. During an injury a tendon can be partially torn, this will cause swelling, but if the patient had maintained a good strength a non-surgical repairmen is indicated[53]. If the tendon breaks completely the joint suffer from a complete loss of movement and the stumps retract from one another[54]. In these cases, a surgical procedure is mandatory. The most common cases of tendon injuries concern forearm/hand extensor and flexor tendon, the Achilles tendon, the tearing of the patellar or quadriceps tendons at the knee, and the rotator cuff tears.[55]

Ligaments have a different function, keeping the bones of a joint together and allow them to move only in predetermined directions. Ligament injuries are usually caused by a wrong movement normally not allowed by the joint. Ligaments injuries are a common sport accident because of the strong and sudden forces that can be suffered. The severity of the damage depends on the portion of the ligaments that was torn. Ligaments lack of blood vessels so it is hard for them, if not impossible, to recover from a serious injury without external healing[56,57]. A broken ligament can therefore allow a joint movement normally restricted which can lead to other serious damages. The most common ligament injuries concern the acromioclavicular ligament, the anterior cruciate ligament (ACL), the posterior cruciate ligament (PCL) and the collateral ligament.[55]

1.3: State of the art of tendons and ligaments replacement

In the last decades many attempts were made to deal with tendons and ligaments injuries: primary repair, biological grafts, synthetic grafts and tissue engineered scaffolds[42,45]. All of them present advantages and disadvantages, and their use varies depending on many factors like the type of the injury, the age of the patient, its occupation and others[58]. A common feature of these techniques is that, if the seriousness of the problem excludes a spontaneous remission of the injury, a surgery is needed. This can be done with a primary repair, which involves the suturing of the proximal and distal ends of the ruptured ligament or tendon by approximating them[45]. This technique, which does not include augmentation, often gives rise to many complications like decrease of the joint function and adhesions[59]. The results are mixed, with some successes, for example in the patellar tendon healing[60], and failures that resulted in the abandonment of this method for ACL treatment in 1982[61]. Other methods involve the tissue augmentation using biological grafts which can be divided in three groups: autograft, allograft and xenograft. Autograft are patches of tissue harvested from the own body of the patient[45]. They usually came from bone patellar bone tendon, hamstring tendon, quadriceps tendon and iliotibial band[45]. Originating from patients' own body, problems like rejection or disease transmission are avoided but the donor-site morbidity remains a drawback[62]. Despite this, autograft are still the most popular used for example for ACL reconstruction[45]. Allograft are tissue patches collected from patellar tendon, Achilles tendon, semitendinosus or fascia Lata of another human donor[63]. The advantages of this technique is to reduce the operative times, to obtain larger patches but on the disadvantages it may involves diseases transmission, immune rejection, tunnel enlargement or weakness derived from the mandatory decellularization of the graft[45]. In the next section the two remaining techniques, synthetic biostable devices and tissue engineered bio-resorbable scaffold will be reviewed. The former is intended as a permanent replacement for the injured tissue, the latter have to promote the healing of the injury, being later reabsorbed by the body.

1.3.1: Synthetic biostable materials and devices for tendon and ligament replacement

The use of synthetic materials became popular in the 1980s when researchers were looking for something which can eliminate the rejection, diseases transmission and donor-site morbidity problems[57,64–69]. Many of them had been abandoned later for the poor biocompatibility and long term complications revealed by studies, such failures, inflammation response because the prosthesis were identified as foreign body, implant degenerations or severe synovist.[42] Among those, can be mentioned filamentous carbon implant, a cord like structure with fibers of 9-10 μm diameter which was strong and flexible. It had been used both for ligament and tendon replacement but was later withdrawn from the market because it was identified as the cause of mild effusion, pain, synovial thickening and an excessive grown of fibrous sheath over it.[70]

Gore-Tex was another permanent prosthesis made of thermomechanically expanded polytetrafluoroethylene (PTFE) fibers (Fig. 1.3.1). It was in braided configuration and widely used for ACL reconstruction but, after initial encouraging results, was discharged due to evidence of bone tunnel widening and a non-biologically inert behaviour in the synovial environment[45]. It is still used in many kind of surgery but no longer to repair or replace tendons or ligaments[42].

Figure 1.3.1: A Gore-Tex implant[71].

Dacron devices were also used for ACL reconstruction between 1989 and 1997 but showed high failure rate[72].

Trevira-Hochfest is another prosthesis made of a woven PET band with longitudinal and cross-direction threads, each with 200 filaments of 23 micrometres of diameter. Although studies exhibited no synovitis and no increase of leukocytes, a slight concentration of PET wear particles and solitary multinuclear giant foreign body were observed in histological analysis[73]. Moreover, up to 2015, only 3 studies about the outcome of this device were found[72].

Leeds-Keio graft (Fig. 1.3.2) are a non-absorbable prosthesis for tendon and ligament reconstruction that became popular since 1980s[74]. It is made of polyester (ethylene terephthalate) and has an open-weave architecture. Its failure stress without tissue ingrowth is 850N, its stiffness is 200 N/mm (similar to the ligament one) and it is inert but encourages the in-growth of a new ligament so it acts also like a scaffold[45 75].

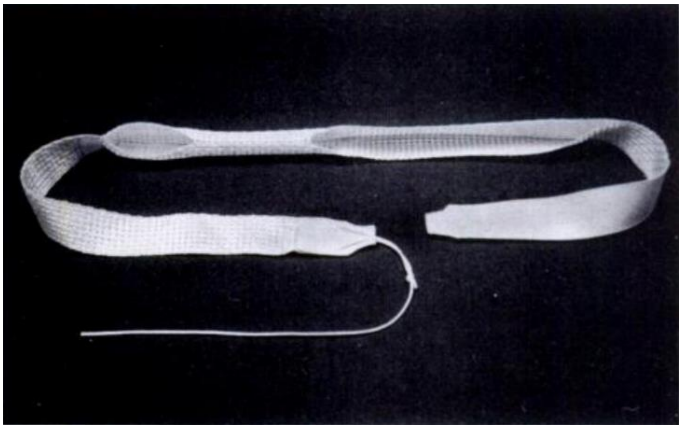

Figure 1.3.2: A Leeds-Keio artificial ligament[74].

Although it has encountered numerous drawbacks in follow up works like failure, bone tunnel enlargement, synovitis because of loosen particles, laxity and degenerative changes[76], this device has also been used with favourable results to repair rotator cuff tear, knee extensor, Achilles tendon rupture, iliofemoral ligament and ankle lateral ligament[42].

Ligament augmentation device (LAD) was invented by Dr. John Kennedy (Fig. 1.3.3) and it is a flat polypropylene high tenacity yarn with nine strands, each one made up of 180 fibers. It is braided in a string of 6mm width and 1mm thick[77].

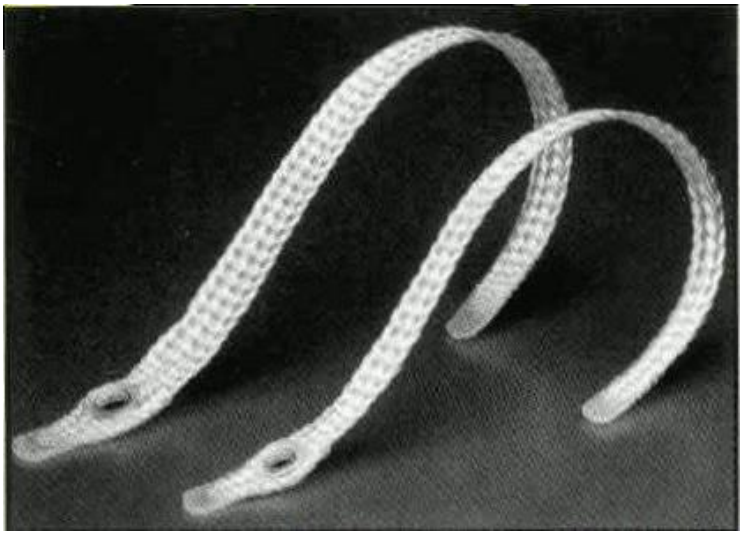

Figure 1.3.3: The Kennedy LAD ligament[78].

Despite the forces tolerated by this device are lower than other synthetic permanent prosthesis[45], it was proposed as an aid device aimed to bear some of the stress while the ligament is being cured by an autogenous graft or after a primary repair. However, studies reported effusion and wear particles originating from LAD. After a long follow-up it emerged that where was no stability advantages in using this device in ACL reconstruction and therefore it is not widely used anymore[79].

Artelon and Sportmesh are devices made of biodegradable polyurethane urea polymer and are intended as a reinforcement for soft tissues[80]. It has been tested for healing of biceps, Achilles and patellar tendons and for the rotator cuff with good results both *in vitro* and *in vivo* (animals). The device showed a good degradation and tissue ingrowth was observed[42].

LARS (Ligament Augmentation and Reconstruction System) is the synthetic prosthesis device for ACL repair that had more success and longevity in this 16 years on the market[72]. It is made of terephthalic polyethylene polyester fibers knitted in the extra-articular part and longitudinal in the articular one (Fig. 1.3.4) to be able to better provide strength and resistance to elongation[45]. It is normally intended for ACL[81–83] repair but it was proposed also for Achilles tendon and patellar reconstruction and for acromioclavicular and collateral ligament repairs[42]. This device has high biocompatibility, no risky complications like foreign body rejection, synovitis, osteolysis were observed although some minor

complications like knee stiffness and bone tunnel enlargement were reported in animal tests[84]. Another advantage of this device is that it showed fibroblast in-growth aligned with the fibers in *in vitro* and *in vivo* studies. These cells (even osteoblasts-like ones) build a capsule all around the fibrous structure of the LARS connecting it to the surrounding tissue enhancing the biocompatibility[85]. However, the tissue in-growth is also probably responsible for a 25% loss in strength and a 70% increase in elongation but, as the same time, exhibited a J-Shaped curve very similar to the natural ligament one[86].

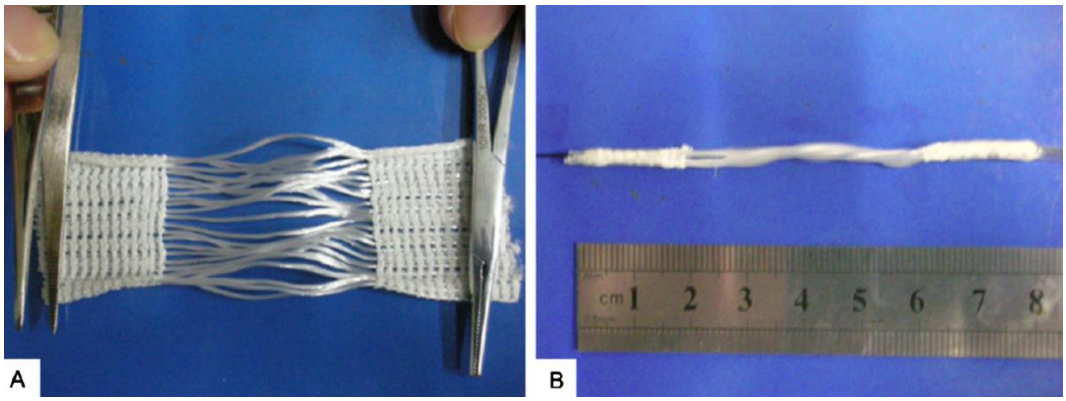

Figure 1.3.4: LARS device in its unfolded (A) and folded (B) form.

The devices presented above, have in common the aim to mimic as better as possible the mechanical behaviour of the corresponding biological one that they have to replace or heal. This is due to the need of prevent joint instability and therefore begin the rehabilitation process as soon as possible. However, those characteristics are often quite lower than the biological original counterpart. In fact, a prosthetic device, in particular for tendon and ligament replacement, should never be stronger than the tissue that it has to replace. This to prevent that another injury can occur in another part of the healthy tendon, or in the bone or muscle. In case of an excessive stress a device replacement is advised compared to another site of injury[37]. For example, anterior cruciate ligament is reported to be able to bear a force of about 1250N[87]. Leeds-keio ligament stops at about 850N[45] and LARS can reach 1000N[88]. However, this can be considered as an advantage of the synthetic devices because biological derived ones have dramatically lower values, ranging

from 27 to 229N[42]. The aim of a prosthesis of this type is to handle at least the 50% of the maximum load of the original one so that the risk of failure during daily activities is lowered. For this need and the others presented above, (Table. 1.3.1) from a 2009 review of Chen et al.[42] shows the outcome of the clinical studies of Gore-Tex, LARS and Leeds-Keio devices for tendon and ligament injuries.

Study type	Year	Tendon involved	Cases (n)	Follow-up	Complication or procedure failure	Opinion
Gore-Tex						
Retrospective	2000	ACL	123	5–11 years	26 rerupture, 50% loosen, 63% osteoarthritis	Against
Retrospective	2002	Rotator cuff	28	44 months	3 failed, no complication	Support
Retrospective	2004	Patellar tendon	7	24 months	None	Support
Retrospective	2005	ACL	17	13–15 years	15 patients had tibia bone tunnel widened	Against
Case report	2006	ACL	1	NA	Extensive periprosthetic osteolysis	Aginst
LARS						
Retrospective	2000	ACL	47	8–45 months	3 rerupture	Support
Prospective controlled	2002	ACL	27 Autograft 26 Lars	24 months	One revision in Lars group	Support
Retrospective	2004	ACL and LCL	21	27.4 months	NA	Neutral
Retrospective	2005	ACL	14	36 months	Stiffness in 5 patients	Support
Retrospective	2006	Knee extensor	22	44 months	Infection rate 18%	Support
Retrospective	2008	LCL	26	43 months	NA	NA
Leeds–Keio						
Retrospective	1991	ACL	20	2–4 years	Synovitis	Against
Retrospective	1992	ACL	25	5 years	NA	Support
Retrospective	1993	ACL	62	8–36	NA	Neutral
Retrospective	1995	ACL	24	2 years	3 rerupture	Against
Retrospective	1995	ACL	50	5–7 years	5 failures	Against
Retrospective	1999	ACL	82	40 days	NA	Support
Retrospective	2000	Ankle lateral Ligament	451 feet	5 years and 8 months	NA	Support
Retrospective	2000	Knee extensor	27 knee	5.9 years	NA	Support
Retrospective	2003	Knee extensor	12 knee	3 years	NA	Support
Case report	2003	Iliofemoral ligament	1	12 months	NA	Support
Retrospective	2004	ACL	18	13.3 years	28% rerupture 51% increase laxity	Against
Case report	2005	Medial patellofemoral ligament	2	6.1 & 8.5 years	NA	Support
Retrospective	2005	Knee extensor	15 knee	53 months	NA	Support
Case report	2005	Knee extensor	3 knee	12–48 months	NA	Support
Prospective, controlled	2006	Rotator Cuff	20 Leeds Keio 19 Autograft	2 years	NA	Support
Retrospective	2006	ACL	13	12 months	NA	Support
Retrospective	2006	ACL	30	24 months	Tunnel enlargement	Support
Retrospective	2007	ACL	50	10–20 years	6 rerupture	Support

Table 1.3.1: Clinical studies reports about three synthetic devices: Gore-Tex, LARS and Leeds-Keio[42]

One last example, concerns a synthetic device directly produced to replace a corrupted tendon. Even for tendons, the conventional method is to harvest donor ones. In this study S.Abdullah et al.[89] used a device called Ortho-tape, a polyethylene terephthalate non-absorbable, woven tendon. Even if is non-absorbable, it has an open structure which can facilitate the tissue in-growth and is

supposed to be not permanent. However, after healing a patient with massive polytrauma that lost 7cm of the extensor forearm tendon, she refused the last stage of the treatment which involved the replacement of the Ortho-Tape with autografts because her function was already satisfying. The authors suggest at the end the usage of this kind of synthetic device when the tendon loss is considered "massive".

1.3.2: Tissue engineering with 3D scaffolds

In the last years, research for tendon and ligament regeneration, has focused on a different approach: the mimicking of the hierarchical structure of the extracellular matrix of the tendon with 3D scaffolds[90–96]. This to encourage the growth of fibroblasts and other cells on the device and the subsequent reformation of the original tissue which then degenerates the scaffold[53,95–98]. This path was already taken with the use of biological graft but, as seen before, presents many drawbacks. Newer scaffolds are made via the polymerization of protein molecules like for example collagen and elastin[42,99]. This lead to a great cytocompatibility, biocompatibility and biodegradability. The main challenge involves the growth of the tissue aligned to the scaffold (and therefore to the tendon/ligament original fibers) avoiding a chaotic proliferation which would lead to a fibrotic tissue. Other aims are a good water uptake and adequate porosity so that the cells can penetrate the scaffold and reform the tissue not only on the surface[42]. Apart from the cell proliferation, these scaffolds aim to provide a structural support that can work in parallel with the tissue regeneration[42,95,96]; the scaffold would bear the load during the recovery of the tendon/ligament, stimulating at the same time the cells with loads in the same direction of the physiological one. The scaffold should therefore be able to withstand loads at least equal to the biological ones under normal usage that is usually in the range between 7% and 40% of the failure load[53]. Stiffness is also important because, to obtain the load-sharing behaviour, the biological tissue and the scaffold should present similar stiffness[53,100]. These specifications are hardly met all together. In the next chapter will be discussed a technique, that is becoming more and more popular in the production of biological scaffold: the electrospinning.

1.4: The Electrospinning technique

Electrospinning is a term coined in the early 90's derived from the two words "electrostatic spinning". The process was actually patented over a century ago but drew the focus of the researchers only in the last twenty years[101]. This is probably due to the revolution brought from the development of nanotechnology which impacted most of the branches of science. At nanometric size, the properties of materials change considerably, compared to the typical macroscopic size ones. The most important factor which have in common these new structures is the huge surface area to volume ratio[102]. Some examples like nanorods, nanotubes, nanowires, nanospheres or nanofibers can be mentioned[102–106]. In particular the electrospinning technique is suitable for its capability to produce fibers in the micro/nanoscale size and to tune their dimensions and alignment. This process can produce fibers with one to two order of magnitude greater surface area to volume ratio compared to other conventional methods such melting and dry/wet spinning[93]. Moreover, from a biomechanical point of view, this technique became very interesting because the nanofibers produced have a structure, a dimension and a porosity comparable to the ones found in the fibrous system of the extra cellular matrix[97]. This can therefore be extended to almost all of the tissues like bone, cartilages, blood vessels, nerves and, of course, tendons and ligaments[95,107–109]. Another advantage of this process is the ability to use a wide range of polymeric materials, both biological or synthetic ones[110].

1.4.1 The Operating Principles

The Electrospinning technique is based on the electrostatic stretching of a polymer droplet to form ultra-fine nanofibers[111]. The basic configuration of an electrospinning machine (Fig. 1.4.1) is composed by a syringe pump, which control the flow rate of one or more syringes, loaded with a solution derived from a polymer (or a blend of polymers), solved in a solvent system (of one or more solvents). An high electrostatic field, usually between 5 to 30kv[93], is applied from a DC power supply to the fluid via the metallic needle of the syringe (spinneret).

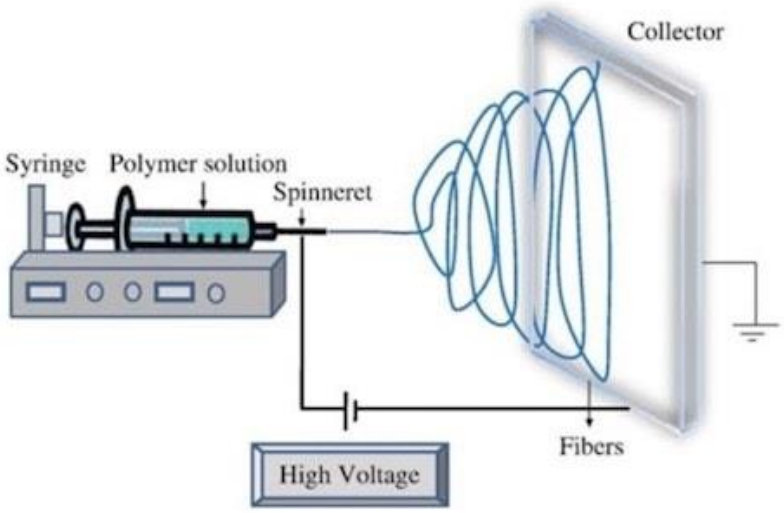

Figure 1.4.1: The Electrospinning technique[112].

At a certain distance from the needle is placed the collector. This metallic part, connected to the ground, constitutes the negative. An electrostatic field is formed in this way between the needle and the collector. When the pump is activated, a droplet appears on the tip of the needle. The electric charges, inducted by the power supply on the droplet, causes instability because the reciprocal repulsion of charges is opposed to the surface tension of the liquid. These forces elongate the droplet from the original shape to form a sort of cone named as "Taylor cone" (Fig. 1.4.2).

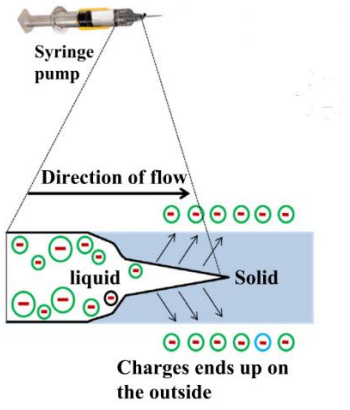

Figure 1.4.2: Taylors' cone formed on the droplet on the tip of the syringe. [113]

When the electrostatic field is high enough to overcome the surface tension, nanofibers emerges from the Taylor cone and travel toward the collector driven by the electrostatic field. The trajectory is straight in the first section but then the

internal and external charge forces cause the whipping of the path of the liquid jet. This movement causes the stretching, shrinking and elongation of the viscoelastic fibers, making them even thinner[113,114]. The whipping movement promote also the evaporation of the solvent system, solidifying the fibers before being deposited on the collector[115].

1.4.2 Working Parameters

The simple operating principle of this technique smacks against quite complex parameters tuning. The process and its outcome are in fact regulated by several factors regarding the solution, the machine setup and the environment[113]. The first ones include the raw polymer type, the solvent used, the concentration, the viscosity and the conductivity of the solution[116]. The second ones consist in the applied electrostatic field, the distance between the tip and the collector, eventually the velocity of a rotating collector, the flow rate, the needle diameter[117]. The environment parameters that must be controlled are the temperature and the relative humidity.

Speaking about the solution, the concentration plays an important role in the integrity of the polymer chains. If it is too low, the chains break before reaching the collector causing beads. If otherwise it is too high, the viscosity of the solution will increase causing a clog in the needle.[118] The conductivity of the solution impact the shape of the Taylor cone and also the diameter of the nanofibers[119 120]. This is quite self-evident thinking about the principle of the electrospinning. If the conductivity of the solution is too low, it will not react to the electric field and the cone will not be formed. A conductive solution will instead have free charges which can move inside the liquid and therefore deform the droplet to form the cone. Even the air-travel from the tip to the collector can take place only if the solution reacts enough to the electrostatic field. Speaking about the solvent, it has to be able to completely dissolve the raw polymer. It should also have a moderate boiling point because if it is too high the jet will dry up too early before leaving the tip. Otherwise, if it is too low, even the solvent will reach the collector melting the fibers that are already deposited on it originating beads[121 113].

The most important machine parameter is the voltage applied to form the electrostatic field[122]. The optimal value varies from polymer to polymer. Raising the voltage, theoretically the fiber will be stretched more before reaching the collector causing a lower fiber diameter. This is true until a critical value; exceeding it will result in the formation of beads and thicker nanofibers because of the increased jet velocity[113]. The flow rate is a critical value and should be balanced with the rate of formation of the nanofibers from the droplet. Increasing it too much will result again in the formation of beads or unspun droplets that will fall from the tip because of the gravity[123]. The correct distance from the needle to the collector must be determined in order to obtain a stable smooth and uniform flux of nanofibers. If the distance is kept to short, this will lead to defective and large-diameter nanofibers[113], or in a not complete evaporation of the solvent system.

The collector is a crucial part of the electrospinning machine. Upon it shape, position and movements, depends the morphology and alignment of the nanofibers[101]. Different collection systems are also used to obtain different architectures of nanofibers: bundles, that are groups of straight nanofibers aligned in the same direction, or yarns, that are aligned but also contain an imparted twist in order to enhance the mechanical properties[101,124]. The most basic collector consists of a metal grounded plate that draw the nanofibers toward it[125] (Fig. 1.4.1). The fibers, in this way, deposit in a random configuration on the plate surface[126]. Other techniques, involving high-speed rotating drum collectors, are mainly used to obtain stretched and aligned fibers[126]. Besides these two major categories of collectors, many different techniques had been researched to obtain fibers with a desired alignment of with better mechanical features[111,116] (Fig. 1.4.3). Theron et al[127] and Xu et al.[128] proposed a rotating disk collector with a tapered edge in order to obtain aligned nanofibers due to the high velocity of the disk. The drawbacks are that the length of the fibers is limited and necking was observed[101]. Dalton et al.[129] used grounded parallel annular collectors in the path of the jet with one of them rotating in order to produce yarns (twisted fibers) of up to 50mm length. Teo and Ramakrishna[111] proposed two negatively charged steel blades perpendicular to the direction of the jet to obtain highly aligned fibers. The methods above are only able to obtain short bundles or yarns. Other methods were proposed with the aim to

produce continuous fibers. For example, Khil et al.[130] and Smit et al.[131] directed the jet inside a water bath with a grounded electrode and collected the continuous yarn with a take-up roller. Teo et al.[132] also directed the jet into the water but they then collected the yarn from a hole on the base of the water collector. Wang et al.[90] reported a method to directly collect continuous bundle in the air by placing a rotating drum at a set distance. The speed of rotation must be investigated to match the production and the collection rate.

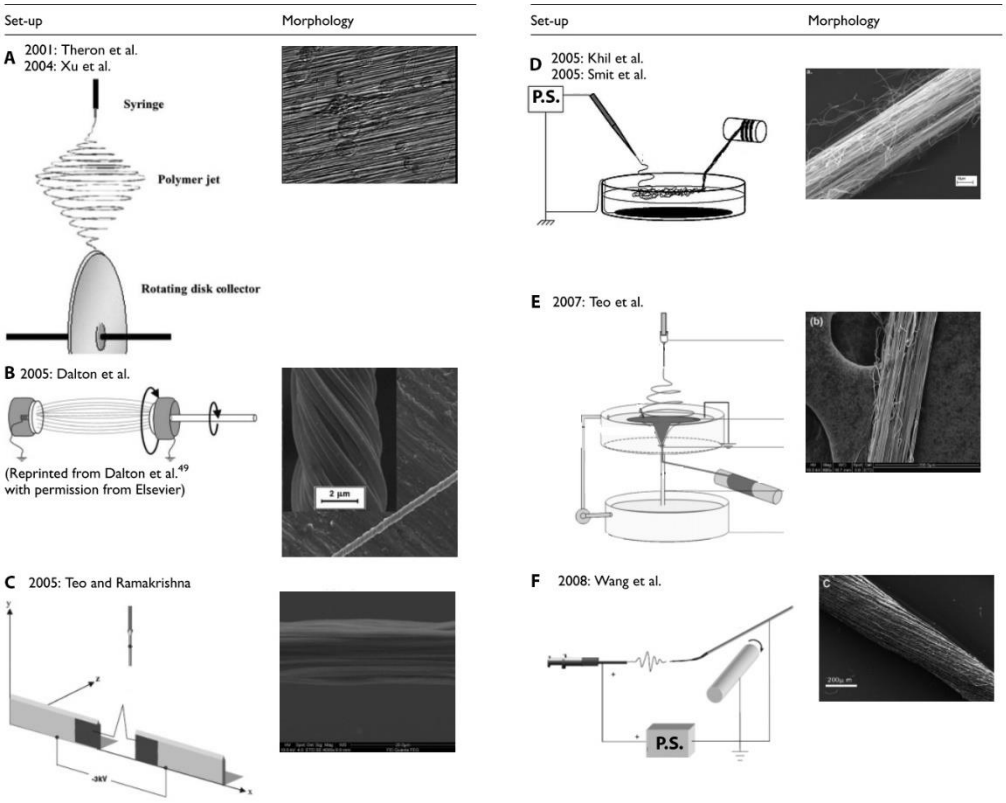

Figure 1.4.3: Several collector types for electrospinning. Modified from O'Connor et al.[101]

Lastly, the environmental parameters act an important role on the outcome of electrospinning. Relative humidity is recommended to be under 35%[93]: if it is too high it will often lead to beaded fibers or impair the electrospinning at all[113]. The solidification process of the fiber in the jet also depends on the humidity of the air. Temperature can change the rate of evaporation of the solvent and therefore even change the viscosity of the solution before the spinning process. If it is increased, this will lead to a decrease in the diameters of fibers for both these causes[113].

1.4.3 Electrospinning in tendon and ligament tissue replacement

At the present day, many researches are currently being carried out on synthetic and resorbable scaffolds for tendons and ligaments, but very few animal trials had been evaluated. To improve the mechanical properties and the biocompatibility, in the last years the research on scaffolds focused its attention on the electrospinning technique[97]. Electrospun scaffolds have a surface area to volume ratio higher than with other production methods[98,101,133]. This is crucial to obtain a better cell penetration and proliferation in the scaffold[111,128]. The alignment and the dimension of the electrospun fibers can also be tuned to mimic as much as possible the ones of the extracellular matrix. This will also enhance the mechanical properties of the scaffolds with fibers aligned to the load. With this production method, many attempts have been made[92,93,97,102,108], trying to reproduce every part of a tendon/ligament. Fibers and fascicles are the starting low level structures that had been investigated[101] aiming to mimic their characteristics and mechanical behaviour[94,134–144]. Tendon/ligament-to-bone insertion site were also investigated due to their particular composition[107,145,146]. Upper level structures like multiscale tendons had been later investigated[147–149], trying also to mimic the tendon/ligament sheath[91,150].

This technique permits the production of nanofibers from a wide range of polymers, both synthetic and biological[151]. One common problem of electrospun proteins like collagen and elastin is the loss of these molecules after ageing in physiological environment[138]. Recently Sensini et al.[94] aimed to the production of an electrospun scaffold for the human Achilles tendon two different blends of PLLA and Collagen (75-25 and 50-50) were cross linked *ad hoc* to both reduce the collagen early loss and increase the mechanical properties before seeding them with human tenocytes.

1.5: Developments and applications: soft-robotics – an overview

1.5.1: Soft Robots: actuation modes and prototypes

In this chapter, Soft Robotic will be discussed. This can be considered a newly born field that can be a promising alternative way of use of synthetic tendons. This area of research is in continuous growth and relies on the development of robotic devices mimicking the mechanisms of movement and locomotion of soft bodied animals found in nature[152]. Classic robots, have structures made of stiff materials such as steel, aluminium, titanium or alloys, hard polymers connected with rigid links and operated by numerical control machines (CNC) and motors. They have the advantages of being very precise, fast and powerful when used in their specific field, but lack adaptability when the environment of work is not well known[153]. In soft-robotic, robots differ in many features compared to the conventional ones because they are designed using soft materials, in order to mimic the living beings, we find in nature. To allow movements, negative pressures systems, chemical reactions or advanced polymers, substitute the classical motors. For example, when considering animals with a structural skeleton, this rigid component is almost never directly exposed to the environment. As a matter of fact, the soft tissue which covers it constitutes the majority of body mass. Indeed, only 11% of the weight of an adult human male is made by the skeleton, whereas more than 42 % is soft tissues[152].
Just like living being's evolutionary curve adapted to their complex and unpredictable environment, the same rule applied to soft robotics. Indeed, an important principle for soft robotic is compliance matching; as proposed by a perspective from Majidi[154], compliance matching "*is the principle that materials that come into contact with each other should share similar mechanical rigidity in order to evenly distribute internal load and minimize interfacial stress concentrations*". Soft robots are usually made of materials with a Young's modulus ranging from 10^4 to 10^9 MPa[153], contrarily to conventional ones characterized by a modulus over 10^{10} MPa[154]. This leads to the ability to safely interact with humans and the environment and to prevent or absorb collisions even if unable to precisely detect the position of their target. They are deformable and soft but with an adaptable shape, which is a keystone in the scalability of their use. However, their

soft structure also represents a disadvantage; as a matter of fact, this implies an inability to produce high forces and makes them harder to be controlled[153].
In this section, a first overview on the actuation and transmission modes of soft robots will be discussed. A brief on the prototypes of soft robots will follow.
The kind of actuation is possibly the most important feature as it is very challenging to produce localized forces without being able to use rigid parts like, for example, an electric motor.

One of these actuation systems is obtained using **SMAs (Shape Memory Alloys)**, a particular type of alloys which can change shape when warmed through an electric current. When the stimulus is removed, they revert to their original shape. These have many advantages like having a high force-weight ratio, a high resistance to fatigue and they can also be used as sensors. The drawbacks are the high currents needed and a marked hysteresis[155]. An example of a SMA coil is shown in (Fig. 1.5.1 B)

Another actuation system is based on **SMPs (Shape Memory Polymers)** which have the same functioning of SMAs but can be triggered by different types of stimuli: chemical, electric, thermic, light or magnetic. Their advantages are being flexible and often biocompatible.

Electro Active Polymers (EAPs) can also be used as they exhibit a change in shape or size in response to an electric field. They can be used both as actuators of sensors. Being able to undergo a large amount of deformation while sustaining large forces, EAPs are an interesting way to mimic biological muscles; in fact, they have even higher power density. The drawbacks of these materials are the slow response time and, once again, the high currents needed for them to work[156 153].

One of the simplest ways to actuate soft robots are **hydraulic** or **pneumatic** systems, which are based on the introduction of liquids or air inside expansion chambers embedded in the structure so that these parts will show different stiffness; in this way it can be produced a change in the shape and/or a folding.
Bearing in mind that this work is focused on tendons, which transfer the force made by actuators (muscles), it will be investigated a particular actuation system of soft robotics in which the forces are **cable-driven** in a similar way. This technique is usually chosen to design hybrid soft robots, which are made of soft components and

are often actuated by rigid motors. With cables it can be detached, even with a long range, the motor from the actuation target site (like with fingers and corresponding muscles in the forearm). Many problems could be overcome this way; for example, the weight and the volume can be lowered leading to less inertia and, accordingly, a faster movement response[157]. On the other hand, the main drawback is that it is very challenging to minimise or eliminate all backlashes, leading to potential instability.

Firstly, it will now be overviewed the soft robots that were designed as prototypes in order to investigate materials and locomotion strategies rather than being made for a specific use. They are all inspired by different soft animals.

The first prototypes involve **worm-like** robot, based on the principle that worms are fixed-volume hydrostats and their locomotion is achieved by the contraction of the longitudinal muscles: this will shorten their body and at the same time increases its diameter; conversely contracting the circumferential muscles they decrease the diameter therefore elongating the body. One example is the Meshworm[158], it uses SMA like actuators. This robot can steer using longitudinal SMA coil muscles in place of the tendons (Fig. 1.5.1 A).

Octopus-like robots are based on the movement techniques of ones of the most complex and evolved soft-bodied animals: the cephalopod. They have the ability to completely modify their shape to pass through tiny holes or cracks. The manipulators inspired by these animals were developed on the concept of compartmentalized deformations used to produce locomotion. They can be actuated by pneumatic muscles[159] or, alternatively[160], SMA springs are considered; these can be arranged both transversely and longitudinally to produce local deformation, and cables are employed to obtain the global bending, like tendons. These are surrounded by a plastic fiber braid (Fig. 1.5.1 B).

Caterpillar-like robots differ from worms because they have a totally different muscular system and imply different locomotion strategies. They only exhibit longitudinal and oblique muscles used to locally increase or decrease the body stiffness. The same principle is mimicked by the GoQbot[161] (Fig. 1.5.1 C), made of silicone rubber and capable to flex ventrally thanks to two tensile SMA coils which can separately control the anterior or posterior flexion. When this

motion is executed quickly enough it can produce a ballistic rolling locomotion up to 2 m/s for a 10-cm long robot.

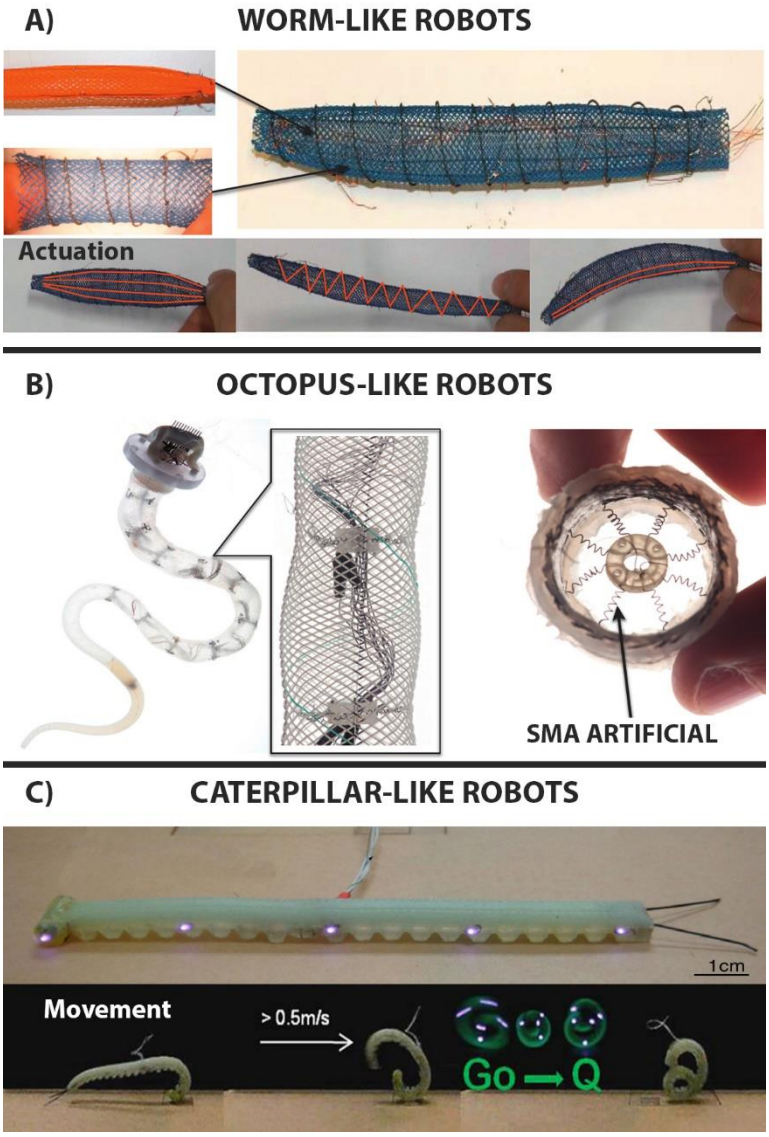

Figure 1.5.1: Animal-inspired soft robots. A) Meshworm: structure and actuation modes[152]*. B)Octopus-like robot. mechanical structure of the arm, allowing for local and global deformations while keeping the arm shape. Focus on the SMAs radial muscles which causes radial restriction*[152]*. C)GoQBot. It has a composite body consisting of several mixtures of silicone. GoQbot simulating a ballistic rolling. The name "Go Q" is due to its shape assumed during the movement* [161]

These examples were developed to propose a different interaction of rigid robots with a partially known environment. In fact, some of the characteristics of these robots such as the locomotion system, the actuators, the compliance materials

etc. are considered attractive by many fields of research. One of this is, of course, the biomedical field. It can be imagined miniaturized robots for body exploration, drug delivery, minimal invasive surgery, soft wearable robots or prosthesis (like manipulators for hand replacement).

1.5.2: Soft exoskeletons and prosthesis

Inspired from the soft robot prototypes presented above, the development of some soft exoskeletons has begun with a possible large impact on movement rehabilitation. This strategy has been successfully employed in the construction of many wearable soft robots in which the function of the rigid frame, showed in the conventional robots, is carried out by the natural skeleton. In literature these devices are often referred to as soft exoskeletons, soft wearable robots, exosuits, exotendons etc. and, in the vast majority of cases, they are actuated with a cable-driven system. In the following part some examples of these devices are presented, focusing on their design.

BiomHED (Biomimetic Hand Exotendon Device[162]) is proposed to assist stroke survivors in which significant upper extremity impairment is prevalent[163]. The goal of this exoskeleton designed by Lee et al. is to help patients in producing complex, task-oriented hand gestures with high intensity, since it has been shown that this leads to maximized outcomes in stroke rehabilitation[162]. The main problem is that survivors often have uncontrolled spasticity and weakness with a typical clenched-hand posture. This point is where the BiomHED helps patients, trying to assist their movements reflecting the dynamic functions of the impaired hand. As previously mentioned, this is a cable driven soft exoskeleton that is worn as a glove. The actuation is achieved by DC motors placed on the forearm and the force is transferred by "exotendons": stainless steel cables (SAVA 1024[164]), four for each finger, that mimic the geometry of the four main natural finger muscle-tendon units (Fig. 1.5.2).

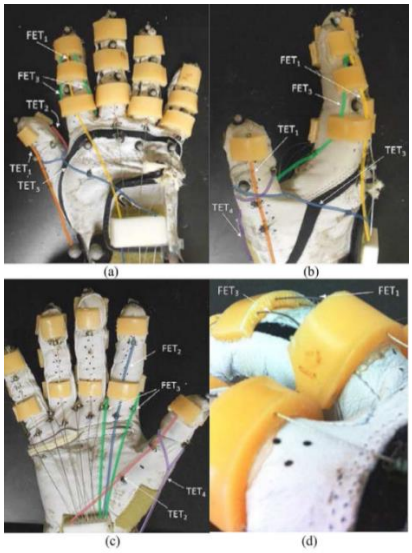

Figure 1.5.2: Exotendon configuration of the BiomHED: (a) dorsal view, (b) radial view, (c) palmar view, and (d)magnified view of the dorsal thermoplastic guides that route exotendons (FET=Finger ExoTendon; TET=Thumb ExoTendon)[162].

Exosuit (Fig. 1.5.3) is a novel soft-cable-driven device proposed by Asbeck et al.[165] [166]whose goal is to assist walking. It is worn like clothing and can generate moments at the ankle and the hip in the order of 18% to 30% of the corresponding natural ones produced during a walk. Even this device lacks rigid parts, and this leads to a minimization of its weight as it uses the natural skeleton as a frame. Indeed, a soft device pretending to actuate forces on the body presents challenges, because the body is compliant and cannot stand high pressures in a comfortable way.

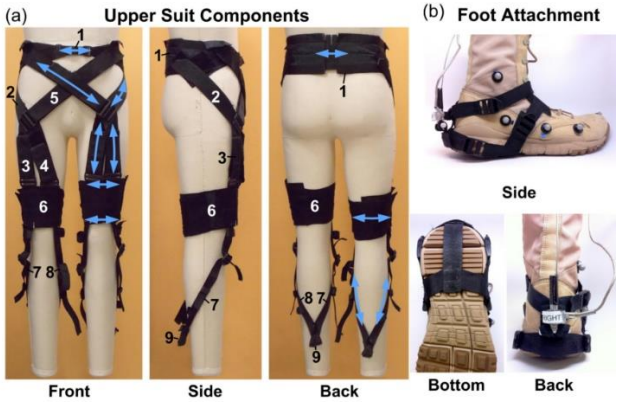

Figure 1.5.3: (a) Views of the upper suit with components labelled. Arrows indicate places where it can be adjusted to fit different sizes of individual. (b) Views of the foot attachment[165]

It attaches around the waist and above the knee. The actuation is applied by a motor located in a backpack with electronics and batteries, making it a portable device. The force is transferred to the back of the calf and the waist through webbing straps. Again, from the back of the calf, a Bowden cable starts extending downwards to another webbing strap placed on the back of the heel. A key feature of this device is that the forces generated are both active and passive; the active ones by the motor and the Bowden cable and the passive ones by the natural kinematics of walking through the elastic straps. From the work of Asbeck the material which is made the cable by is not known.

Exoglove (Fig. 1.5.4), proposed by Hyunki In et al.[167] [168] , is another device based on the structure of a human hand. Its design consists of two tendons for each finger and for the thumb, fixed in position with fabric straps that act as pulleys. The straps length and position can be adjusted but they are inextensible in order to maintain the moment arms of the tendons. The cables run inside Teflon tubes to minimize the friction. Even in this case the actuation is obtained with a motor placed far, reducing the weight to 194g and the consequent inertia. The results presented by this work, conducted on a healthy subject, showed a pinch force of 20N and a wrap grasp force of 40N during daily life tasks. The glove could also grasp objects with a maximum size of 76mm. The authors propose this device for people incapable of opening or closing their hands but who are still able to use upper limb joints like shoulders, elbows and wrists. It is also proposed to assist individuals with medium to low finger spasticity, only if the degree of spasticity is the same for all fingers.

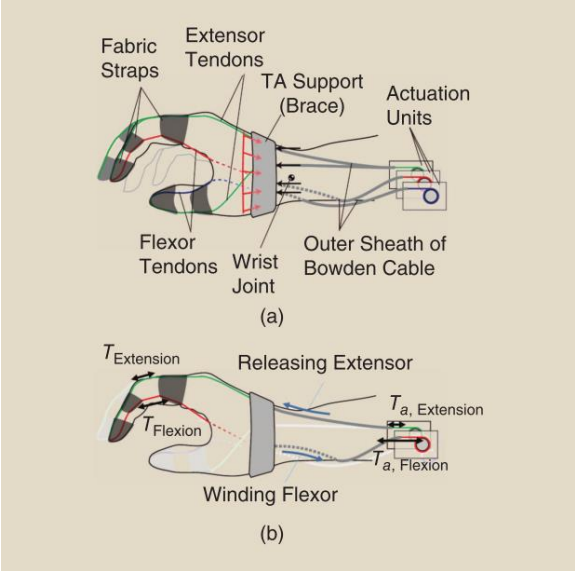

Figure 1.5.4: Exoglove schematics. The dotted lines indicate the sections of tendons and Bowden cables that lie on the far side of the hand. (a) Black arrows indicate the force exerted on the TA (Tendon anchoring) support by the Bowden cables, red arrows indicate the distributed force exerted on the TA support by the hand. (b) While the tendon moves toward the joint, the tension applied to the joint is greater than the tension at the actuator.[167]

Current literature suggests several works which are similar to the above-mentioned examples in that they involve a wearable soft glove which aims at assisting the impaired hand[153]. The designs are macroscopically similar as they involve detached motors with Bowden cables connected to the fingers with a soft glove. The cables are mostly made of stainless steel[162,165,167], which is a very strong material that exhibits an almost linear behaviour in the range corresponding to the tensions sustained by a tendon; this is quite different from the behaviour of the natural counterpart, lacking the typical toe-region due to the fibers which not yet totally aligned. One exception is the soft robotic glove proposed by Nycz et al.[169] in which they use dyneema cables for the actuation. This commercial fiber is made from Ultra High Molecular Weigh Polyethylene[170] and, as declared by the manufacturers, "*is produced in a patented gel spinning process in which the fibres are drawn, heated, elongated, and cooled. Stretching and spinning leads to molecular alignment, high crystallization, and low density*." However, it can be

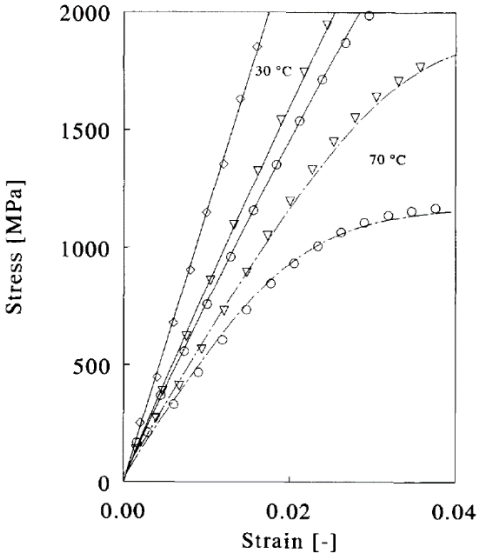

Figure 1.5.5: Dyneema constant-strain-rate experiments at various temperatures and strain rates of 10-4 s-1(O), 10-3s-1 (◊) and 10s-1 (▽), compared with model predictions (curves).[171]

seen in (Fig. 1.5.5) that these fibers present a much stronger and rigid behaviour than a natural tendon[171]. Furthermore, from this graph the large difference in terms of elastic modulus from natural human tendon to dyneema fibers is quite noticeable. The former has a modulus ranging from tens to hundreds of MPa[172], conversely the latter which ranges from 50 to 100 GPa at different temperatures and speeds. For the above-mentioned reason, it will be taken into account another work that goes beyond the strict definition of "soft-robotic" since it can be seen as the use of soft material in a rigid robotic environment. **The Anatomically Correct Testbed (ACT) Hand**[173] is a robotic device that tries to mimic the mechanisms and controls of the human hand with a design as close as possible to the biological one, including bone structures and tendon arrangements[174]. Xu et al.[175] proposed as a refinement of the ACT Hand (Fig. 1.5.6). This device is focused on replicating the main features of the biological ligaments and tendons using artificial materials. The aim is to replicate the extensor hood, a collagen-based structure composed of ligaments and tendons located on the dorsal side of each fingers bone. It is a connective attachment by which the extensor tendon inserts into the phalanges. For this reason, it is a key element to allow hand motion. The authors propose a crochet technique with a 0.46mm *Spectra fiber* to achieve complex shapes, controlled fiber orientation, integrity and strength. In (Fig. 1.5.7) the results of mechanical tests on specimens, which differ from each other by the crochet technique, are shown.

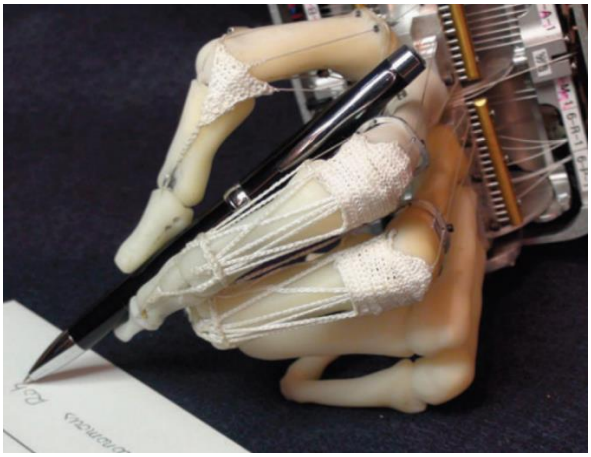

Figure 1.5.6: Crocheted extensor hood implemented in the Anatomically Corrected Testbed Hand (ACT) Hand[175]

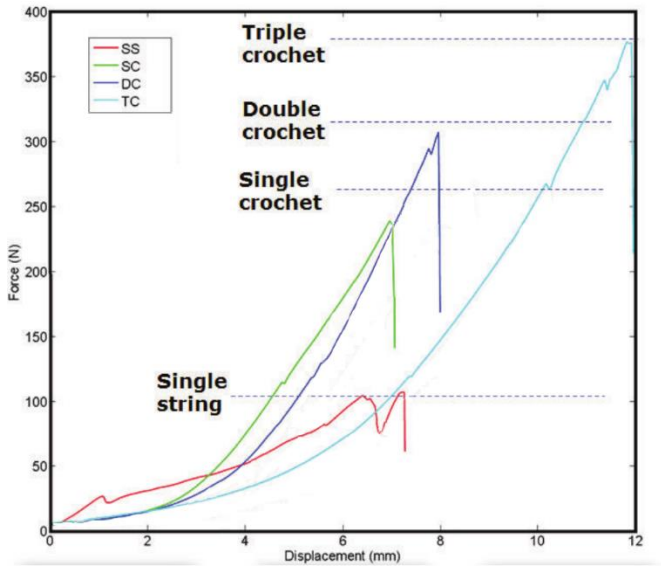

Figure 1.5.7: Typical load-displacement curves from crocheted specimens. Note: Dashed lines indicate the corresponding breaking forces (adapted form Xu et al.)[175]

Although from the graph above the stress-strain characteristics of the extensor cannot be obtained, there is an evidence of the typical nonlinear toe-region followed by a mostly linear curve. Although this behaviour is probably due to the stretching of the crocheted mesh rather than the material itself, it is still interesting to see how, in this field, efforts are made to make transmission devices that better mimic the biological counterpart.

Another attempt to overcome the problem of a lack of nonlinear regions was done by Bundhoo et al[176] in a paper proposing a SMA-based **tendon-driven actuation system** for artificial fingers (Fig. 1.5.8). This device consists in a system for wearable robotic hand applications which contains a combination of tendon cables, springs and SMA wires to form an agonist-antagonist artificial finger muscle. SMAs are a typical choice in the soft robotic field, usually because in these contexts they eliminate the need for complex transmissions devices, they can operate silently and are quite lightweight. However, cons like limited life cycles, hysteretic behaviour and low actuation strains should be considered[177]. The contribution of this paper consists in the addition of a compliance element (a tendon with a spring-slack part) to each SMA muscle wires. This allows the formation of agonist-antagonist artificial muscle pairs for the actuation of the flexion/extension and abduction/adduction of the metacarpophalangeal (MCP) joint and the flexion/extension of the proximal interphalangeal (PIP) joint for the artificial finger[177].

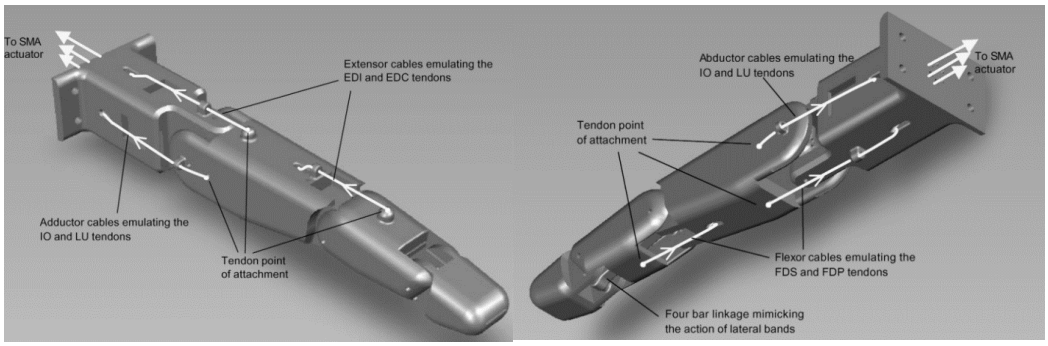

Figure 1.5.8: (a) Extensor and adductor tendon cable configuration. (b) Flexor and abductor tendon cable configuration.[176]

The spring-biased SMA mechanism consists in a spring opposed to the contraction of the SMA element; once the latter is activated it heats up shortening itself and accordingly elongating the spring; then, when deactivated, the spring helps the SMA wire (which is cooling and elongating) to return to the original length. Moreover, each spring is added in parallel to a slack portion of the corresponding tendon (Fig. 1.5.9) to introduce the nonlinear stiffness: the "first stiffness" corresponds to the modulus of the spring, then, when the tendon is taut, the stiffness

increases to tend to infinity. This is another way of mimicking the toe-region of a tendon in order to introduce a certain compliance that is a necessary element in soft robotics, as mentioned above.

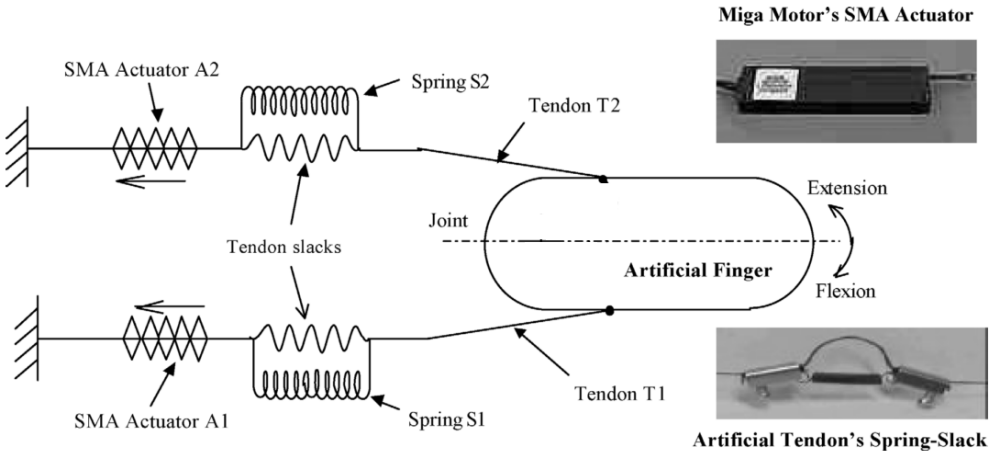

Figure 1.5.9: Differential spring-biased SMA joint actuation mechanism. The insets show the actual SMA actuator and spring-slack element implemented.(Adapted by Bundhoo et al.)[176]

Another type of soft actuation under investigation is the use of nylon6.6 artificial muscles[178] (Fig. 1.5.10). In this work a 3D printed human hand is actuated by a twisted and coiled nylon cable. In a paper from the same research group[179] Haines et al. introduced this type of muscle (TCP) made of polymer fibers used for fishing line; it was also demonstrated that these fibers contract in response to thermal o electrothermal stimuli[179]. The advantages are many, the stroke of the muscle can be adjusted setting the spring index of the twisted nylon fiber, it works silently and shows minimal or no hysteresis compared to SMA muscles. Furthermore, it is significantly cheaper than SMAs. The hand developed in this paper is five-fingered and electro-thermally powered by TCP muscles. The efficiency of this muscle was reported as 1.08%, this low value can be mitigated using a locking device which can hold the load without power consumption.

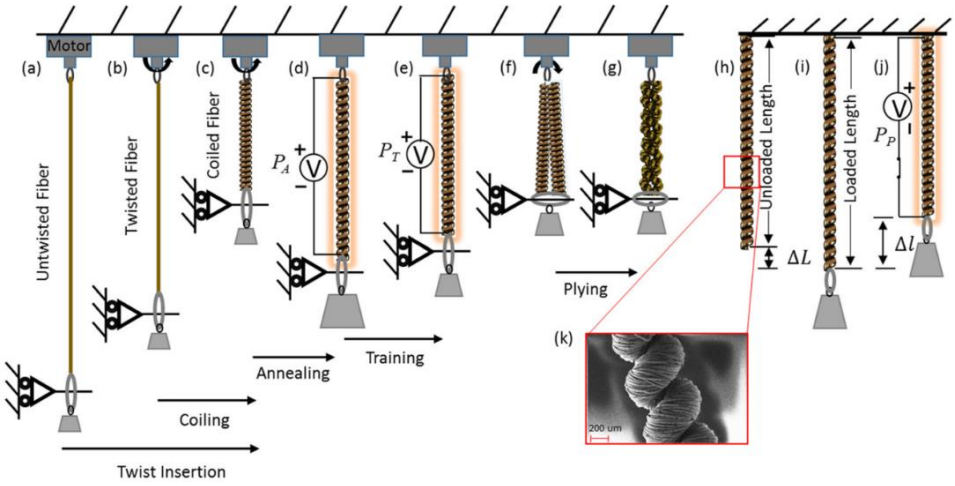

Figure 1.5.10: TCP Nylon muscle fabrication process. Description below.[178]

This process is divided in two main steps: the first one is Twist insertion and coiling, the second one is Annealing and Training. First of all, the top end of the precursor fiber is attached to a motor and a weight is suspended at the bottom to keep the precursor fiber straight (a). By rotating the motor, the fiber is twisted (b). A 1-ply twisted TCP muscle is obtained (c). Annealing via electro-thermal heating applies power P_a to the ends (d). The muscle is then trained again by electro-thermal heating with power P_t (e). These processes are needed to obtain the reversibility of actuation of the muscle and a good intercoil spacing. Then a 2-ply muscle is obtained plying two 1-ply muscles together (f). At the end the muscle has an unloaded length L (h); applying the load it will elongate of a ΔL (i). At the end the muscle is tested applying a power Pp to the ends, showing the contraction of Δl (j). In (k) a scanning electron microscope image if a 1-ply muscle is shown. Apart from the benefits of using TCP muscles as actuations, the two main problems appear to be the response speed of the force when the thermal heating is applied, and the maximum force obtained. In this paper the first experiment on the robotic hand was done with a heating time of 25s and a cooling time of 45s for the actuation of the muscles. Then they managed to reduce this time to 1 second to achieve fast finger motion using short pulse with high electrical power (another problem). Focusing on the maximum force, it was showed that the peak value of 0.93N was obtained with a pulse power of 2.24 $\frac{W}{cm^{-1}}$. It is enough for some grasping tasks of lightweight objects but still not suitable for the daily use of a prosthesis.

1.6: *In vitro* tendon and ligament simulators

Educators today are looking for tools able to simulate the most varied anatomical structures. This is well represented, for example, by the use of SAWBONES®. This brand design, produces and distributes, in particular composite bones for mechanical simulations, *in vitro* testing of orthopaedic devices and investigation and validation of new surgical techniques. However, nowadays only few devices are available to simulate tendons and ligaments tissues. Despite the use of the classical animal models[180] (with their intrinsic problems of conservation, reproducibility and loss of mechanical properties and morphology over time), some synthetic solutions were proposed. SAWBONES® itself proposes both a surgical simulator for tendon and ligaments sutures (Fig. 1.6.1 A) and some models of different tendons and ligaments (Fig. 1.6.1 B, C). The former is a rope-like structure, the latter are usually made of simple flexible plastic.

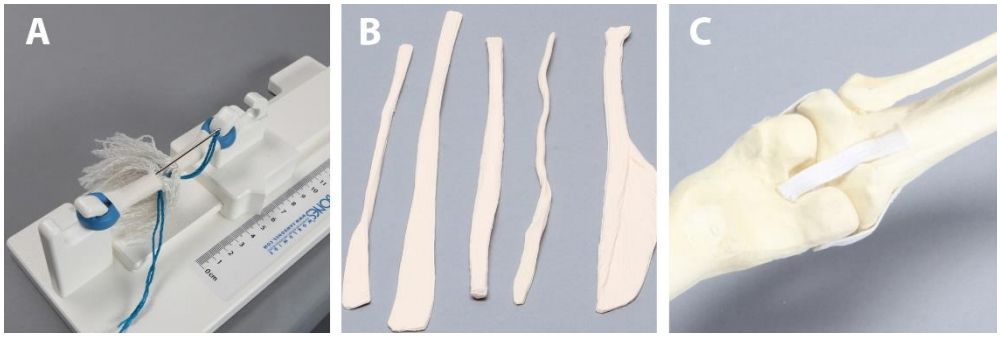

Figure 1.6.1: SAWBONES® products. A) Achilles tendon surgical suturing simulator. B) Various types of tendons. C) Knee ligaments

Some works focused on tendon and ligament surgical sutures simulation tools. Ingraham et al[181]. proposed a rubber, worm-like fishing bait (Fig. 1.6.2 A). Tare[182] et al., instead, proposed the use of compact cotton dental rolls (Fig. 1.6.2 B).

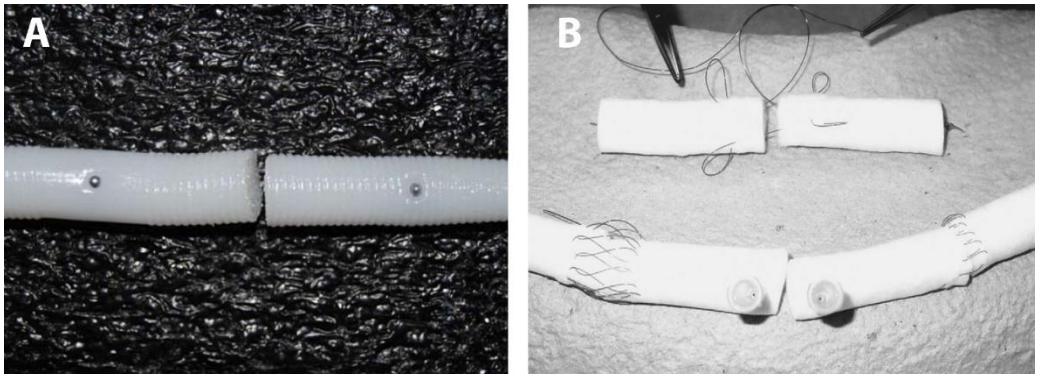

Figure 1.6.2:Synthetic simulation tools. A) Worm-like fishing bait. B) Cotton dental rolls

2: AIMS

The aim of this work is to investigate the possibility to produce a biostable multiscale nylon 6.6 structure, able to mimic the hierarchical structure and the biomechanical properties of tendons and ligaments. The electrospinning technique was chosen as the production method, because of its ability to produce nanofibers with tuneable alignment, with the diameter in the same order of magnitude of the collagen fibrils of tendons and ligaments.

The initial purpose was to produce electrospun bundles using and modifying already investigated techniques[139,147,183]. These bundles were produced to mimic the morphology and mechanical properties of collagen fascicles.

The following aim was to assemble these bundles together through an electrospun randomly oriented nylon 6.6 sheath, produced to pack and narrow the bundles together, mimicking the role of the epitenon/epiligament sheath.

The bundles and the multiscale nylon 6.6 device were morphologically investigated using a scanning electron microscope and an optical microscope.

Ad hoc setups were developed to investigate the mechanical properties of the bundles and the complete multiscale nylon 6.6 device.

NOTE:

According to the Knowledge Transfer Office of Alma Mater Studiorum - Università di Bologna, some images (marked with an asterisk *) in the present thesis will be partially censored to protect some technological innovations under patent.

3: MATERIALS AND METHODS

In this section the experimental workflow of this thesis will be explained. At first, the materials adopted will be listed. Then, the methods used to produce each part of the multiscale scaffold, and the *ad-hoc* setups developed to test them, will be reported. Finally, the chosen procedures to morphologically and mechanically characterize these structures will be explained.

3.1: **Materials**

In order to produce both the electrospun bundles and the multiscale device sheath, a polymeric solution of Poly[imino (1,6 - dioxohexamethylene) iminohexamethylene] was used, trademark name and composition "Zytel Nylon Resin", (Nylon 6.6), purchased by DuPont (Wilmington, Delaware, USA).
The solvents used were Trifluoroacetic acid (TFA), chemical formula CF_3CO_2H, produced by Carlo Erba Reagents S.r.l. (Cornaredo, Milan, Italy) and Acetone (AC), chemical formula $(CH_3)_2CO$ purchased from Sigma Aldrich (Saint Louis, USA).
The electrospun specimens were produced by the following polymeric solution:

13% (weight/volume) of Nylon 6.6 solved in a specific volume (mL) of TFA/AC 50/50 (volume/volume)

For the hydration of the specimens before the mechanical tests, so appointed 'wet' bundles and multiscale nylon 6.6 device were hydrated in a saline solution (NaCl 0.9%) purchased by Carlo Erba Reagents S.r.l. (Cornaredo, Milan, Italy).

3.2: **Production of electrospun nylon 6.6 bundles and ring bundles**

In order to mimic the tendon/ligament fibrils and fascicles, electrospun bundles already investigated (Sensini et al. Journal Microscopy[134]) and new prototypes were produced. The nylon 6.6 solution was firstly prepared by mixing trifluoroacetic acid and acetone in equal volumes, stirring it until the temperature dropped to room temperature (because of the exothermic reaction) and then adding nylon pellets. The solution was then stirred again at 45-50 °C to properly dissolve the pellets for a time depending to the volume of the solution.

The electrospinning system (Fig. 3.2.2) used consists in:

- Custom made electrospinning machine "Lab Unit" (Fig. 3.2.1) designed by Alma Mater Studiorum – University of Bologna and distributed by Spinbow (Bologna, Italy).
- Syringe pump (KDScientific 200 series (Holliston, USA)
- 4x5ml glass syringes Fortuna Optima purchased by Sigma Aldrich (Saint Louis, USA) loaded with the polymeric solution
- 4 teflon tubes and connectors Bola (Grunsfeld, Germany)
- 4 stainless steel needles branded Hamilton (Reno, USA) with an internal diameter of d=0.84mm

Figure 3.2.1: Lab Unit

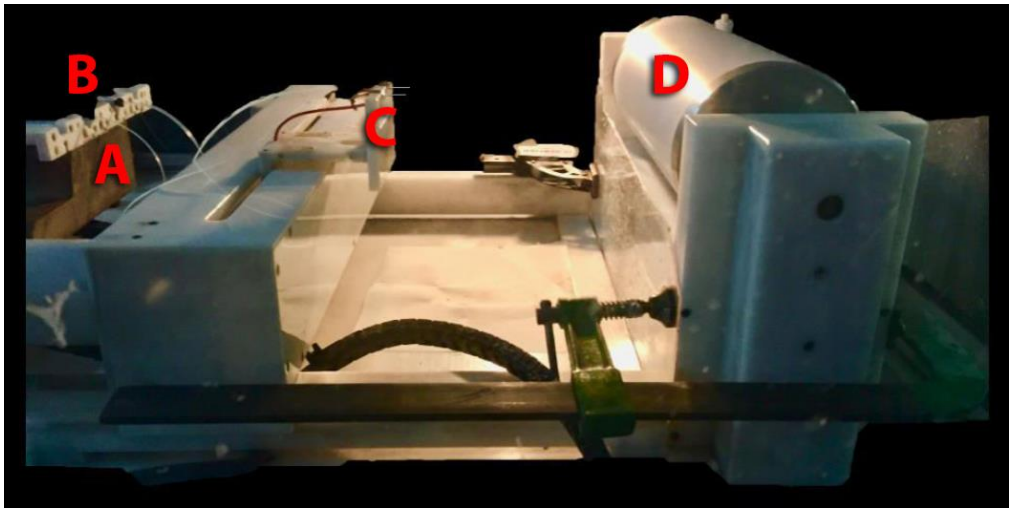

Figure 3.2.2: Electrospinning system

The syringes loaded with the polymeric solution were loaded onto the pump (A) and connected via Teflon tubes (B) to the needles rack placed onto the moving tower (C). This tower strafes back and forth to do a more even distribution of the jet on the collector. The needles are connected to the positive. At a certain distance the collector (D) is placed, meaning a rotating drum collector of 150mm of diameter. In order to obtain aligned nanofibers, the drum collector was rotated at high-speed.

The parameters used for the spinning were:

- Needle-Collector distance = 160mm
- Voltage = 20kV
- Drum rotating speed = 2900 rpm
- Tower speed = 1500 mm/min
- Tower limits: left=140mm – Right=240mm
- Pump syringe flow rate = 0.5 ml/h
- Electrospinning time = 180 min
- Room temperature and humidity

In order to easily retrieve the fibers without ruining the drum surface, the collector was covered with polyethylene-paper fixed with double-sided tape taking care not

to overlap it. Then, once the machine was activated, the collector was set in rotation before starting the syringe pump.

Once the process was finished the collector was covered with a layer of nanofibers. This mat was cut with a cutter into circumferential stripes of 50mm width; each stripe was then rolled up into a bundle by hand (Fig. 3.2.3), using gloves to improve the grip (and for safety reasons). In this way seven bundles were obtained for each electrospinning session.

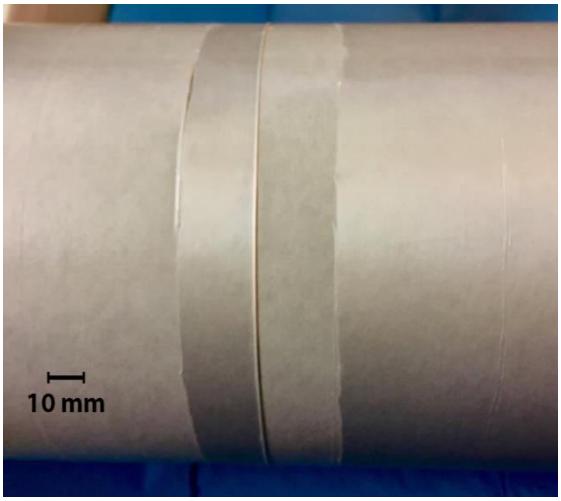

Figure 3.2.3: A bundle rolled by hand

In order to put the bundles off from the drum, in the first three processes the bundles were cut (Fig. 3.2.4 A). In another configuration, bundles were slit on one side of the collector in which the axis of the drum was freed making it possible to take off the intact "ring" bundles (Fig. 3.2.4 B).

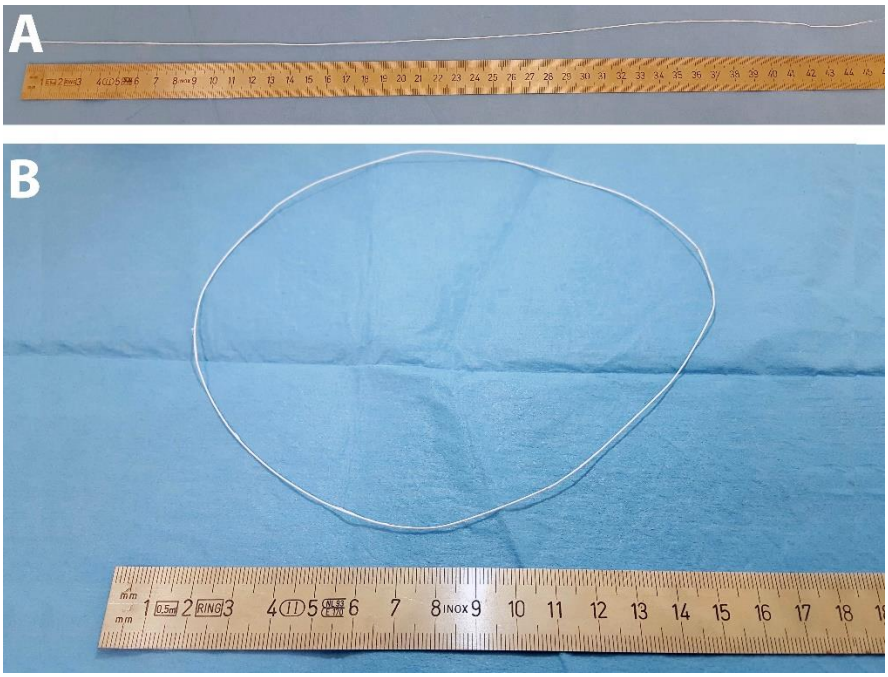

Figure 3.2.4: A) Single bundle. B) Ring bundle

3.3: **Production of the multiscale nylon 6.6 device and sheath**

In order to produce the multiscale nylon 6.6 device and a random electrospun epitenon/epiligament like sheath, the same Nylon 6.6 solution and custom-made electrospinning system were used, specifically:

- Custom made stainless steel capstan grips were used to assemble the ring bundles together which used also as additional collectors.
- Motorized device for the rotation of the bundles custom made by Alma Mater Studiorum – University of Bologna and modified for this work
- 30kV power supply model Fug DC HCP 35-35000 (Schechen, Germany)
- Syringe pump KDScientific Legato 110 (Holliston, USA)
- Syringe pump New Era Pump System NE-300 (Farmingdale, USA)
- 2x5ml glass syringes Fortuna Optima purchased by Sigma Aldrich (Saint Louis, USA) loaded with the polymeric solution
- 2 Teflon tubes and connectors Bola (Grunsfeld, Germany)
- 2 stainless steel needles branded Hamilton (Reno, USA) with an internal diameter of d=0.84mm
- Containment case with air extraction system

24 “ring” bundles (4x6 arms of the grips) were assembled on the custom grips and then placed in the rotating support of the device (Fig. 3.3.1). The bundles have a circular shape that permits to simply hook them to the grips.

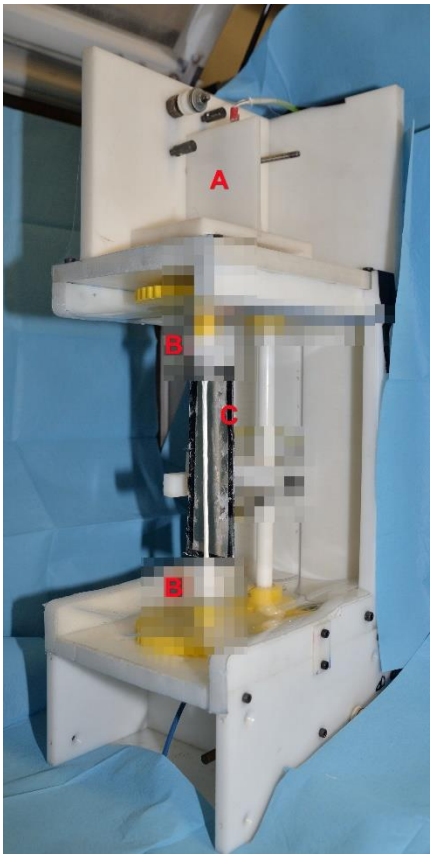

Figure 3.3.1: Rotating machine for the production of multiscale nylon 6.6 device sheath. This machine has a motor (A – not visible) that can rotate both clockwise and counter clockwise at different speeds, set by a potentiometer. The two grips (B) are connected by gears, so they rotate in the same direction at the same speed. This was done in order to avoid any torque of the specimen. The ground collector consists in an aluminium plate (C) placed behind the bundles (and also the grips), attached on a positioner with 3 degrees of freedom.*

The entire system is shown in (Fig. 3.3.2). The syringes, loaded with the same polymeric solution used for the bundles production, were placed onto the two syringe pumps(D). Two Teflon tubes connect them to the needles placed into a Delrin rack adjustable in height (E – and focused in Fig. 3.3.3). Here the needles were connected via a copper cable to the high-tension clamp. The tower with the needles rack (F) could be narrowed and aligned at will to the rotating machine (G).

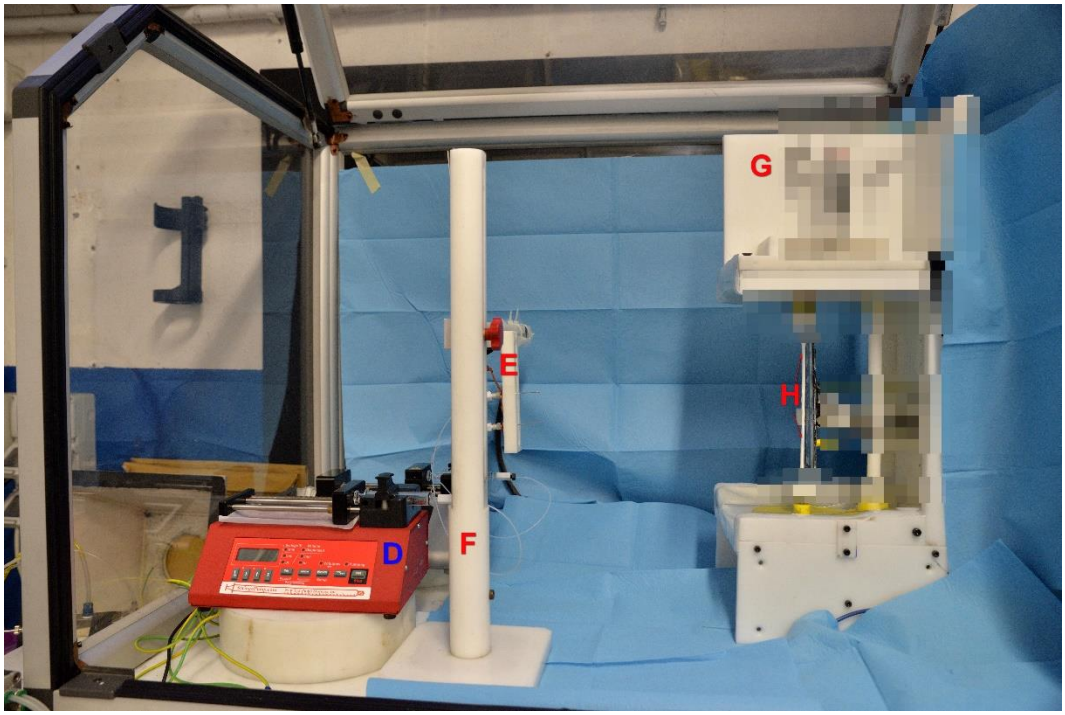

Figure 3.3.2: Electrospinning system for multiscale nylon 6.6 device sheath*

When the process was activated the solution was ejected by the pumps on the tip of the needles. The electrostatic field between the needles and the collector permitted the spinning of the fibers through a jet stream; the nanofibers then reached the collector plate. In front of the collector they encounter the bundles (H); in this way the fibers were deposited randomly on both the bundles and the plate, forming a mat. When the rotation of the bundles was activated, the mat fixed onto the bundles rolled itself dragging the part of mat deposited on the plate until it teared up. The torque generated by this rotation permitted the tight winding of the fibers around the group of bundles. Once the mat was broken it was necessary to wait a variable amount of time to permit the reformation of the electrospun membrane. The process was then repeated until a desirable thickness of the sheath was achieved. The electrospinning from a needle produced a gaussian-like distribution of the nanofibers along the length of the bundles centred about in the middle of the plate (and of the bundles).

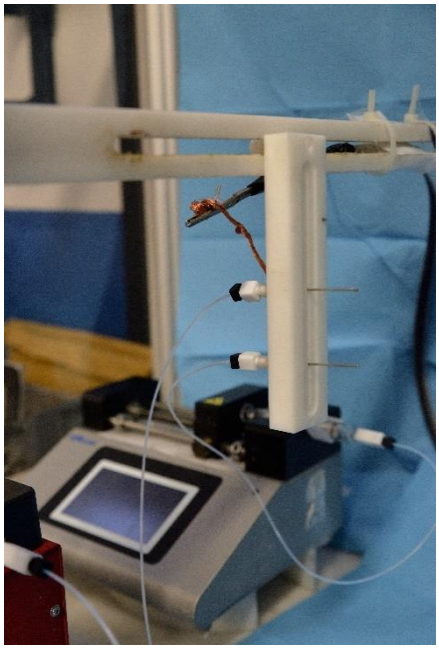

Figure 3.3.3: Needles connected to High-Tension clamp. Syringe pumps in the background

To produce a sheath uniform as much as possible an electrospinning process with one syringe was alternated to another one with two syringes (and two pumps with the same settings) spinning at the same time. The electrostatic field interactions of the two charged needles and jet produced two symmetric gaussian-like distribution of nanofibers centred toward the distal parts of the bundles. Once the production of the sheath was over, the multiscale nylon 6.6 device was complete and could be extracted from the machine together with the grips which were the same used for the tensile stress. The following parameters were used for the process:

- Voltage = 20kV
- Needle-Collector distance = 160mm
- Bundles-Collector distance = about 5mm
- Rotating speed = 15 rpm
- Rotation period = about every 5 minutes
- Pump syringe flow rate = 0.5 ml/h
- Room temperature and relative humidity
- Time = 10 hours

In the next section the grips prototyping, along with the rotating machine modification, will be discussed.

3.4: **Design of grips and modification of electrospinning machine**

In this work the full tendon was mimicked by the assemblage of 24 ring-shape bundles surrounded by a thin sheath. With the nooses at the end of the bundles it was sufficient to have hook-like grips capable to reduce the stress-concentration. Symmetry was another requirement in order to keep the bundles as tight as possible. The grips were used both connected to the rotating support of the machine dedicated to the sheath production, and to the tensile stress machine for mechanical characterization. The prototypes of those grips were designed using Autodesk Fusion 360 (San Rafael, CA, USA). In (Fig. 3.4.1) the top grip is shown. It consists in 3 crossed cylinders of 8mm diameter with a ledge at the ends to prevent the nooses of the bundles to disengage from the grip. The central, vertical cylinder was used as a connection for the two machines and the horizontal holes are meant as sockets for two screws for its locking.

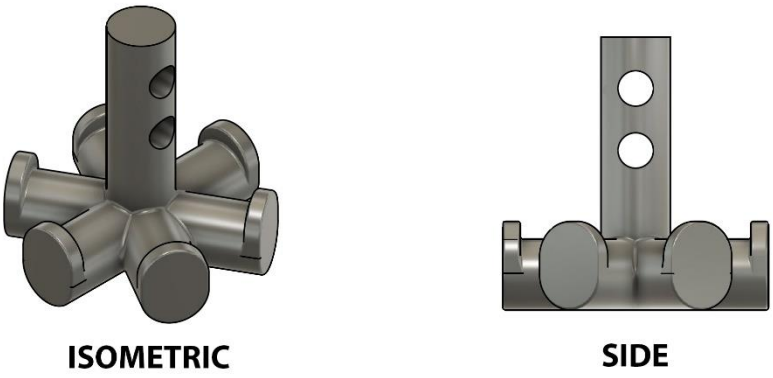

Figure 3.4.1: Schematics of upper custom-made grip

The bottom grip has the same structure, three cylinders of the same size crossed with the ledges in the opposite direction to block the lower nooses. In the next figure (fig 3.4.2) the grip is shown. The hole in the centre of the bottom grip is meant for the inclusion of a threaded rod. Note that the bottom face of the bottom grip should face the bottom one of the top grip.

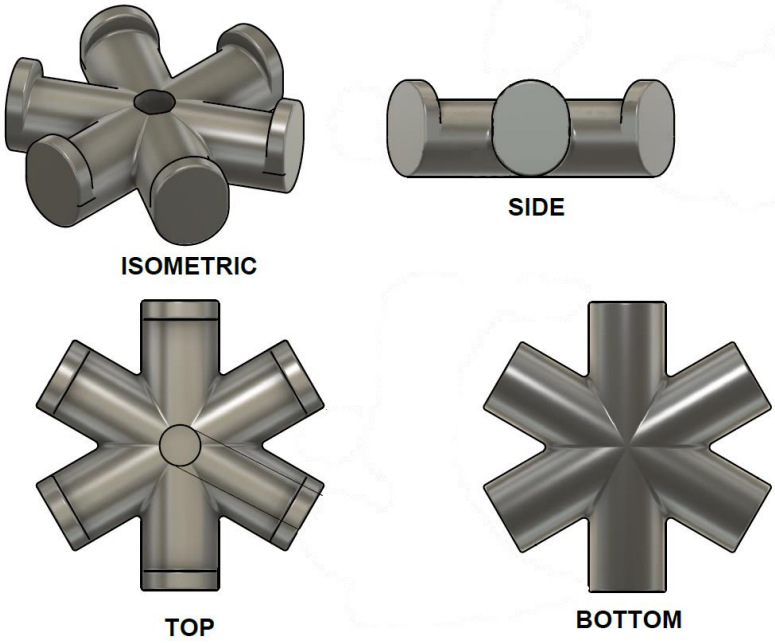

Figure 3.4.2: Schematics of bottom custom-made grip

The grips were then fast prototyped (Fig. 3.4.3) with a 3D printer custom made by Carlo Gotti, modified from a Tarantula kit (Tevo, Zhanjiang, China), with layer height 0.1mm. The slicing and printing process was done via the software Simplify3D. The material used was polylactic acid (PLA), in filament, produced by Bq (Las Rozas de Madrid, Spain).

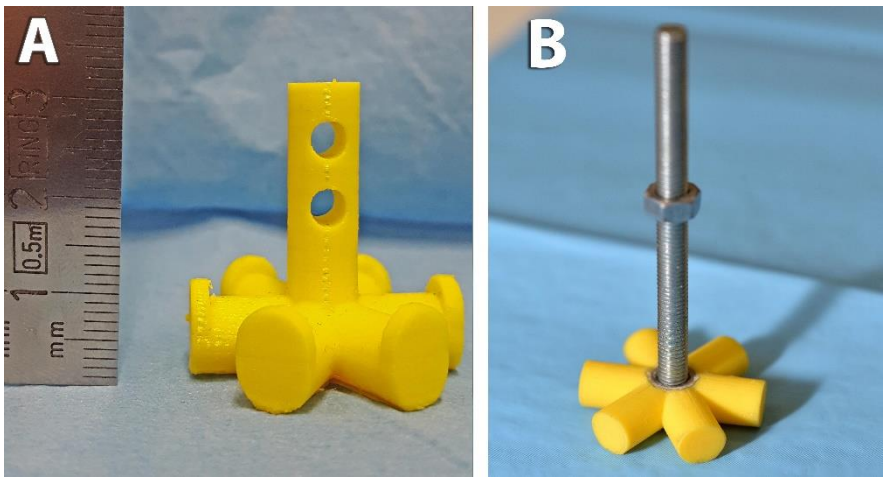

Figure 3.4.3: Grips prototypes. A) Top B) Bottom.

These prototypes present some differences compared to the definitive one, the upper one (A) had a threaded top and the lower one (B) included a socket for a nut

in order to insert a threaded rod of iron. Once the prototypes were evaluated, the project (Fig. 3.4.1 and Fig. 3.4.2) finally was printed thanks to the collaboration of the Spin-off Nextema of the University of Bologna. A 3D metal printer was used to laser sinter the grips from stainless steel powder AISI316L, produced by LPW Technology (Runcorn, UK). The machine used was MySint 100RM, layer height was set at 0.02 mm. The definitive grips are shown in (Fig 3.4.4).

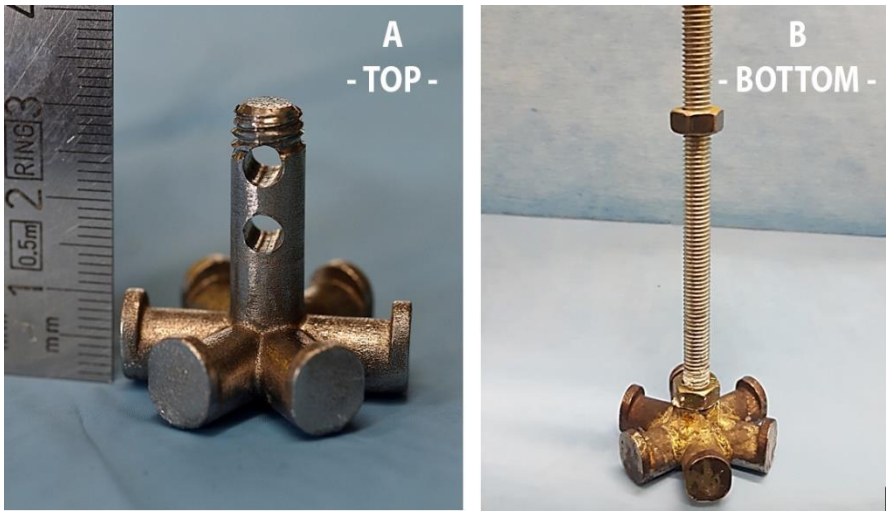

Figure 3.4.4: Stainless Steel grips

In the bottom grip (B) a nut was welded to the grip to enhance the locking system for the threaded screw.

The machine showed in (Fig. 3.3.1) for the nylon 6.6 sheath production was also modified *ad hoc*. The original machine had only the upper part that could rotate and the lower was a pin free to spin in a passive way dragged by the bundles and the upper part.

This could lead to an unwanted twist or torque in the bundles. A focus on the modified parts of the machine is shown in (Fig. 3.4.5); this picture represents a

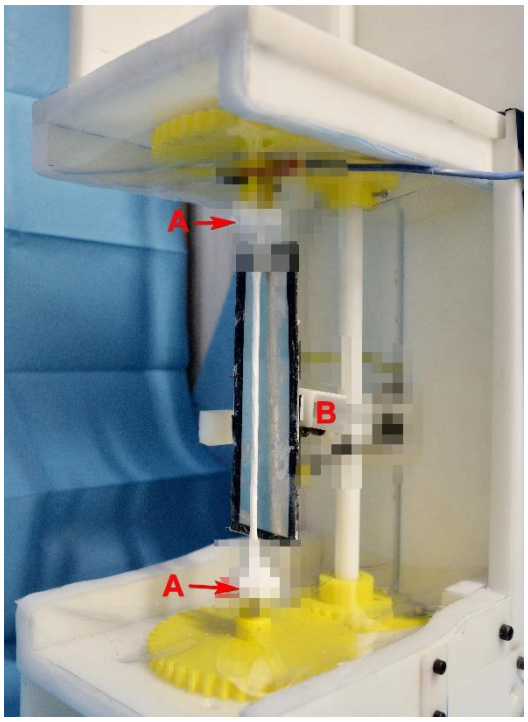

Figure 3.4.5: A close up of the modification of the rotating machine. A) Stainless steel Grips B) Collector Support*

moment of the electrospinning of the sheath. The bundles were hooked to the grips presented above (A), four for each cylinder end. Within the grips a small band of Parafilm was used to preliminary keep as close as possible the bundles; it was removed as soon as the sheath was resistant enough. The collector plate was fixed to a support(B) which can be moved in each direction to be able to approach the bundles without hindering the gears. In (Fig. 3.4.6) a zoom-in of the upper gear is presented. The gears were designed using AutoDesk Tinkercad (San Rafael, CA, USA) and 3D printed with the same printer in PLA. Gear (A) was directly connected to the motor located above, the hollow central cylinder(B) acts as a socket for the upper grip with which was locked with a transversal plug. A copper wire(C) was positioned to ground with the collector plate also the grip. The main gear transmitted the rotation to a smaller gear(D) fixed to a rotation shaft made of Delrin(E), a low-friction plastic. The rotation was then transferred to the lower part of the machine, as presented in (Fig. 3.4.7). In the central part of the bigger gear the lower grip was fixed with a transversal screw. The threaded screw of the grip crosses the floor of the machine and was

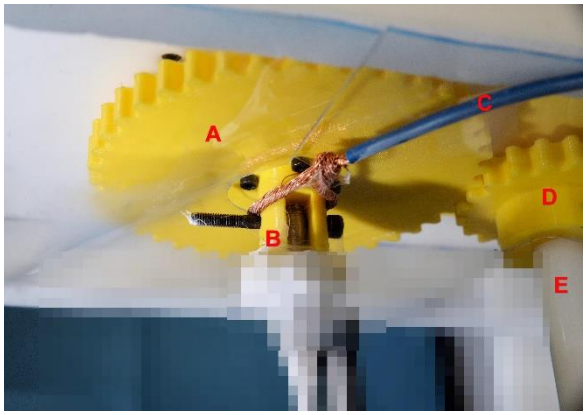

Figure 3.4.6: Upper Gears. A) Main gear. B) Socket for the grip. C) Copper ground wire. D) Shaft Gear. E) Shaft*

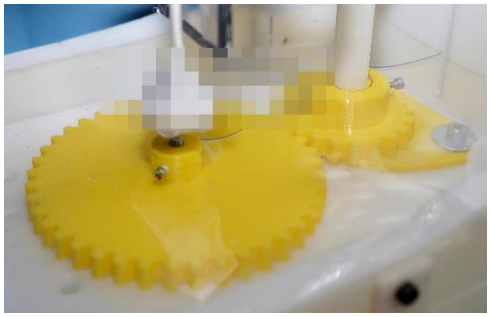

Figure 3.4.7: Lower Gears*

locked on the opposite side with a bearing and a nut. Another copper wire was connected to the screw to ground the lower grip. These modifications allowed a synchronous rotation of the grips, avoiding the problems mentioned above.

3.5: **Morphological characterization: optical microscopy and scanning electron microscopy**

The electrospun bundles were morphological characterized using the optical microscope Zeiss Observer A1m AX10 (Fig. 3.5.1). From the first bundles 20 specimen were cut. Their diameter (mean and standard deviation) was obtained by the mean of five diameters calculated for each specimen with this microscope. The ring bundles were also analysed; four sections of the ring were taken in a cross pattern (mean and standard deviation). In each section the diameter was taken five times and mediated.

Figure 3.5.1: Zeiss Observer A1m AX10

In order to understand the level of alignment and the diameters of the nanofibers, a portion of the electrospun mat was investigated. A specimen of the mat was cut and fixed on a stub, then a metallization with a gold-platinum alloy in argon environment was done using a sputter coater produced by Quorum (Laughton, UK). Then images were taken using a scanning electron microscope (SEM) model Phenom Pro-X, produced by PhenomWorld (Eindhoven, The Nederlands) (Fig. 3.5.2). The diameters of the fibers were calculated on the SEM images on 200 different fibers using ImageJ software. The alignment of the fibers was analysed on the same images using the software Directionality, a plugin of ImageJ. The scanning electron microscope was also used to take a picture of a section of a multiscale nylon 6.6 device.

Figure 3.5.2: Scanning Electron Microscope Phenom Pro-X

3.6: **Mechanical characterization of single bundles, ring bundles and multiscale nylon 6.6 device**

3.6.1 Mechanical characterization of single bundles

The first step of the mechanical characterization was done with the cut specimens obtained from the electrospun bundles. Twenty segments, 110 mm length each, were cut from the bundles, four from each one. From these, a half were assigned to the group "dry" and the other half to the "wet" one. Once obtained the diameters, the wet ones were hydrated in a saline solution for 120 seconds before the tensile test; the dry ones were used as spun. The specimens were then placed on custom-made capstan grips made in a previous work by Sensini et al.[94] (Fig. 3.6.1 B) wrapping the bundle around two aluminium cylinders (diameter = 8mm) to reduce the stress concentrations. For each side, the bundle makes one and a quarter turn around the cylinder before being inserted into a through hole and then, being hold by a rubber O-Ring. During the setup the two ends of the capstan grip were kept still by a bar screwed on one side. The gauge length was so calculated, in accordance to ISO 2062/2009[184], EN12562[185] and ASTM D2256[186] standards:

- Cylinder circumference = $2*\pi*(8/2) = 25.13$mm
- Distance between the axis of the two cylinders = 16mm
- Total Gauge length = $2* (25.13 + 25.13/4) + 16 = 78.83$ mm

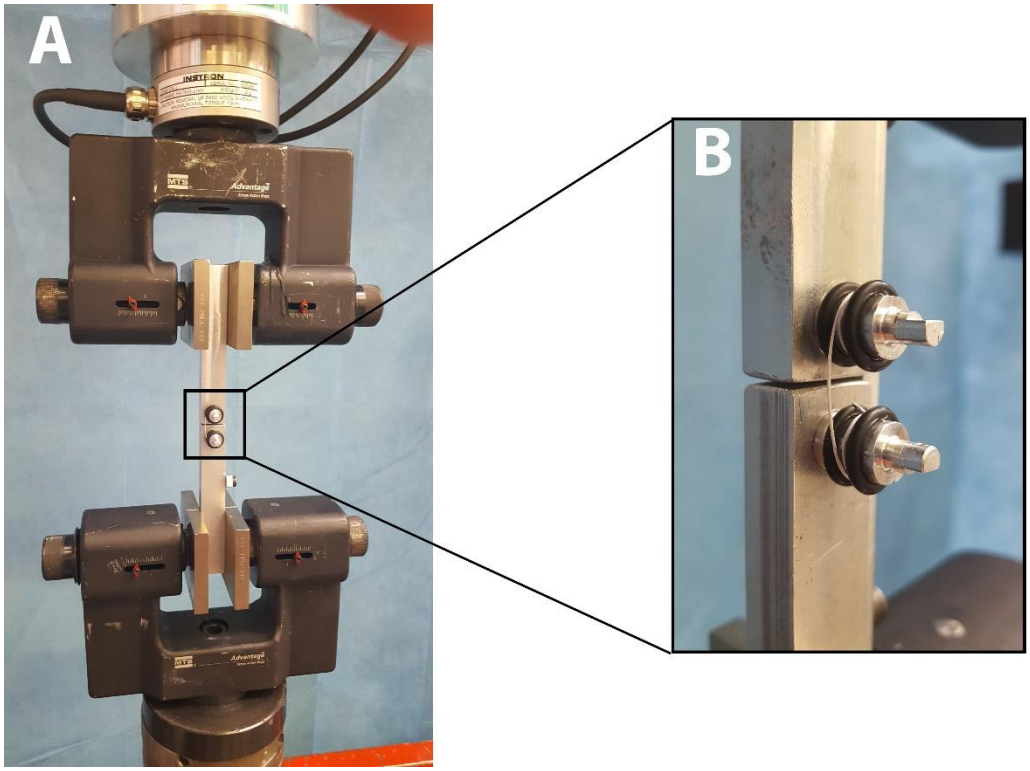

Figure 3.6.1: Setup of single bundles mechanical test. A) Capstan grips mounted on Instron machine. B) Bundles mounted on custom-made capstan grips.

The grips were then fixed in MTS advance clamps which were screwed in the tensile test machine Instron 8500 digital control, model 8032 (Canton, Massachusetts, USA), using a Instron load cell of 1 kN (Fig. 3.6.1 A). The strain rate was set to 20% strain/s. The machine worked in displacement-control mode. It was calibrated with the clamps and capstan grips mounted. All tests continued until the complete rupture of the bundles. A NI-PXIe-1078 system, manufactured by National Instruments (Austin, Texas, USA), was used for data acquisition. Data acquisition rate was set at 1000Hz.

3.6.2 Mechanical characterization of ring bundles

Five ring bundle specimens were tested. The method of test was the same above except for the following:

Figure 3.6.2: Setup for "ring" bundles test

- The rings were simply “hooked” to the same capstan grips pre-positioned at the correct distance to keep the bundles in place but not pre-tensioned. The upper capstan grip was directly screwed into the load cell, the bottom one was hold by the clamp like in the previous setup (Fig. 3.6.2).
- All specimens were bathed in saline solution for 120 seconds.
- The initial length was calculated in accordance to the standard ASTM D1414[187] as the circumference of the entire ring. During the test the instantaneous length was calculated as the contact length between the bundle and the two aluminium cylinders of the capstans plus twice the distance between the centres of the capstan grips.
- The area was calculated as twice the cross-sectional area calculated from axial thickness, obtained in the morphological analysis.
- The strain rate was set to 100% strain/s.

3.6.3 Mechanical characterization of multiscale nylon 6.6 device

For the completed multiscale nylon 6.6 device, the same grips (Fig. 3.4.4) used during the sheath production were used. To do this, a custom-made adapter was built to connect the upper grip directly to the load cell through a threaded rod and a plug (Fig. 3.6.3). The threaded part of the bottom grip was instead fixed in an aluminium block and then held by one MTS advance clamp.

Figure 3.6.3: Custom-made adapter used to connect the upper grip directly to the load cell

In (Fig. 3.6.4), the complete setup before the test is shown. Three specimens had been tested, all previously bathed in a saline solution for 120 seconds. The cross-sectional area of the multiscale nylon 6.6 device was calculated through the diameter obtained with the morphological analysis. The initial length and the length of the multiscale nylon 6.6 device during the test were calculated with the same method described for the ring bundle. The strain rate was set to 100% strain/s.

3.6.4: Data analysis

The steps taken for the data analysis were:

- Measure the diameter of each specimen from the morphological analysis.
- Filter the data with Matlab with a median filter of n=81 samples.
- Offset displacement data with the mean value of the first 400 samples of the acquisition in which the actuator was idling, before starting the test.
- Offset load data with the mean value of the last 400 samples of the acquisition in which the actuator had stopped after the specimen had completely broken.

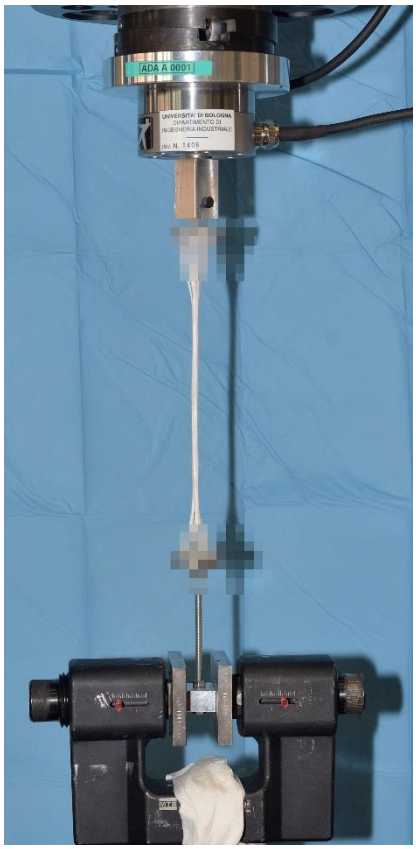

Figure 3.6.4: Setup of multiscale nylon 6.6 device tensile test*

- Search the first valid force value at which the force values stopped to oscillate and began the ramp.
- Calculate the engineering stress as $\frac{Force}{Area} = \frac{N}{mm^2} = [MPa]$
- Calculate the engineering strain as $\frac{Displacement}{Gauge\ length} * 100 = \frac{[mm]}{[mm]} = []$
- Produce Stress-strain curve

To obtain the Young's modulus and the elastic limit, the process used was the following (referred to a typical stress-strain curve depicted in Fig. 3.6.5):

- Identify the failure stress value as the highest stress (E);
- The stress value corresponding to the 20% of the failure stress value was defined as the starting point of the linear region (A);
- The yielding point was visually estimated as initial guess with the stress-strain graph (C);
- The value corresponding to the 50% of the stress between the estimated yielding point and the point (A) was identified as the half-way of the linear region (B);

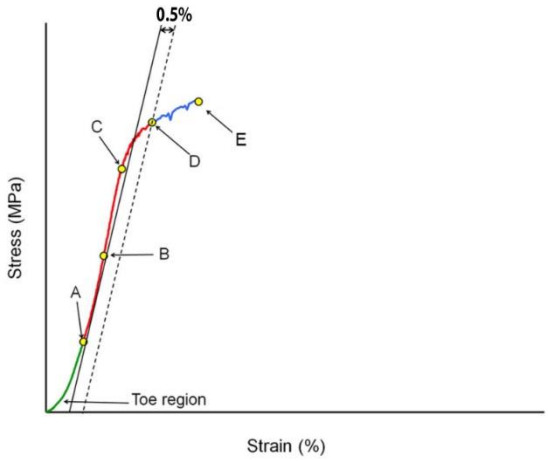

Figure 3.6.5: Sketch of method use to analyse the stress-strain curve. Adapted from Sensini et al.[183]

- A linear regression from the point (A) to (B) was made (solid line);
- A second line was drawn parallel to the solid one obtained with the regression mentioned above, shifted of +0.5% relative strain (dashed line);
- The crossing point between the parallel line and the stress-strain curve was identified as the Elastic Limit (D);
- A linear regression from the starting point of the linear region (A) and the elastic limit (D) was done. The value of the slope of this line was identified as the Young's Modulus.

- The work to failure was calculated as the area under the stress-strain curve until the failure stress point with the trapezoids method.
- The work to yield was calculated as the area under the stress-strain curve until the Elastic Limit using the trapezoids method.

4: RESULTS

4.1: Morphological properties

4.1.1 Morphology of nanofibers and bundles

Investigating sections of the bundles, image like (Fig. 4.1.1) were taken using the scanning electron microscope.

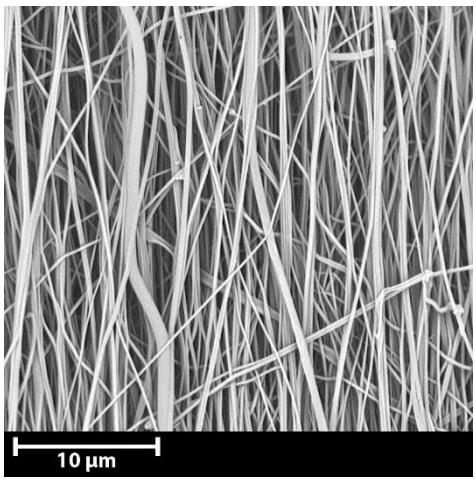

Figure 4.1.1: SEM image of a section of a bundle

The diameters of the nanofibers were therefore calculated:

Diameters of the Electrospun Fibers		
Mean	257	nm
Standard Deviation	43	nm

Table 4.1.1: Diameters of the electrospun fibers

With a mean diameter of 257 nm, it was demonstrated that the fibers were produced at nanoscale level, with low scatter.

On the same scanning electron microscope images, the alignment of the nanofibers was quantified (Fig. 4.1.2). The graph shows the percentage of amount of nanofibers (y-axis) and their deviation, expressed in degrees, from the direction

of rotation of the collector (x-axis). About 75% of the fibers present a maximum deviation of ±15° [134].

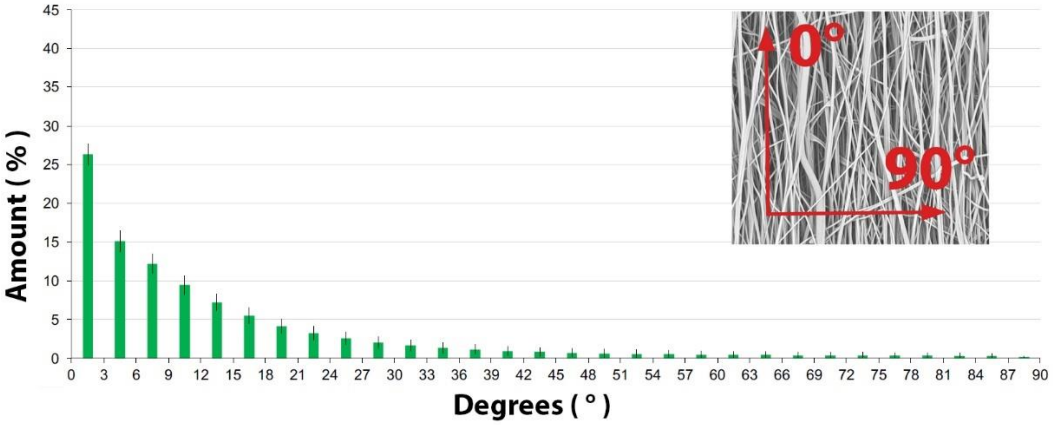

Figure 4.1.2: Percentage of amount of alignment of the nanofibers

An example of a cut bundle specimen obtained with the manual wrapping on the drum of the nanofiber mat is showed in (Fig. 4.1.3 A). A close up of a bundle obtained with the optical microscope is showed in (Fig. 4.1.3 B).

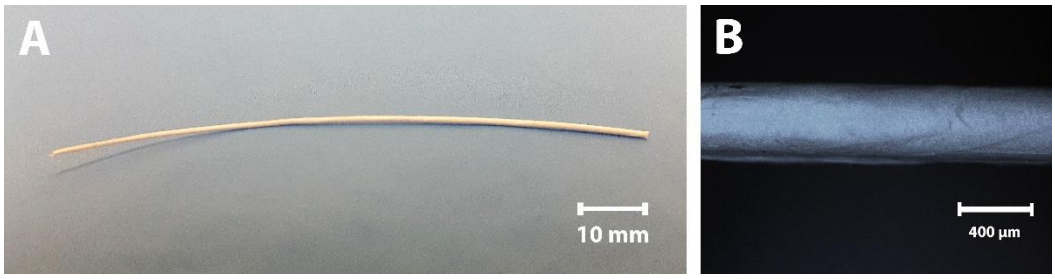

Figure 4.1.3: A) Cut bundle B) Magnification with optical microscope

The mean diameter of these single bundles is showed in (Table 4.1.2).

Diameters of the Single Bundles		
Mean	0.450	mm
Standard Deviation	0.038	mm

Table 4.1.2: Diameters of the single bundles (measured on 20 specimens)

The same morphological analysis on the ring bundles reported the mean diameter showed in (Table 4.1.3). Single bundles are a portion of ring bundles, directly cut on the collector. The diameter should be the same; the measures was repeated on uncut ring bundles to check any possible change due to the dragging on the drum to free them.

Diameters of the Ring Bundles		
Mean	0.475	mm
Standard Deviation	0.048	mm

Table 4.1.3: Diameters of the ring bundles (measured on five specimens)

4.1.2 Morphology of multiscale nylon 6.6 device

Three multiscale nylon 6.6 devices were morphologically investigated. (Fig. 4.1.4) shows an example of the multiscale nylon 6.6 device before the mechanical test. The electrospun sheath was uniform on its length and, tightening the bundle one another, reduced the cross-sectional area of the multiscale device.

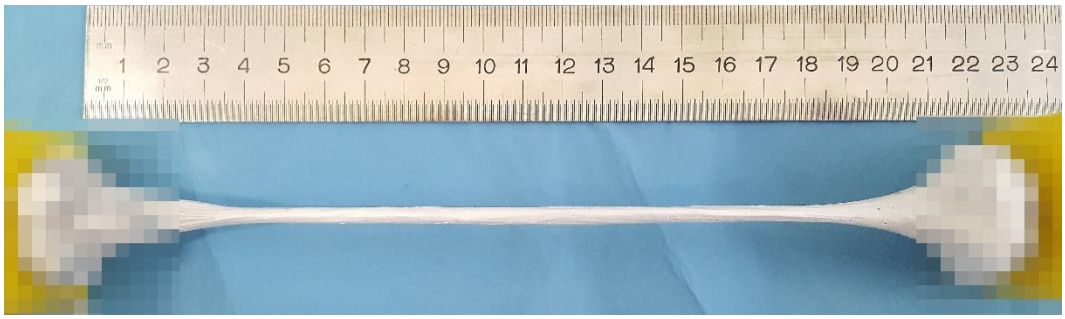

Figure 4.1.4: Multiscale nylon 6.6 device*

In (Fig 4.1.5) a close-up of the multiscale nylon 6.6 device exhibits how the bundles are tightened even in the proximity of the grips until they separate to be hooked in the cylinders.

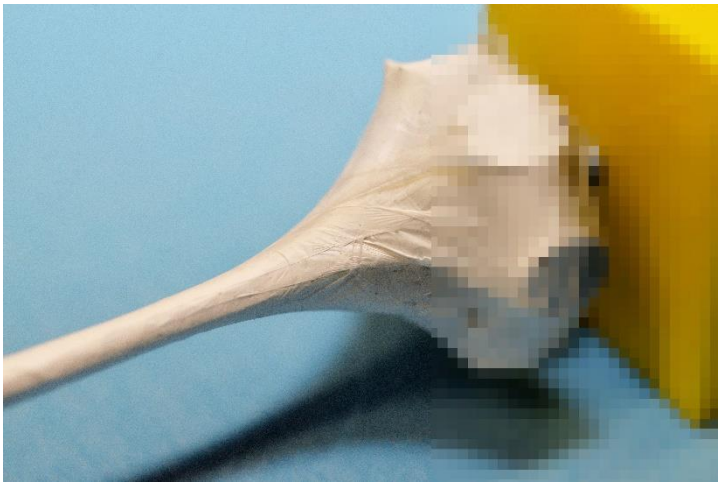

Figure 4.1.5: Multiscale nylon 6.6 device in proximity of the grips*

The diameters obtained from three multiscale nylon 6.6 device are presented in (Table 4.1.4).

Diameters of multiscale nylon 6.6 device		
Mean	4.9	mm
Standard Deviation	0.42	mm

Table 4.1.4: Diameters of multiscale nylon 6.6 device (measured on three specimens)

A cut portion of the multiscale nylon 6.6 device was investigated via scanning electron microscope. The outcome is shown in (Fig. 4.1.6) in which are visible three bundles and the random sheath on the left.

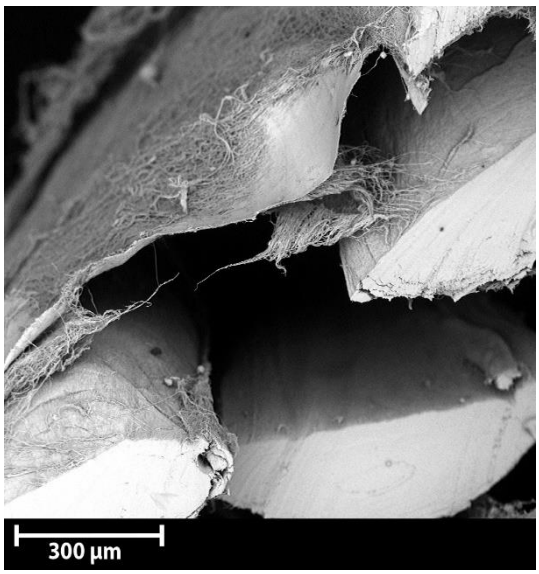

Figure 4.1.6: Cut section of the multiscale nylon 6.6 device

4.2: Mechanical properties

4.2.1: Mechanical properties of single bundles

The first specimens tested were the cut bundles. The bundles ruptured in the middle section between the capstan grips, demonstrating that these grips deconcentrated the stress adequately. In (Fig. 4.2.1) is showed the moment of a bundle rupture.

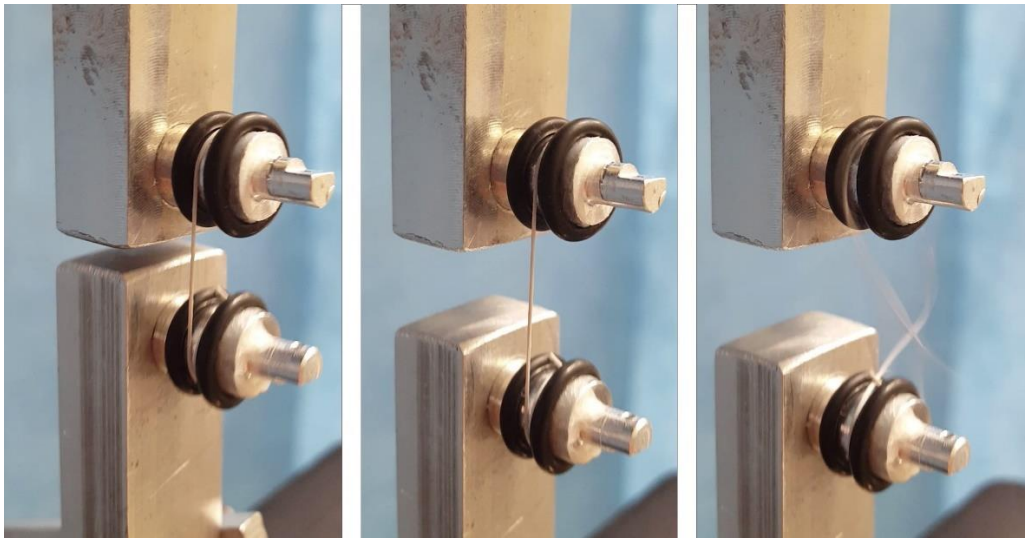

Figure 4.2.1: Frames of the moment of the rupture of the cut bundle specimen (form left to right)

Ten specimens from each group, dry and wet, were tested. The results are shown in (Table 4.2.1).

SINGLE BUNDLES	DRY	WET	
Failure Load	11.8±1.6	10.1 ± 0.9	[N]
Failure Stress	72 ± 6.8	66 ± 14	[MPa]

Failure Strain	12.7±1.3	11.0 ± 3.0	[%]
Young's Modulus	709 ± 76.8	684 ± 63	[MPa]
Elastic Limit	----------	62 ± 12	[MPa]
Work to Failure	440 ± 56.3	395 ± 188	[MPa]
Work to Yield	----------	337 ± 137	[MPa]

Table 4.2.1: Results of mechanical characterization of single bundles

The dry group exhibited an elastic-brittle behaviour. The Young's modulus was thus calculated as the slope of the linear regression between the point corresponding to 20% of the failure stress, to the failure stress.

4.2.2: Mechanical properties of ring bundles

The results for the mechanical characterization of the ring bundles are shown in (Table 4.2.2). All of them were hydrated in saline solution before the test.

RING BUNDLES	**WET**	
Failure Load	22.1 ± 1.6	[N]
Failure Stress	63 ± 11	[MPa]
Failure Strain	10.0 ± 1.2	[%]
Young's Modulus	808 ± 89	[MPa]
Work to Failure	287 ± 94	[MPa]

Table 4.2.2: Results of the mechanical characterization of the ring bundles. Due to the brittle behaviour the work to yield and elastic limit were not calculated.

Even with the ring bundles the behaviour was brittle. The Young's modulus was thus calculated as the slope of the linear regression between the point corresponding to 20% of the failure stress, to the failure stress. The work to yield and elastic limit were not calculated.

4.2.3: Mechanical properties of multiscale nylon 6.6 device

Three multiscale nylon 6.6 devices were tested. In all three cases the rupture occurred at the interface with the grip. The results of the mechanical characterization of multiscale nylon 6.6 device are shown in (Table 4.2.3). All of them were hydrated before the test.

MULTISCALE NYLON 6.6 DEVICE	WET	
Failure Load	333 ± 11.6	[N]
Failure Stress	23.1 ± 5	[MPa]
Failure Strain	9.0 ± 0.2	[%]
Young's Modulus	321 ± 81	[MPa]
Work to Failure	86 ± 22	[MPa]

Table 4.2.3: Results of the mechanical characterization of multiscale nylon 6.6 device

The behaviour was again elastic-brittle. The Young's modulus was thus calculated as the slope of the linear regression between the point corresponding to 20% of the failure stress, to the failure stress. The work to yield and elastic limit were not calculated.

In (Fig. 4.2.2) the stress – strain behaviours of the three structures investigated are compared

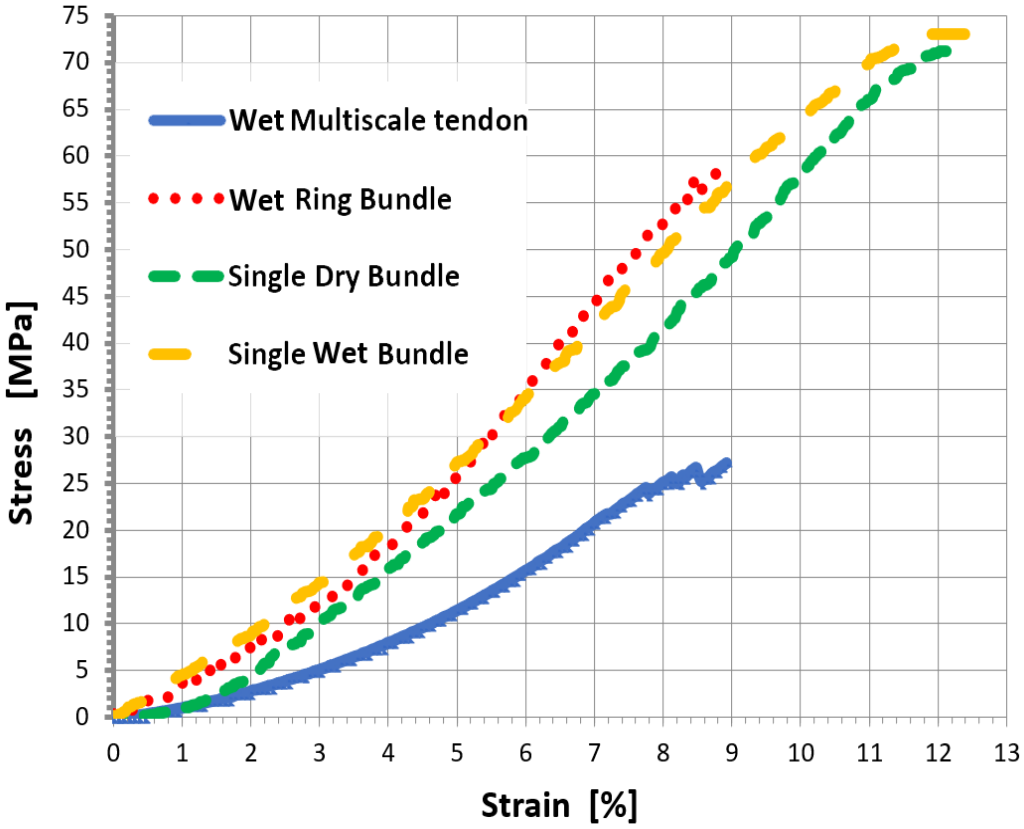

Figure 4.2.2: Stress - strain comparison of single bundles, ring bundles and multiscale nylon 6.6 devices

In (Fig. 4.2.3) the same structures are compared in terms of a load – strain relationship.

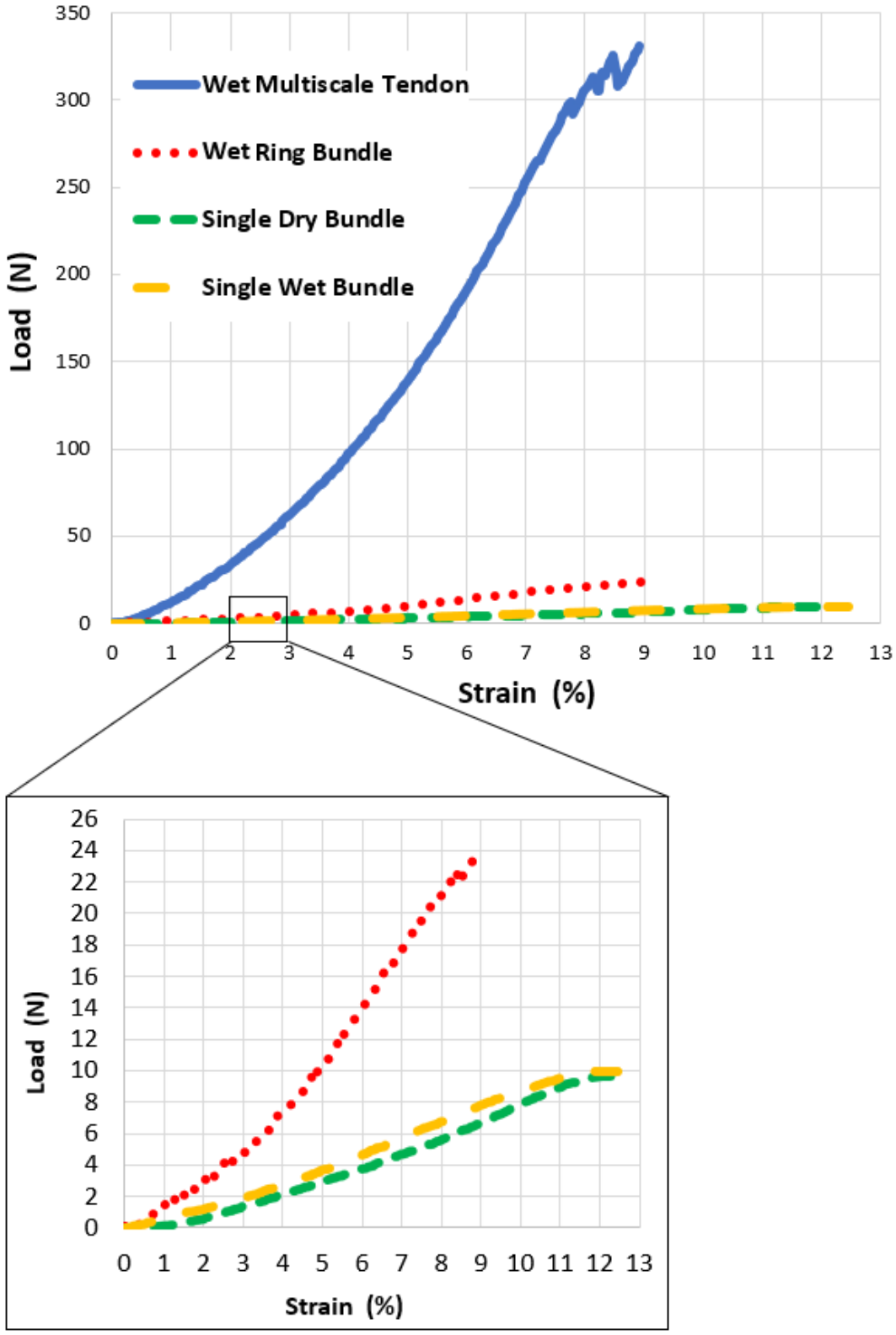

Figure 4.2.3: Load - strain comparison of single bundles, ring bundles and multiscale nylon 6.6 devices

5: DISCUSSION

5.1: Morphological Characterization

In this work an innovative electrospun, multiscale, nylon 6.6 nanofibrous device, for tendons and ligaments replacement and simulation was developed. In order to confirm that its hierarchical structure and biomechanical properties were similar with the ones of tendons and ligaments, a morphological and mechanical multiscale characterization was performed.

The SEM investigation reported electrospun nylon 6.6 well defined nanofibers, without beads, of 257 ± 43 nm. These measures are in line with literature when compared to the diameter of collagen fibrils[1,3,8]. The directionality analysis on the SEM images of the surface of the bundles (Fig. 4.1.2), confirmed that the nanofibers were aligned to the axis of the bundles, with a dispersion of ±15°. This distribution contributes to obtain better biomimicking the physiological disposition of collagen fibrils of tendons[1,188]. In addition, this misalignment of the nanofibers, and their slightly crimp, contributed to give the desired non-linearity of the stress – strain curve according to their progressively stretch, depending on their alignment to the load. This process resembles the recruitment of the fibers found in tendons and ligaments[1,3,8]. From SEM images it was possible to notice a certain amount of porosity determined by the spacing between the nanofibers. This free space may reduce the friction between nanofibers, when mechanically tested and, can eventually be filled up with gelatinous substances to better mimic the presence of proteoglycans of the biological counterpart.

The bundles investigation with optical microscope, reported a diameter of 0.45 ± 0.04 mm, that was consistent with collagen tendons and ligaments fascicles diameter as found in literature[7,8]. The bundles specimens were obtained by manual wrapping a portion of the electrospun mat directly on the drum. The thickness of the mat along the drum was uniform, and this allowed to obtain bundles with consistent diameters both inter-specimen and intra-specimen. This method of production has proved to be reproducible and scalable. Reproducible because, once the electrospinning parameters were tuned properly, the outcome of the process in

terms of mat thickness and nanofibers disposition was almost constant. Scalable because the diameters of the bundles can be set, cutting and wrapping band of the mat of different width. The final diameter of the bundles – and thus the band width to be cut - can be predicted with an empirical formula given an estimated thickness of the mats. It should also be noted that, with this procedure, bundles of every kind of diameter, can be obtained, with greater diameters compared to the ones reported in literature[101,116]. This permits to obtain patient specific models of bundles, based on the effective values of the tendons and ligaments fascicles under evaluation.

Ring bundles are a novel kind of electrospun bundle and this production method brings many advantages. At first, they facilitate the suture during implant, preventing the sliding of the suture wires when fixed inside the nooses of the ring bundles. The uninterrupted circular shape ensure also that they can be assembled together and hooked to any kind capstan grips, without being forced to use cement to hold them during the mechanical tests. In fact, it is well established, that the stress-concentration always occurs in the contact points with the blocking mechanism[186]. Finally, another advantage is that the final diameter of these rings (or their length, if cut), is tuneable choosing a drum collector with a different diameter. So, this technique permits to obtain multiscale devices, with a patient's specific final length, able to simulate the length of every tendon or ligament of the human body. The morphological investigation of the multiscale tendon reported a structure that successfully resembles a biological tendon with its hierarchical structure. In the SEM image of a section of the multiscale device (Fig. 4.1.6) a focus on some bundles and a portion of the sheath can be observed. It should be noted that the not circular shape of the bundles observed, is due to the pressure of the blade used to cut the specimen; normally, bundles were observed with an almost circular cross-sectional area (Fig. 4.1.3). The bundles, after the alignment in the sheath machine, were kept together by the electrospun sheath. In fact this patented method to produce an electrospun sheath[147], permitted to tight the bundles each

other, reducing the final diameter of the multiscale nylon 6.6 device, increasing their final mechanical properties (Fig. 5.1.1).

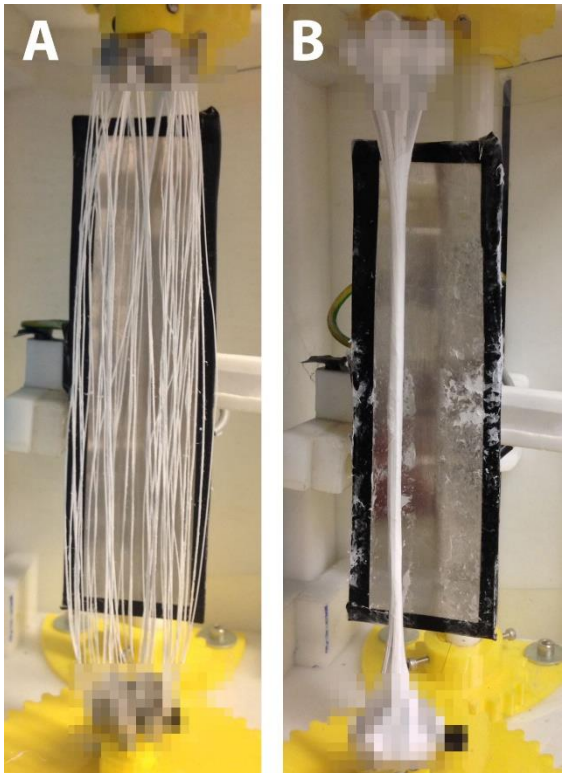

Figure 5.1.1: Electrospinning of the random sheath. A) Ring bundles before the process. B) Multiscale nylon 6.6 device completed, wrapped by the sheath.*

This process permits to form the sheath without using a drum collector in the body of the device during the electrospinning process[189], and to scale the production of the sheath on devices of every desired length. In fact until now, no groups were able to achieve similar results in the electrospinning research field[109,117,189,190], compromising in a critical way the applicability of the electrospun scaffolds and devices in the regeneration and replacement of human soft tissues.

The number of ring bundles used was arbitrary, it can be varied with no influence on the process of sheath production. It is also possible to combine different group of bundles each with their individual sheath to form a unique tendon surrounded by another sheath. In this way the internal subunit with their sheath would mimic a tertiary fascicle instead of a complete tendon. In (Fig. 5.1.2) the

SEM image of the nylon 6.6 multiscale device is again showed, comparing its internal structure with the one typical of biological tendon[191].

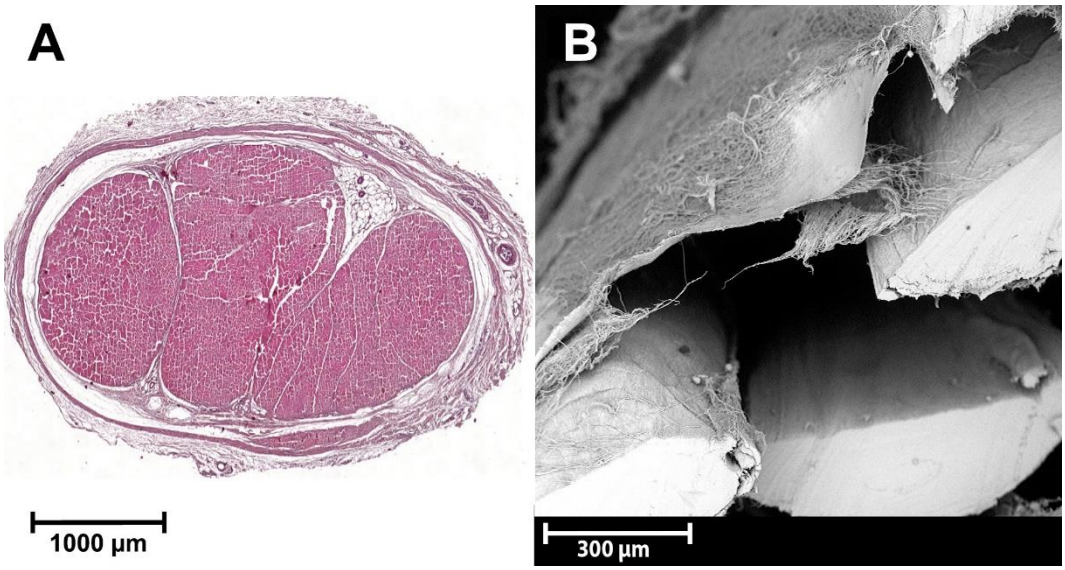

Figure 5.1.2: Comparison of: A) Transversal section of a rabbit Achilles tendon (achieved with dynamic contrast enhanced magnetic resonance imaging and histologic[191]) and B) electrospun nylon 6.6 multiscale tendon

The empty spaces between bundles are present but, as mentioned, reduce the friction between them. Possibly they could be also filled up with gel substances, to mimic the role of proteoglycans. The sheath thickness was uniform along the tendon except for the ends where the nooses of ring bundles has to diverge to be hooked in the grips. Here, the convenience of these ring-shaped bundles is that other types of grips can be easily tested without modifying the production process.

5.2: Mechanical properties

For the mechanical characterization of the electrospun multiscale devices, a bottom-up approach was applied. At first, cutting portions of the ring bundles directly on the drum, the singles bundles specimens were obtained. In order to characterize the electrospun nylon 6.6 material, and also to compare it to the studies[147,183], the mechanical characterization was firstly performed on these kind of single bundles specimens. The *ad hoc* capstan grips designed, permitted to break the bundles in the middle of the gauge length, reducing the underestimation of the ultimate stress. The strain rate was set to $20\%s^{-1}$. This parameter was chosen, according to the physiological strain rate, typical of daily activities as a run reported in literature[192,193]. It was also decided to split the specimens in two groups to investigate the behaviour of the electrospun bundles in both dry and wet environment. Indeed, in the case of an implant, the immersion of the specimens in saline before a mechanical test, is a good starting point to understand if mechanical properties are affected by the hydration. The outcome of mechanical tests (Table 4.2.1), suggests at first instance that there are no marked differences between dry and wet group. This is probably due to the intrinsic hydrophobic nature of nylon 6.6[194], that does not interact with the saline solution. In (Table 5.2.1), results obtained from wet bundles are compared with those obtained from human Caucasian fascicle characterization, from literature[34]. It should be noted that the Achilles tendon fascicles reported by this work from Hanson et al.[34], had a mean diameter of 0.7 mm, comparable to the nylon bundles one.

	Single Wet Bundles	**Human Fascicles**[34]	**[]**
Failure Stress	66 ± 14	28.1 ± 9.8	[MPa]
Young's Modulus	684 ± 63	317 ± 110	[MPa]
Failure Strain	11.0 ± 3.0	13.8 ± 4.4	[%]

Table 5.2.1: Comparison between mechanical behaviour of single wet bundles and human fascicles

It can be seen how the failure strain is comparable. The failure stress and the Young's modulus are in the same order of magnitude but higher in nylon 6.6 bundles. This is firstly due to the different mechanical characteristics of the two materials (nylon 6.6 and collagen) but also for the different strain rate applied during the tests. Hanson et al.[34] specimens were tested at a displacement rate 0.5 mm/min compared to the 16 mm/s used to characterize the nylon 6.6 single bundles. These differences in the strain rate, could have a relevant impact on the failure stress values and the Young's modulus, in order to the fact that both collagen fascicles and nylon 6.6 bundles are viscoelastic materials. As reported by Robinson et al.[195], who tested rat tail tendon fascicles both at 0.5%/s and 50%/s, the mean values of failure stress increased from 30 MPa (at 0.5%/s) to 60 MPa (at 50%/s), and the Young's modulus from 450 (at 0.5%/s) to about 550 MPa (at 50%/s). It should be noted that the nylon 6.6 bundles were tested about 1920 times faster than Hanson's fascicles. Moreover, results by Robinson et al.[195] at 50%/s, even if obtained from a different species, were in line with the nylon 6.6 bundles. The stress – strain curve (Fig. 4.2.2) showed a non-linear shape typical of tendons and ligaments fibers and fascicles (Fig. 1.1.4)[34]. The curves had a toe-region that is typically due to the progressive alignment and stretching of the nanofibers inside the bundles. This demonstrates the suitability of the electrospinning process to produce materials with this behaviour, starting from bulk materials with totally different mechanical characteristics[196]. In (Fig 5.2.1) a nylon 6.6 bulk filament (A) is compared to the electrospun one (B). The shape of the curve is different, not showing the sigmoid

trend. The Young's modulus reported for bulk nylon 6.6 is greater than 3000MPa[196], compared to the 684MPa of electrospun bundles.

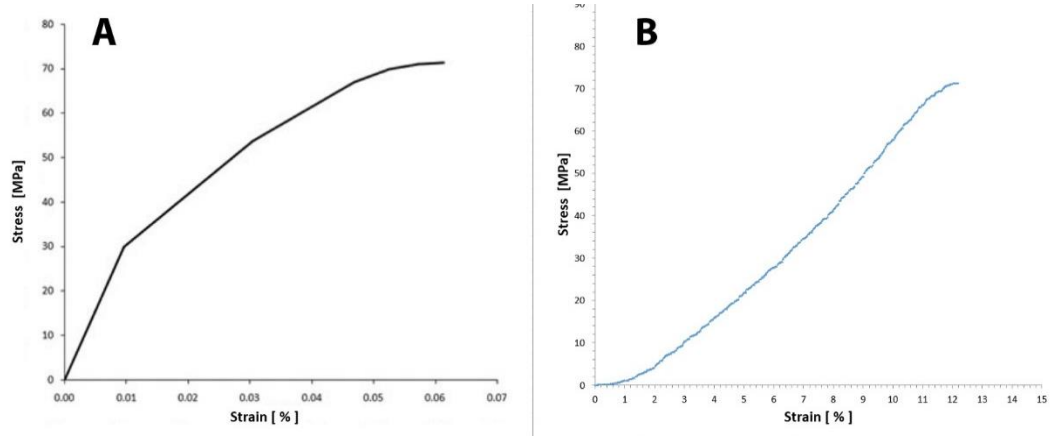

Figure 5.2.1: Comparison between bulk nylon 6.6[196] (A) and electrospun bundle made of nylon 6.6 nanofibers

The results obtained from the mechanical test of ring bundles (Table 4.2.2) were, as expected, in line with the single bundles (the difference was less than 10% for failure stress and strain and 20% for Young's modulus). The Young's modulus was higher than the single bundles one. A strain rate of 100%/s was used for the ring bundles, in order to simulate a physiological worst-case scenario of rupture for a ligament or tendon[193]. This again confirmed that the strain rate contributes heavily to increase the stiffness of the bundle.

The multiscale nylon 6.6 device was tested at a strain rate of 100%/s, as the ring bundles. In (Fig 4.2.2 and Fig. 4.2.3) the typical non-linear behaviour of the curves of tendons is showed. The values of the mechanical properties of the multiscale nylon 6.6 device (Table 4.2.3), were compared to the literature[106]. From the review of Peppas et.al[106], it is reported how there is a huge variability between different natural tendons and ligaments and even between different tests on the same type of tendon and ligament carried out by different groups of researchers[106]. In addition, a certain amount of uncertainty should be added to the mechanical properties reported in literature considering that biological specimens are often tested as a composite of bone-ligament-bone or muscle-tendon-bone because it was easier to clamp them[106]. The mechanical properties of the multiscale nylon 6.6 device are, for example, in the same range of the patellar tendon[106]. Even Anterior longitudinal

spine ligament, medial collateral ankle ligament and anterior/posterior cruciate ligaments, shared the same range of mechanical characteristics in term of failure stress, Young's modulus and failure strain.

The multiscale nylon 6.6 device was composed of 24 ring bundles (so 48 filaments) with a mean diameter of 0.450 mm. It should also be noted that, calculating the cross-sectional area of the entire structure as a sum of the cross-sectional areas of the bundles, the failure stress would increase to about 45 MPa and the Young's Modulus to 550 MPa, narrowing the values obtained by biological tests reported by Hanson et al[34]. This problem could be overcame, tightening more the bundles with the sheath or adding gel substances "proteoglycans-like" that, compressing by the sheath around the bundles, could help to increase the mechanical properties. Moreover, it must be taken into account that, some research groups reported much different values of the mechanical properties of the same tendon or ligament. For example, Thermann et al.[197], calculating the cross-sectional area with a different approximation instead of Wren et al.[198], concluded that the failure strength at a strain rate of 30%/s, was 41 ± 10 MPa. The mean failure load of the multiscale nylon 6.6 device of 333 N was lower when compared to the theoretically sum of the contributes of the 24 ring bundles, that should be around 530N. This is due to the fact that the complex structure of the multiscale nylon 6.6 device was harder to test compared to the single ring bundle. Considering the high-velocity of the test, the different ring bundles could had been tensioned in different moment, without being able to reposition themselves, due to their not perfect symmetric placing. Moreover, some of the bundles were ruptured in the proximity of the grips, according to the superficial roughness caused by the 3D printing production process, indicating that the load to failure was under-estimated and should be instead in the range between 333 and 530 N. The main role of the electrospun random sheath was to tighten the ring bundles together, and to simulate the behaviour of the epitenon/epiligament. The electrospun sheath did not contribute to the traction mechanical properties of the multiscale nylon 6.6 device. However, the sheath underwent radial stresses, opposing to the opening of the group of bundles that, when stretched, tend to vertically align.

5.3 Future directions

Talking about the applications of the multiscale nylon 6.6 device produced in this work, it could be proposed as an innovative synthetic biostable implant, compared to the currently available devices. These devices are mainly targeted to the replacement of ligaments[42,73,75,79,81–83] with only few findings of their use in tendon applications[42,89]. Today, even though the trend of research on tendon and ligament repair is focused on resorbable scaffold[53,95–98], this practice is not always suggested, like for example in the treatment of injuries on elderly where the regenerative activity of the cells is limited[199]. Nylon is a biostable polymer already used for suture wires and thus a medical grade material[200]. As an implant, the production of the multiscale nylon 6.6 device could be easily industrialized to match the target tendon/ligament to replace. The process has also proven to be highly reproducible.

The multiscale nylon 6.6 tendon can't be directly proposed as a multiscale scaffold for tendon and ligament repair, but a replacement, because of the non-resorbable nature of nylon polymer. However, this novel structure can be also proposed, using different polymers, pure or in blends, even resorbable, to overcome this limitation, as reported in literature[135,147,148,183].

Moreover, the multiscale nylon 6.6 device could be suitable also for soft robotic and exoskeletons. In this field, the principle of the compliance matching states that materials that come into contact with each other should share similar mechanical rigidity. Some examples of exoskeletons, showed in this work[153,162,167–169], proposed cable-driven actuators using steel[162,165,167] or dyneema[170] wires. Both share a Young's modulus ranging from tens to hundreds of GPa with the former that is also harder than any biological tissue. These cables, proposed in literature, are intended to play the role of tendons but have totally different structures and properties. Moreover, stainless steel and dyneema wires lack of the toe-region that provides the non-linearity typical of tendons. Here the use of the multiscale electrospun nylon 6.6 device is proposed to mimic better both mechanical behaviour and the hardness of the biological tendons and ligaments. As an example, in the work of Xu et al.[175], the authors proposed a crochet technique with spectra fiber to reproduce the extensor hood of ACT Hand. The crochet technique was introduced because is capable to provide a non-linearity in the stress – strain curve.

The electrospun multiscale nylon 6.6 device, produced in this work, may be proposed to reproduce the extensor hood and its non-linearity, avoiding the need to use an unlikely biological structure like crocheted strings. The TCP muscles, proposed by Wu et al.[178], are made of the same material used in this work, nylon 6.6. The authors did not use electrospinning to reproduce the fibers but twisted and coiled fishing line. It might be interesting to test electrospun nylon 6.6 bundles as an alternative.

Finally, in order to mimic the hierarchical morphology and the mechanical properties of the multiscale nylon 6.6 device, it could be a valid alternative to the few currently available tools for mechanical simulations, *in vitro* testing of orthopaedic devices and investigation and validation of new surgical techniques on tendons and ligaments. In fact, as showed above, the available devices investigated in literature,[181,182] and commercial products (SAWBONES®), are far from both the multiscale morphology (intrinsic and also macroscopic) and mechanical performance of human tendons and ligaments.

The production method proposed in this work leaves open to many possible further developments. It was shown how the process is already reproducible and scalable, but it can be easily industrialized to obtain faster and even more reproducible results. It was shown the potential of the electrospun random sheath to tighten and pack the bundles one another but it did not contribute to the mechanical properties when longitudinally stressed. It may be suggested the use of a more ductile polymer for the sheath production. It would probably tighten better the bundles during the sheath production process yielding itself around the bundles. This would lead to a minor cross-sectional area and thus to an improved failure stress calculation. In the sheath production would be also useful to control the shape and uniformity of the electric field, especially if the sheath has to be electrospun on a long structure like the bundles of this work. Even the bundles polymer can be substituted but the outcome and the mechanical properties have to be investigated. It was even reported how the hydration in saline solution did not affect the mechanical properties. This was an advantage, considering that this structure does not change in an aqueous environment, but it could be interesting to introduce a gel within the bundles to

mimic the proteoglycans and hopefully enhance even the mechanical properties. Other types of grips for the multiscale nylon 6.6 device could be designed according to the desired target tendon or ligament. This, in order to mimic in the best possible way its distal parts and the level of tightening of the bundles. This would allow a better formation of the sheath and lower radial stresses when tested. Finally, electrospinning the mats on the drum collector, it could be introduced a rotation of the jet, in such a way that the fibers would be deposited aligned but with an intrinsic twist. This would simulate the hierarchical structure of collagen even at a lower level, mimicking the triple helix of tropo-collagen, even if at a higher dimensional scale. Creep, stress-relaxation and fatigue tests would also be interesting to investigate deeply the mechanical characterization of these structures.

6: CONCLUSIONS

The principal aim of this work was to produce a nylon 6.6 multiscale device able to mimic the hierarchical structure and biomechanical properties of tendons and ligaments tissue. The morphological analysis, carried out with a scanning electron microscope and an optical microscope, demonstrated that the multiscale nylon 6.6 device reproduced the complex hierarchical structure of a tendon or ligament with a high degree of precision, compared to the currently available devices for tendons/ligaments reconstruction and the *in vitro* simulation tools for biomechanical tests and surgical techniques. Mechanical characterization of the bundles and the multiscale nylon 6.6 device reported satisfactory results, comparable to several biological tendons and ligaments. Further investigation on this device may include cyclic loading tests to determine whether and how it changes its mechanical behaviour. The nylon 6.6 was chosen due to its already known medical biostability and its low cost. Results showed that, even though starting from nylon 6.6 bulk material, characterized by marked mechanical difference from tendons and ligaments tissue, the electrospinning process used was able to reproduce the non-linear behaviour of the biological counterpart. This outcome confirmed the important role of the electrospinning technique to obtain aligned nanofibers mimicking the intrinsic structure of collagen in both animal and human bodies, like already reported by several works in literature. The tuning of this technique, the choice of adequate parameters, has proven to be extremely important for the success of the production process. The customization of the machine for the tendon sheath production and the *ad hoc* grips made for the mechanical testing, represent a first step toward the industrialization of the production process. This will lead to further improvements in the scalability and reproducibility of the outcome, as well as the mechanical properties of bundles and the sheath. From this perspective, the production method proposed in this work leaves room for many possible further developments: different polymers, even resorbable, more complex structures, gel addition within the bundles and more. The development and further investigation of this electrospun multiscale nylon 6.6 device and, more generally, of this production method in fields such synthetic

implants for tendon/ligaments regeneration and replacement, or *in vitro* simulation tool for biomechanical tests and surgical simulation, is strongly advised.

7: REFERENCES

1. Kannus, P. Structure of the tendon connective tissue. *Scand. J. Med. Sci. Sport.* **10,** 312–320 (2000).

2. Khan, S. & Hashmi, G. S. HISTOLOGY AND FUNCTIONS OF CONNECTIVE TISSUES: a review article. *Univ. J. Dent. Sci.* **1,** 1–2 (2015).

3. Kastelic, J., Galeski, A. & Baer, E. The multicomposite ultrastructure of tendon. *Connect. Tissue Res.* **6,** 11–23 (1978).

4. Minns, R. J., Soden, P. D. & Jackson, D. S. The role of the fibrous components and ground substance in the mechanical properties of biological tissues: A preliminary investigation. *J. Biomech.* **6,** 153–165 (1973).

5. Kirkendall, D. T. & Garrett, W. E. Function and biomechanics of tendons. *Scand. J. Med. Sci. Sports* **7,** 62–66 (1997).

6. Doschak, M. R. & Zernicke, R. F. Structure, function and adaptation of bone-tendon and bone-ligament complexes. *J. Musculoskelet. Neuronal Interact.* **5,** 35–40 (2005).

7. Elliott, D. Structure and function of mammalian tendon. *Biol. Rev.* **40,** 392–421 (1965).

8. Goh, K. L., Listrat, A. & Béchet, D. Hierarchical mechanics of connective tissues: Integrating insights from nano to macroscopic studies. *J. Biomed. Nanotechnol.* **10,** 2464–2507 (2014).

9. Mitchell, R., Chesney, A., Seal, S., McKnight, L. & Thoma, A. Anatomical variations of the carpal tunnel structures. *Can. J. Plast. Surg.* **17,** e3-7 (2009).

10. Ferreira, R. *et al.* Achilles Tendon Vascularization of Proximal, Medial, and Distal Portion Before and After Partial Lesion in Rats Treated with Phototherapy. *Photomed. Laser Surg.* **33,** 579–584 (2015).

11. Ippolito Ernesto, Natali, P. G., Postacchini, F., Accinni, L. & De Martino, C. Morphological, Immunochemical, and Biochemical Study of Rabbit Achilles Tendon at Various Ages. *J. Bone Jt. Surg.* 1535–1539 (1980).

12. Holmes, D. F. *et al.* Corneal collagen fibril structure in three dimensions: Structural insights into fibril assembly, mechanical properties, and tissue organization. *Proc. Natl. Acad. Sci.* **98,** 7307–7312 (2001).

13. Moore, M. J. & De Beaux, A. A quantitative ultrastructural study of rat tendon from birth to maturity. *J. Anat.* **153,** 163–169 (1987).

14. Hess, G. P., Cappiello, W. L., Poole, R. M. & Hunter, S. C. Prevention and

treatment of overuse tendon injuries. *Sport. Med.* **8,** 371–384 (1989).

15. Finni, T. Structural and functional features of human muscle-tendon unit. *Scand. J. Med. Sci. Sport.* **16,** 147–158 (2006).

16. Charvet, B., Ruggiero, F. & Le Guellec, D. The development of the myotendinous junction. A review. *Muscles. Ligaments Tendons J.* **2,** 53–63 (2012).

17. Liu, Y., Ramanath, H. S. & Wang, D. A. Tendon tissue engineering using scaffold enhancing strategies. *Trends Biotechnol.* **26,** 201–209 (2008).

18. David, L., Grood, E. S., Noyes, F. R. & Zernicke, R. E. Biomechanics of ligaments and tendons. *Exerc. Sport Sci. Rev.* **6,** 125–182 (1978).

19. Neumann, D. A. *Kinesiology of the Musculoskeletal System-E-Book: Foundations for Rehabilitation*. (Elsevier Health Sciences, 2013).

20. Bozec, L. & Horton, M. Topography and mechanical properties of single molecules of type I collagen using atomic force microscopy. *Biophys. J.* **88,** 4223–4231 (2005).

21. Yang, L., van der Werf, K. O., Dijkstra, P. J., Feijen, J. & Bennink, M. L. Micromechanical analysis of native and cross-linked collagen type I fibrils supports the existence of microfibrils. *J. Mech. Behav. Biomed. Mater.* **6,** 148–158 (2012).

22. Eppell, S. ., Smith, B. ., Kahn, H. & Ballarini, R. Nano measurements with micro-devices: mechanical properties of hydrated collagen fibrils. *J. R. Soc. Interface* **3,** 117–121 (2006).

23. Goh, K. L., Aspden, R. M., Mathias, K. J. & Hukins, D. W. L. Effect of fibre shape on the stresses within fibres in fibre-reinforced composite materials. *Proc. R. Soc. A Math. Phys. Eng. Sci.* **455,** 3351–3361 (1999).

24. Goh, K. ., Meakin, J. ., Aspden, R. . & Hukins, D. W. . Influence of fibril taper on the function of collagen to reinforce extracellular matrix. *Proc. R. Soc. B Biol. Sci.* **272,** 1979–1983 (2005).

25. Szczesny, S. E. & Elliott, D. M. Interfibrillar shear stress is the loading mechanism of collagen fibrils in tendon. *Acta Biomater.* **10,** 2582–2590 (2014).

26. Edwards, A., Bull, A. M. J. & Amis, A. A. The attachments of the anteromedial and posterolateral fibre bundles of the anterior cruciate ligament : PPPart 2: Femoral attachment. *Knee Surgery, Sport. Traumatol. Arthrosc.* **16,** 29–36 (2008).

27. Cheong, V. S. *et al.* Magnetic resonance imaging of the human anterior cruciate ligament: Three-dimensional computer reconstruction and structural analysis. *J. Med. Imaging Heal. Informatics* **2,** 378–385 (2012).

28. Newsham-West, R., Nicholson, H., Walton, M. & Milburn, P. Long-term morphology of a healing bone-tendon interface: A histological observation in the sheep model. *J. Anat.* **210,** 318–327 (2007).

29. Screen, H. R. C., Bader, D. L., Lee, D. A. & Shelton, J. C. Local Strain Measurement within Tendon. *Strain* **40,** 157–163 (2004).

30. Screen, H. R. C., Lee, D. A., Bader, D. L. & Shelton, J. C. An investigation into the effects of the hierarchical structure of tendon fascicles on micromechanical properties. *Proc. Inst. Mech. Eng. Part H J. Eng. Med.* **218,** 109–119 (2004).

31. Hansen, K. A., Weiss, J. A. & Barton, J. K. Recruitment of Tendon Crimp With Applied Tensile Strain. *J. Biomech. Eng.* **124,** 72 (2002).

32. Franchi, M. *et al.* Crimp morphology in relaxed and stretched rat Achilles tendon. *J. Anat.* **210,** 1–7 (2007).

33. Benjamin, M., Kaiser, E. & Milz, S. Structure-function relationships in tendons: A review. *J. Anat.* **212,** 211–228 (2008).

34. Hanson, P., Aagaard, P. & Magnusson, S. P. Biomechanical properties of isolated fascicles of the Iliopsoas and Achilles tendons in African American and Caucasian men. *Ann. Anat.* **194,** 457–460 (2012).

35. Tendon healing mechanobiology. Available at: https://www.shoulderdoc.co.uk/article/1029.

36. Campbell-kyureghyan, N. H. & Marras, W. S. Combined Experimental and Analytical Model of the Lumbar Spine Subjected to Large Displacement Cyclic Loads Part II –. **2,** (2009).

37. Cristofolini, L. Slide from 'Biological Tissue Characterization' lessons. (2015).

38. Pioletti, D. P., Rakotomanana, L. R., Benvenuti, J. F. & Leyvraz, P. F. Viscoelastic constitutive law in large deformations: Application to human knee ligaments and tendons. *J. Biomech.* **31,** 753–757 (1998).

39. Duenwald, S. E., Vanderby, R. & Lakes, R. S. Stress relaxation and recovery in tendon and ligament: Experiment and modeling. *Biorheology* **47,** 1–14 (2010).

40. Wren, T. A. L., Lindsey, D. P., Beaupré, G. S. & Carter, D. R. Effects of creep and cyclic loading on the mechanical properties and failure of human Achilles tendons. *Ann. Biomed. Eng.* **31,** 710–717 (2003).

41. Sasaki, N. & Odajima, S. Elongation mechanisms of collagen fibrils and force-strain relations of tendons at each level of structural hierarchy. *J. Biomech.* **29,** 1131–1136 (1996).

42. Chen, J., Xu, J., Wang, A. & Zheng, M. Scaffolds for tendon and ligament

repair: Review of the efficacy of commercial products. *Expert Rev. Med. Devices* **6,** 61–73 (2009).

43. Walden, G. *et al.* A Clinical, Biological, and Biomaterials Perspective into Tendon Injuries and Regeneration. *Tissue Eng. Part B Rev.* **23,** 44–58 (2017).

44. Iliadis, D. P., Bourlos, D. N., Mastrokalos, D. S., Chronopoulos, E. & Babis, G. C. LARS Artificial Ligament Versus ABC Purely Polyester Ligament for Anterior Cruciate Ligament Reconstruction. *Orthop. J. Sport. Med.* **4,** 1–10 (2016).

45. Jamil, T., Ansari, U., Najabat Ali, M. & Mir, M. A Review on Biomechanical and Treatment Aspects Associated with Anterior Cruciate Ligament. *Irbm* **38,** 13–25 (2017).

46. PANKAJ SHARMA, MRCS, AND NICOLA MAFFULLI, MD, MS, PHD, F. ➤. Tendon Injury and Tendinopathy : Healing and Repair. *J. Bone Jt. Surg.* 17–19 (2005).

47. Soldatis, J. J., Goodfellow, D. B. & Wilber, J. H. End-to-End Operative Repair of Achilles Tendon Rupture. *Am. J. Sports Med.* **25,** 90–95 (1997).

48. Docheva, D., Müller, S. A., Majewski, M. & Evans, C. H. Biologics for tendon repair. *Adv. Drug Deliv. Rev.* **84,** 222–239 (2015).

49. Kannus, P. & Jozsa, L. Histopathological changes preceding spontaneous rupture of a tendon. A controlled study of 891 patients. *J. Bone Joint Surg. Am.* **73,** 1507–1525 (1991).

50. ARNER, O., Lindholm, A. & Orell, S. R. Histologic changes in subcutaneous rupture of the Achilles tendon; a study of 74 cases. *Acta Chir. Scand.* **116,** 484 (1959).

51. Selvanetti, A., Cipolla, M. & Puddu, G. Overuse tendon injuries: Basic science and classification. *Oper. Tech. Sports Med.* **5,** 110–117 (1997).

52. Gruchow, H. W. & Pelletier, D. An epidemiologic study of tennis elbow. *Am. J. Sports Med.* **7,** 234–238 (1979).

53. Ratcliffe, A. *et al.* Scaffolds for Tendon and Ligament Repair and Regeneration. *Ann. Biomed. Eng.* **43,** 819–831 (2015).

54. Maffulli, N., Ajis, A., Longo, U. G. & Denaro, V. Chronic Rupture of Tendo Achillis. *Foot Ankle Clin.* **12,** 583–596 (2007).

55. Clayton, R. A. E. & Court-Brown, C. M. The epidemiology of musculoskeletal tendinous and ligamentous injuries. *Injury* **39,** 1338–1344 (2008).

56. Duthon, V. B. *et al.* Anatomy of the anterior cruciate ligament. *Knee Surgery, Sport. Traumatol. Arthrosc.* **14,** 204–213 (2006).

57. Zantop, T., Petersen, W. & Fu, F. H. Anatomy of the anterior cruciate ligament. *Oper. Tech. Orthop.* **15,** 20–28 (2005).

58. Buss, D. D. *et al.* Nonoperative treatment of acute anterior cruciate ligament injuries in a selected group of patients. *Am J Sport. Med* **23,** 160–165 (1995).

59. Nielsen, A. B. & Jensen, P. Ø. Primary flexor tendon repair in 'no man's land'. *J. Hand Surg. Am.* **9,** 279–281 (1984).

60. Marder, R. A. & Timmerman, L. A. Primary repair of patellar tendon rupture without augmentation. *Am. J. Sports Med.* **27,** 304–307 (1999).

61. Meunier, A., Odensten, M. & Good, L. Long-term results after primary repair or non-surgical treatment of anterior cruciate ligament rupture: A randomized study with a 15-year follow-up. *Scand. J. Med. Sci. Sports* **17,** 230–237 (2007).

62. Kartus, J., Movin, T. & Karlsson, J. Donor-site morbidity and anterior knee problems after anterior cruciate ligament reconstruction using autografts. *Arthroscopy* **17,** 971–980 (2001).

63. Jackson, D. W., Corsetti, J. & Simon, T. M. Biologic incorporation of allograft anterior cruciate ligament replacements. *Clin. Orthop. Relat. Res.* **324,** 126–133 (1996).

64. Janssen, R. P. A. & Scheffler, S. U. Remodeling of Hamstring Tendon Grafts After ACL Reconstruction. in *Anterior Cruciate Ligament Reconstruction* 257–265 (Springer, 2014).

65. Sun, K. *et al.* Anterior Cruciate Ligament Reconstruction With Bone-Patellar Tendon-Bone Autograft Versus Allograft. *Arthrosc. - J. Arthrosc. Relat. Surg.* **25,** 750–759 (2009).

66. Fu, F. H. & Cohen, S. *Current concepts in ACL reconstruction*. (SLACK Incorporated, 2008).

67. Lee, G. H., McCulloch, P., Cole, B. J., Bush-Joseph, C. A. & Bach, B. R. The Incidence of Acute Patellar Tendon Harvest Complications for Anterior Cruciate Ligament Reconstruction. *Arthrosc. - J. Arthrosc. Relat. Surg.* **24,** 162–166 (2008).

68. Bartlett, R. J., Bartlett, R. J., Clatworthy, M. G. & Nguyen, T. N. V. Graft Selection in Reconstruction of the Anterior Cruciate Ligament. *J Bone Jt. Surg [Br]* **83,** 625–34 (2001).

69. Prokopis, P. M. & Schepsis, A. A. Allograft use in ACL reconstruction. *Knee* **6,** 75–85 (1999).

70. Jenkins, D. H. The repair of cruciate ligaments with flexible carbon fibre. A longer term study of the induction of new ligaments and of the fate of the

implanted carbon. *Bone Joint J.* **60,** 520–522 (1978).

71. Gore-Tex prothesis. Available at: http://medapparatus.com/Gallery/Gallery_JointArthroplasty_Page5.html.

72. Batty, L. M. *et al.* Synthetic devices for reconstructive surgery of the cruciate ligaments: a systematic review. *Arthroscopy* **31,** 957–968 (2015).

73. Seitz, H., Marlovits, S., Schwendenwein, I., Müller, E. & Vécsei, V. Biocompatibility of polyethylene terephthalate (Trevira® hochfest) augmentation device in repair of the anterior cruciate ligament. *Biomaterials* **19,** 189–196 (1998).

74. Fujikawa, K., Ohtani, T., Matsumoto, H. & Seedhom, B. B. Reconstruction of the extensor apparatus of the knee with the Leeds-Keio ligament. *Bone Joint J.* **76,** 200–203 (1994).

75. Fujikawa, K., Iseki, F. & Seedhom, B. B. Arthroscopy after anterior cruciate reconstruction with the Leeds-Keio ligament. *Bone Joint J.* **71,** 566–570 (1989).

76. Murray, A. W. & Macnicol, M. F. 10–16 year results of Leeds-Keio anterior cruciate ligament reconstruction. *Knee* **11,** 9–14 (2004).

77. McPherson, G. K. *et al.* Experimental Mechanical and Histologic Evaluation of the Kennedy Ligament Augmentation Device. (1084).

78. Something New. *Orthopedics.* (1992). Available at: https://www.healio.com/orthopedics/journals/ortho/1992-9-15-9/%7Bed6f1b43-efc3-4ec4-ad32-5d29a0e19d25%7D/something-new.

79. Drogset, J. O. & Grøntvedt, T. Anterior cruciate ligament reconstruction with and without a ligament augmentation device: results at 8-year follow-up. *Am. J. Sports Med.* **30,** 851–856 (2002).

80. Longo, U. G., Lamberti, A., Maffulli, N. & Denaro, V. Tendon augmentation grafts: a systematic review. *Br. Med. Bull.* **94,** 165–188 (2010).

81. Nau, T., Lavoie, P. & Duval, N. A new generation of artificial ligaments in reconstruction of the anterior cruciate ligament. *Bone Joint J.* **84,** 356–360 (2002).

82. Liu, Z., Zhang, X., Jiang, Y. & Zeng, B.-F. Four-strand hamstring tendon autograft versus LARS artificial ligament for anterior cruciate ligament reconstruction. *Int. Orthop.* **34,** 45–49 (2010).

83. Machotka, Z., Scarborough, I., Duncan, W., Kumar, S. & Perraton, L. Anterior cruciate ligament repair with LARS (ligament advanced reinforcement system): a systematic review. *BMC Sports Sci. Med. Rehabil.* **2,** 29 (2010).

84. Guerard, S. *et al.* Biomechanical evaluation of a bioactive artificial anterior

cruciate ligament. *Adv. Biomech. Appl.* **1,** 239–252 (2014).

85. Trieb, K. *et al.* In vivo and in vitro cellular ingrowth into a new generation of artificial ligaments. *Eur. Surg. Res.* **36,** 148–151 (2004).

86. WANG, C.-L., HSIAO, C.-K., HSU, A.-T., DUNG, C.-Z. & CHANG, C.-H. Biocompatibility and Mechanical Property of Lars Artificial Ligament With Tissue Ingrowth. *J. Mech. Med. Biol.* **12,** 1250012 (2012).

87. Handl, M. *et al.* Reconstruction of the anterior cruciate ligament: Dynamic strain evaluation of the graft. *Knee Surgery, Sport. Traumatol. Arthrosc.* **15,** 233–241 (2007).

88. Leduc, S., Yahia, L., Boudreault, F., Fernandes, J. C. & Duval, N. Mechanical evaluation of a ligament fixation system for ACL reconstruction at the tibia in a canine cadaver model. in *Annales de chirurgie* **53,** 735–741 (1999).

89. Abdullah, S. Usage of synthetic tendons in tendon reconstruction. *BMC Proc.* **9,** A68 (2015).

90. Wang, X. *et al.* Continuous polymer nanofiber yarns prepared by self-bundling electrospinning method. *Polymer (Guildf).* **49,** 2755–2761 (2008).

91. Liu, S. *et al.* Biomimetic sheath membrane via electrospinning for antiadhesion of repaired tendon. *Biomacromolecules* **13,** 3611–3619 (2012).

92. Xu, Y. *et al.* Fabrication of Electrospun Poly(L-Lactide-co-ε-Caprolactone)/Collagen Nanoyarn Network as a Novel, Three-Dimensional, Macroporous, Aligned Scaffold for Tendon Tissue Engineering. *Tissue Eng. Part C Methods* **19,** 925–936 (2013).

93. Liu, H. Electrospining of nanofibers for tissue engineering applications. *J. Nanomater.* **2013,** 1–31 (2013).

94. Sensini, A. *et al.* Biofabrication of bundles of poly (lactic acid) -collagen blends mimicking the fascicles of the human Achille tendon. *Biofabrication* (2017).

95. Liu, W., Thomopoulos, S. & Xia, Y. Electrospun nanofibers for regenerative medicine. *Adv. Healthc. Mater.* **1,** 10–25 (2012).

96. Chainani, A., Little, D. & Little, B. S. Current Status of Tissue-Engineered Scaffolds for Rotator Cuff Repair. *HHS Public Access* **344,** 1173–1178 (2015).

97. Wang, X., Ding, B. & Li, B. Biomimetic electrospun nanofibrous structures for tissue engineering. *Mater. Today* **16,** 229–241 (2013).

98. Jiang, T., Carbone, E. J., Lo, K. W. H. & Laurencin, C. T. Electrospinning of polymer nanofibers for tissue regeneration. *Prog. Polym. Sci.* **46,** 1–24 (2015).

99. Dahlin, R. L., Kasper, F. K. & Mikos, A. G. Polymeric Nanofibers in Tissue Engineering. *Tissue Eng. Part B Rev.* **17,** 349–364 (2011).

100. McCarron, J. A., Milks, R. A., Chen, X., Iannotti, J. P. & Derwin, K. A. Improved time-zero biomechanical properties using poly-L-lactic acid graft augmentation in a cadaveric rotator cuff repair model. *J. Shoulder Elb. Surg.* **19,** 688–696 (2010).

101. O'Connor, R. A. & McGuinness, G. B. Electrospun nanofibre bundles and yarns for tissue engineering applications: A review. *Proc. Inst. Mech. Eng. Part H J. Eng. Med.* **230,** 987–998 (2016).

102. Kumbar, S. G., James, R., Nukavarapu, S. P. & Laurencin, C. T. Electrospun nanofiber scaffolds: Engineering soft tissues. *Biomed. Mater.* **3,** (2008).

103. Huang, Z. M., Zhang, Y. Z., Kotaki, M. & Ramakrishna, S. A review on polymer nanofibers by electrospinning and their applications in nanocomposites. *Compos. Sci. Technol.* **63,** 2223–2253 (2003).

104. Kumbar, S. G., Kofron, M. D., Nair, L. S. & Laurencin, C. T. Cell behavior toward nanostructured surfaces. *Biomed. Nanostructures* 261–295 (2007).

105. Nalwa, H. S. *Handbook of nanostructured materials and nanotechnology, five-volume set*. (Academic Press, 1999).

106. Peppas, N. A. *Handbook of Biomaterial Properties*. *Journal of Controlled Release* **65,** (2000).

107. Li, X. *et al.* Nanofiber scaffolds with gradations in mineral content for mimicking the tendon-to-bone insertion site. *Nano Lett.* **9,** 2763–2768 (2009).

108. Sahoo, S., Ouyang, H., Goh, J. C.-H., Tay, T. E. & Toh, S. L. Characterization of a Novel Polymeric Scaffold for Potential Application in Tendon/Ligament Tissue Engineering. *Tissue Eng.* **12,** 91–99 (2006).

109. Verdiyeva, G., Koshy, K., Glibbery, N., Mann, H. & Seifalian, A. M. Tendon reconstruction with tissue engineering approach - A review. *J. Biomed. Nanotechnol.* **11,** 1495–1523 (2015).

110. Xie, J. & Hsieh, Y.-L. Ultra-high surface fibrous membranes from electrospinning of natural proteins: casein and lipase enzyme. *J. Mater. Sci.* **38,** 2125–2133 (2003).

111. Teo, W. E. & Ramakrishna, S. A review on electrospinning design and nanofibre assemblies. *Nanotechnology* **17,** (2006).

112. Bartolo, F. Electrospinning. Available at: http://www.chimica-online.it/materiali/fibre-tessili/electrospinning.htm.

113. Haider, A., Haider, S. & Kang, I. K. A comprehensive review summarizing the effect of electrospinning parameters and potential applications of

nanofibers in biomedical and biotechnology. *Arab. J. Chem.* (2015). doi:10.1016/j.arabjc.2015.11.015

114. Bae, H. S. H. *et al.* Fabrication of highly porous PMMA electrospun fibers and their application in the removal of phenol and iodine. *J. Polym. …* **20,** 158 (2013).

115. Sell, S. A., McClure, M. J., Garg, K., Wolfe, P. S. & Bowlin, G. L. Electrospinning of collagen/biopolymers for regenerative medicine and cardiovascular tissue engineering. *Adv. Drug Deliv. Rev.* **61,** 1007–1019 (2009).

116. Ali, U., Zhou, Y., Wang, X. & Lin, T. Electrospinning of Continuous Nanofiber Bundles and Twisted Nanofiber Yarns. *Nanofibers - Prod. Prop. Funct. Appl.* 153–174 (2011). doi:10.2106/JBJS.J.01112

117. Ngadiman, N. H. A., Noordin, M. Y., Idris, A. & Kurniawan, D. A review of evolution of electrospun tissue engineering scaffold: From two dimensions to three dimensions. *Proc. Inst. Mech. Eng. Part H J. Eng. Med.* **231,** 597–616 (2017).

118. Gupta, P., Elkins, C., Long, T. E. & Wilkes, G. L. Electrospinning of linear homopolymers of poly (methyl methacrylate): exploring relationships between fiber formation, viscosity, molecular weight and concentration in a good solvent. *Polymer (Guildf).* **46,** 4799–4810 (2005).

119. Son, W. K., Youk, J. H., Lee, T. S. & Park, W. H. The effects of solution properties and polyelectrolyte on electrospinning of ultrafine poly(ethylene oxide) fibers. *Polymer (Guildf).* **45,** 2959–2966 (2004).

120. Fong, H., Chun, I. & Reneker, D. H. Beaded nanofibers formed during electrospinning. *Polymer (Guildf).* **40,** 4585–4592 (1999).

121. Shenoy, S. L., Bates, W. D., Frisch, H. L. & Wnek, G. E. Role of chain entanglements on fiber formation during electrospinning of polymer solutions: good solvent, non-specific polymer–polymer interaction limit. *Polymer (Guildf).* **46,** 3372–3384 (2005).

122. Deitzel, J. ., Kleinmeyer, J., Harris, D. & Beck Tan, N. . The effect of processing variables on the morphology of electrospun nanofibers and textiles. *Polymer (Guildf).* **42,** 261–272 (2001).

123. Fridrikh, S. V., Yu, J. H., Brenner, M. P. & Rutledge, G. C. Controlling the Fiber Diameter during Electrospinning. *Phys. Rev. Lett.* **90,** 4 (2003).

124. Fennessey, S. F. & Farris, R. J. Fabrication of aligned and molecularly oriented electrospun polyacrylonitrile nanofibers and the mechanical behavior of their twisted yarns. *Polymer (Guildf).* **45,** 4217–4225 (2004).

125. Li, D. & Xia, Y. Electrospinning of nanofibers: Reinventing the wheel? *Adv. Mater.* **16,** 1151–1170 (2004).

126. Rutledge, G. C. & Fridrikh, S. V. Formation of fibers by electrospinning. *Adv. Drug Deliv. Rev.* **59,** 1384–1391 (2007).

127. A., T., E., Z. & A.L, Y. Electrostatic field-assisted alignment of electrospun nanofibers. *Nanotechnology* **12,** 384 (2001).

128. Xu, C. Y., Inai, R., Kotaki, M. & Ramakrishna, S. Aligned biodegradable nanofibrous structure: a potential scaffold for blood vessel engineering. *Biomaterials* **25,** 877–886 (2004).

129. Dalton, P. D., Klee, D. & Möller, M. Electrospinning with dual collection rings. *Polymer (Guildf).* **46,** 611–614 (2005).

130. Khil, M., Bhattarai, S. R., Kim, H., Kim, S. & Lee, K. Novel fabricated matrix via electrospinning for tissue engineering. *J. Biomed. Mater. Res. Part B Appl. Biomater.* **72,** 117–124 (2005).

131. Smit, E., Bűttner, U. & Sanderson, R. D. Continuous yarns from electrospun fibers. *Polymer (Guildf).* **46,** 2419–2423 (2005).

132. Teo, W.-E., Gopal, R., Ramaseshan, R., Fujihara, K. & Ramakrishna, S. A dynamic liquid support system for continuous electrospun yarn fabrication. *Polymer (Guildf).* **48,** 3400–3405 (2007).

133. Rothrauff, B. B. *et al.* Braided and Stacked Electrospun Nanofibrous Scaffolds for Tendon and Ligament Tissue Engineering. *Tissue Eng. Part A* **23,** 378–389 (2017).

134. Sensini, A. High Resolution X-Ray Tomographic Morphological Characterization of Electrospun nanofibrous bundles for tendon and ligament regeneration and replacement. *J. Microsc.* (2018).

135. Sensini, A. *et al.* Tendon Fascicle-Inspired Nanofibrous Scaffold of Polylactic acid/Collagen with Enhanced 3D-Structure and Biomechanical Proprieties. *Sci. Rep.*

136. Sensini, A., Focarete, M. L., Gualandi, C., Tozzi, G. & Cristofolini, L. Biomechanical suitability if scaffolds made of electrospun bundles for tendon repair. *Bone Joint J.* (2017).

137. Sensini, A. Individuazione e stima di parametri per la valutazione di ottiche endoscopiche.

138. Sensini, A. *et al.* Fabrication and characterization of electrospun scaffolds for tendon reconstruction. *Proc. 7th Meet. Ital. Chapter Eur. Soc. Biomech. (ESB-ITA 2017), Vairo G. Ed. available online from http//esbiomech.org/esb_archive/ESB-ITA-2017.pdf* 6–8 (2017).

139. A. Sensini, M. L. Focarete, C. Gualandi, A. Zucchelli, G. Tozzi, L. Boyle, G. Reilly, L. C. Fabrication, characterization and high-resolution x-ray tomographic investigation of resorbable electrospun nanofibrous scaffolds

for tendon regeneration. in *Congress of Royal Microscopical Society ToScA-Tomography for Scientific Advancement* (2017).

140. Focarete, M. L. *et al.* Crosslinked Poly(L- lactic acid)/collagen electrospun bundles for tendon reconstruction. in *Congress of European Society of Biomaterials* (2017).

141. Sensini, A. *et al.* Biofabrication and mechanical characterization of an electrospun scaffold for tendon reconstruction. in *23nd Congress of European Society of Biomechanics* (2017).

142. Sensini, A., Focarete, M. L., Gualandi, C. & Cristofolini, L. Development and mechanical characterization of electrospun bundles for tendon reconstruction. in *22nd Congress of European Society of Biomechanics* (2016).

143. Segala, M. Crosslinking of electrospun scaffolds for tendon tissue reconstruction. (Alma Mater Studiorum - Università di Bologna, 2016).

144. Dazzi, C. Characterization of resorbable crosslinked electrospun bundles for tendon tissue reconstruction. (2016).

145. Spalazzi, J. P., Doty, S. B., Moffat, K. L., Levine, W. N. & Lu, H. H. Development of Controlled Matrix Heterogeneity on a Triphasic Scaffold for Orthopedic Interface Tissue Engineering. *Tissue Eng.* **12,** 3497–3508 (2006).

146. Dormer, N. H., Berkland, C. J. & Detamore, M. S. Emerging techniques in stratified designs and continuous gradients for tissue engineering of interfaces. *Ann. Biomed. Eng.* **38,** 2121–2141 (2010).

147. Sensini, A. *et al.* Scaffold multiscala elettrofilato per la rigenerazione e/o sostituzione del tessuto tendineo/legamentoso e metodo di produzione.

148. Sensini, A. *et al.* Multiscale tendon-like resorbable electrospun scaffold for tissue regeneration. *Nat. Mater.* (2018).

149. Bendanti, E. Design and multiscale assembly of electrospun scaffolds for tendon reconstruction. (Alma Mater Studiorum - Univeristà di Bologna, 2016).

150. Moshiri, A., Oryan, A. & Meimandi-Parizi, A. Role of tissue-engineered artificial tendon in healing of a large achilles tendon defect model in rabbits. *J. Am. Coll. Surg.* **217,** 421–441.e8 (2013).

151. Matthews, J. A., Wnek, G. E., Simpson, D. G. & Bowlin, G. L. Electrospinning of collagen nanofibers. *Biomacromolecules* **3,** 232–238 (2002).

152. Kim, S., Laschi, C. & Trimmer, B. Soft robotics: A bioinspired evolution in robotics. *Trends Biotechnol.* **31,** 287–294 (2013).

153. Lee, C. *et al.* Soft robot review. *Int. J. Control. Autom. Syst.* **15,** 3–15 (2017).

154. Majidi, C. Soft Robotics: A Perspective—Current Trends and Prospects for the Future. *Soft Robot.* **1,** 5–11 (2014).

155. Cianchetti, M. Fundamentals on the Use of Shape Memory Alloys in Soft Robotics. *Interdiscip. Mechatronics Eng. Sci. Res. Dev. eds M. K. Habib J. Paulo Davim (Hoboken John Wiley Sons, Inc.)* 227–254 (2013).

156. Kim, K. J. & Tadokoro, S. *Electroactive Polymers for Robotic Applications*. *Bratislavske Lekarske Listy* **93,** (2007).

157. Laschi, C. & Cianchetti, M. Soft Robotics: New Perspectives for Robot Bodyware and Control. *Front. Bioeng. Biotechnol.* **2,** 1–5 (2014).

158. Seok, S. *et al.* Meshworm : A Peristaltic Soft Robot With Antagonistic Nickel Titanium Coil Actuators. *Ieee/Asme Trans. Mechatronics* **18,** 1–13 (2012).

159. Zheng, T. *et al.* Octopus Inspired Walking Robot: Design, Control and Experimental Validation. 816–821 (2013).

160. Laschi, C. *et al.* Soft Robot Arm Inspired by the Octopus. 37–41 (2012). doi:10.1163/156855312X626343

161. Lin, H., Leisk, G. G. & Trimmer, B. GoQBot : a caterpillar-inspired soft-bodied rolling robot. **26007,**

162. Lee, S. W., Landers, K. A. & Park, H. S. Development of a biomimetic hand exotendon device (BiomHED) for restoration of functional hand movement post-stroke. *IEEE Trans. Neural Syst. Rehabil. Eng.* **22,** 886–898 (2014).

163. KWAKKEL, G., WAGENAAR, R. C., KOLLEN, B. J. & LANKHORST, G. J. Predicting Disability in Stroke—A Critical Review of the Literature. *Age Ageing* **25,** 479–489 (1996).

164. Sava Cables. Available at: https://www.savacable.com/pages/LowStretchCable.html.

165. Asbeck, A. T., Dyer, R. J., Larusson, A. F. & Walsh, C. J. Biologically-inspired soft exosuit. *IEEE Int. Conf. Rehabil. Robot.* 1–8 (2013). doi:10.1109/ICORR.2013.6650455

166. Asbeck, A. T., De Rossi, S. M. M., Holt, K. G. & Walsh, C. J. A biologically inspired soft exosuit for walking assistance. *Int. J. Rob. Res.* **34,** 744–762 (2015).

167. In, B. H., Kang, B. B., Sin, M. & Cho, K. A Wearable Robot for the Hand with a Soft Tendon Routing System. 97–105

168. In, H., Cho, K., Kim, K. & Lee, B. Jointless Structure and Under-Actuation Mechanism for Compact Hand Exoskeleton. (2011).

169. Nycz, C. J., Delph, M. A. & Fischer, G. S. Modeling and design of a tendon actuated soft robotic exoskeleton for hemiparetic upper limb rehabilitation. *Proc. Annu. Int. Conf. IEEE Eng. Med. Biol. Soc. EMBS* **2015–Novem,** 3889–3892 (2015).

170. Dyneema. Available at: https://www.dsm.com/products/dyneema/en_GB/technologies/dyneema-form-factors/fiber.html.

171. Govaert, L. E., Bastiaansen, C. W. M. & Leblans, P. J. R. Stress-strain analysis of oriented polyethylene. *Polymer (Guildf).* **34,** 534–540 (1993).

172. Maganaris, C. N. & Paul, J. P. In vivo human tendon mechanical properties. *J Physiol* **521 Pt 1,** 307–13 (1999).

173. Weghe, M. Vande, Rogers, M., Weissert, M. & Matsuoka, Y. The ACT Hand: design of the skeletal structure. *IEEE Int. Conf. Robot. Autom. 2004. Proceedings. ICRA '04. 2004* **4,** 3375–3379 (2004).

174. Deshpande, A. D. *et al.* Testbed Hand. **18,** 238–250 (2013).

175. Xu, Z., Matsuoka, Y. & Deshpande, A. D. Crocheted artificial tendons and ligaments for the anatomically correct testbed (ACT) hand. *2015 IEEE Int. Conf. Robot. Biomimetics, IEEE-ROBIO 2015* 2449–2453 (2015). doi:10.1109/ROBIO.2015.7419706

176. Bundhoo, V., Haslam, E., Birch, B. & Park, E. J. A shape memory alloy-based tendon-driven actuation system for biomimetic artificial fingers, part I: Design and evaluation. *Robotica* **27,** 131–146 (2009).

177. Kyberd, P. J. *et al.* The design of anthropomorphic prosthetic hands: A study of the Southampton Hand. *Robotica* **19,** 593–600 (2001).

178. Wu, L. *et al.* Compact and low-cost humanoid hand powered by nylon artificial muscles. *Bioinspiration and Biomimetics* **12,** (2017).

179. Haines, C. S. *et al.* Artificial muscles from fishing line and sewing thread. *Science (80-.).* **343,** 868–872 (2014).

180. Smith, A. M. *et al.* The porcine forelimb as a model for human flexor tendon surgery. *J. Hand Surg. Am.* **30,** 307–309 (2005).

181. Ingraham, J. M., Weber, R. A. & Weber, R. A. Utilizing a simulated tendon to teach tendon repair technique. *Hand* **4,** 150–155 (2009).

182. Tare, M. Dental rolls: A suitable model for practising tendon repair techniques. *J. Hand Surg. Am.* **29,** 506–507 (2004).

183. Sensini, A. *et al.* Biofabrication of bundles of poly (lactic acid) -collagen

blends mimicking the fascicles of the human Achille tendon. *Biofabrication* (2017).

184. Iso, B. S. E. N. Textiles — Yarns from packages — Determination of single-end breaking force and elongation at break using constant rate of extension (CRE). *Management* (2009).

185. Standard, B. Textiles Para-aramid multifilament yarns BS EN 12562:1999. (1999).

186. ASTM. Standard Test Method for Tensile Properties of Yarns by the Single-Strand Method. *ASTM Int.* **D2256/D225,** 1–13 (2015).

187. ASTM. ASTM D1414 - 15 Rubber O-Rings. *Standardization* 1–11 (2015). doi:10.1520/D1414-15.2

188. Banik, B. L., Lewis, G. S. & Brown, J. L. Multiscale Poly-(ε-caprolactone) Scaffold Mimicking Nonlinearity in Tendon Tissue Mechanics. (2016).

189. Li, D. *et al.* Nerve conduits constructed by electrospun P(LLA-CL) nanofibers and PLLA nanofiber yarns. *J. Mater. Chem. B* **3,** 8823–8831 (2015).

190. Moshiri, A. Tendon and Ligament Tissue Engineering, Healing and Regenerative Medicine. *J. Sports Med. Doping Stud.* **3,** (2013).

191. Tavares, W. C. ampo. *et al.* Healing of the Achilles tendon in rabbits--evaluation by magnetic resonance imaging and histopathology. *J. Orthop. Surg. Res.* **9,** 132 (2014).

192. Peltonen, J., Cronin, N. J., Stenroth, L., Finni, T. & Avela, J. Viscoelastic properties of the achilles tendon in vivo. *Springerplus* **2,** 1–8 (2013).

193. Lewis, G. & Shaw, K. M. Tensile properties of human tendo Achillis: Effect of donor age and strain rate. *J. Foot Ankle Surg.* **36,** 435–445 (1997).

194. Zhao, X. P. & Huang, R. Y. M. Pervaporation separation of ethanol–water mixtures using crosslinked blended polyacrylic acid (PAA)–nylon 66 membranes. *J. Appl. Polym. Sci.* **41,** 2133–2145 (1990).

195. Robinson, P. S. *et al.* Strain-Rate Sensitive Mechanical Properties of Tendon Fascicles From Mice With Genetically Engineered Alterations in Collagen and Decorin. *J. Biomech. Eng.* **126,** 252 (2004).

196. Saadatfar, M., Afaghi Khatibi, A. & Mortazavi, B. Effective parameters on the stress-strain curve of nylon 66/clay nanocomposite using FEM. *Strain* **47,** 442–446 (2011).

197. Thermann, H., Frerichs, O., Biewener, A. & Krettek, C. Healing of the achilles tendon: An experimental study. *Foot Ankle Int.* **22,** 478–483 (2001).

198. Wren, T. A. L., Yerby, S. A., Beaupré, G. S. & Carter, D. R. Mechanical properties of the human achilles tendon. *Clin. Biomech.* **16,** 245–251 (2001).

199. Buckwalter, J. A., Goldberg, V. M., Booth, F. & Eyre, D. R. Soft-Tissue Aging and Musculoskeletal Function. *Curr. Orthop. Pract.* (1993).

200. Maitz, M. F. Applications of synthetic polymers in clinical medicine. *Biosurface and Biotribology* **1,** 161–176 (2015).